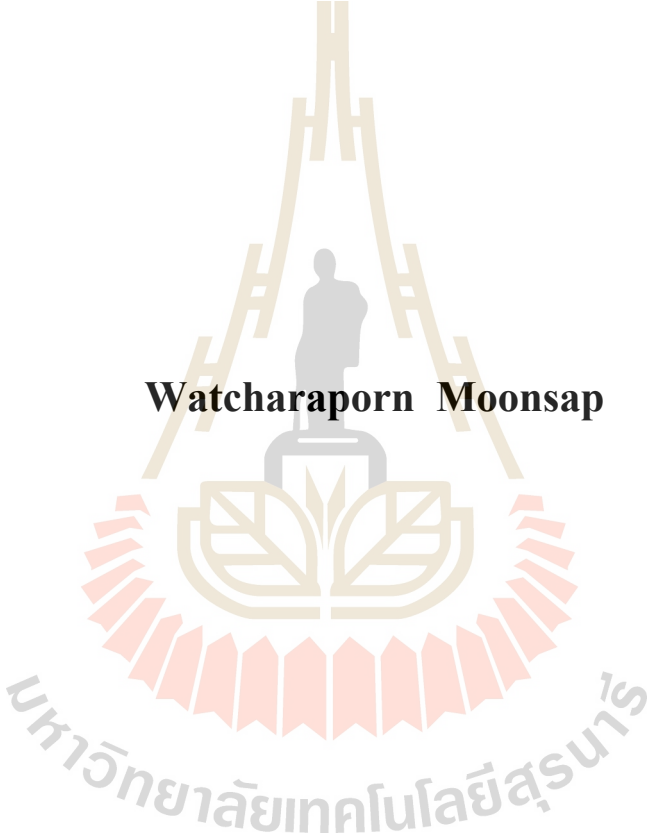


**SUGAR TRANSLOCATION BY AN UNEXPRESSED
PROTEIN CHANNEL IN *E. COLI* : SINGLE
MOLECULE DYNAMICS**



Watcharaporn Moonsap

**A Thesis Submitted in Partial Fulfillment of the Requirements for the
Degree of Master of Science in Physics
Suranaree University of Technology
Academic Year 2018**

การขนส่งน้ำตาลผ่านช่องโปรตีนแผลงใน *E. coli* : พลวัตของโมเลกุลเดี่ยว



วิทยานิพนธ์นี้เป็นส่วนหนึ่งของการศึกษาตามหลักสูตรปริญญาวิทยาศาสตรมหาบัณฑิต
สาขาวิชาฟิสิกส์
มหาวิทยาลัยเทคโนโลยีสุรนารี
ปีการศึกษา 2561

**SUGAR TRANSLOCATION BY AN UNEXPRESSED PROTEIN
CHANNEL IN *E. COLI* : SINGLE MOLECULE DYNAMICS**

Suranaree University of Technology has approved this thesis submitted in partial fulfillment of the requirements for a Master's Degree.

Thesis Examining Committee



(Asst. Prof. Dr. Panomsak Meemon)

Chairperson



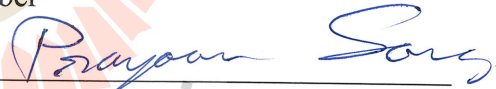
(Asst. Prof. Dr. Michael F. Smith)

Member (Thesis Advisor)



(Prof. Dr. Wipa Suginta)

Member



(Assoc. Prof. Dr. Prayoon Songsiriritthigul)

Member



(Dr. Warintorn Sreethawong)

Member



(Prof. Dr. Santi Maensiri)

Vice Rector for Academic Affairs
and Internationalization



(Assoc. Prof. Dr. Worawat Meevasana)

Dean of Institute of Science

วิทยานิพนธ์ วิชาการ : การขนส่งน้ำตาลผ่านช่องโปรตีนแฝงใน *E. coli* : พลวัตของโมเลกุลเดี่ยว (SUGAR TRANSLOCATION BY AN UNEXPRESSED PROTEIN

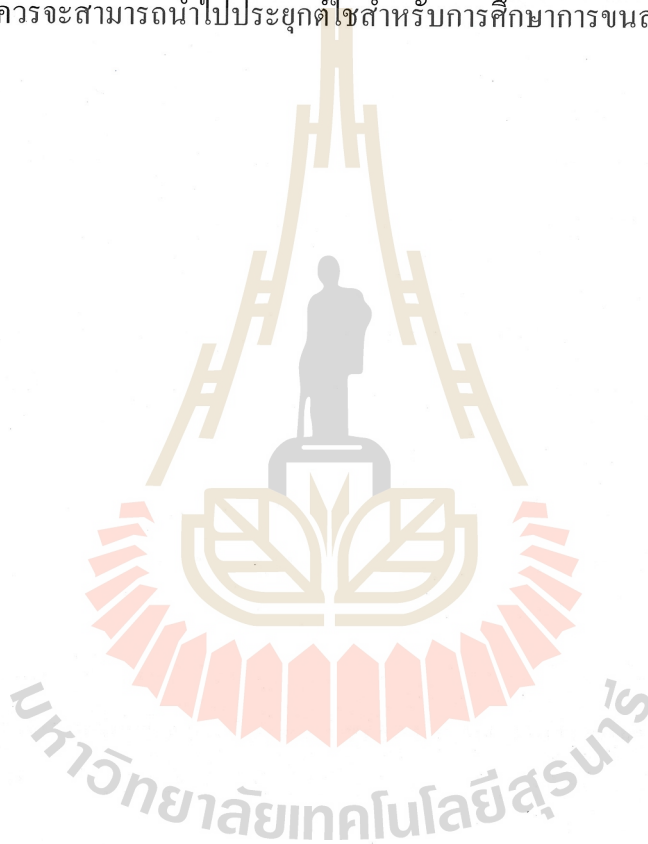
CHANNEL IN *E. COLI* : SINGLE MOLECULE DYNAMICS)

อาจารย์ที่ปรึกษา : ผู้ช่วยศาสตราจารย์ ดร.ไมเคิล เอฟ สมิธ, 92 หน้า

ช่องโปรตีน/ ความน่าจะเป็นของการส่งผ่าน/ ไซโตพอริน/ การวิเคราะห์ช่องโปรตีนเดี่ยว

ช่องโปรตีนที่ฝังอยู่ที่เยื่อหุ้มชั้นนอกของเซลล์แบคทีเรียมีหน้าที่ในการขนส่งสาร เช่น น้ำตาล ระหว่างภายในเซลล์และภายนอกเซลล์ ถ้าหากบริเวณโดยรอบไม่มีน้ำตาลกลูโคส แบคทีเรีย *E. coli* จะใช้น้ำตาลทางเลือกแทน ซึ่งยื่นแฝงที่เกี่ยวข้องกับพัฒนาการของช่องโปรตีนที่มีความจำเพาะต่อน้ำตาลโคติน (น้ำตาลทางเลือกของกลูโคส) ที่เรียกว่า ช่องพอริน *EcChiP* จะแสดงออกในสถานการณ์นี้ ในวิทยานิพนธ์นี้ได้ทำการศึกษาช่องโปรตีนดังกล่าวซึ่งเป็นช่องโปรตีนที่พบได้น้อยมากในธรรมชาติ ซึ่งได้ทำการศึกษาเฉพาะการขนส่งของน้ำตาลผ่านช่องโปรตีนใช้เทคนิค Single channel current measurement เท่านั้น สำหรับเทคนิคนี้กระแสไอออนขนาดเล็กที่ไหลผ่านช่องโปรตีนจะถูกตรวจวัดอย่างต่อเนื่อง ซึ่งสัญญาณของกระแสไอออนจะมีการเปลี่ยนแปลงแบบฉับพลันทุกครั้ง ช่องโปรตีนมีการเข้าออกของน้ำตาลโมเลกุลใหญ่ โดยที่โมเลกุลน้ำตาลที่ถูกกักในช่องโปรตีนจะขัดขวางการเคลื่อนที่ของไอออนไม่ให้ผ่านช่องและเมื่อน้ำตาลออกจากช่องโปรตีนไอออนก็จะสามารถเคลื่อนที่ผ่านช่องไปได้ ทำให้สามารถศึกษาพลวัตของโมเลกุลเดี่ยวในขณะที่น้ำตาลถูกกักในช่องโปรตีนและน้ำตาลหลุดออกจากช่องโปรตีนได้ วัตถุประสงค์ของงานวิจัยชิ้นนี้คือเพื่อพัฒนาวิธีการศึกษาช่องโปรตีนด้วยเทคนิค Single channel current measurement ให้มีความสมบูรณ์มากยิ่งขึ้นโดยมีค่าความน่าจะเป็นที่ช่องโปรตีนขนส่งน้ำตาลไปยังฝั่งตรงข้ามได้สำเร็จรวมอยู่ด้วย ศึกษาสมบัติเฉพาะของช่องพอริน *EcChiP* จากข้อมูลของสัญญาณกระแสไอออนผ่านช่องโปรตีนเดี่ยวและพัฒนาโมเดลอย่างง่ายเพื่อที่จะสามารถนำไปประยุกต์ใช้กับระบบที่คล้ายคลึงกันได้ในงานวิจัยชิ้นนี้ได้วิเคราะห์ข้อมูลของสัญญาณกระแสไอออนผ่านช่องโปรตีนเดี่ยวผลปรากฏว่าอัตราการดักจับโมเลกุลของน้ำตาลไม่ขึ้นกับเวลา อัตราดังกล่าวนี้เกี่ยวข้องกับการเปลี่ยนแปลงจากช่องโปรตีนว่างไปสู่สถานะที่มีน้ำตาลอยู่ในช่องโปรตีน และอัตราการหลุดออกของโมเลกุลน้ำตาลซึ่งเกี่ยวข้องกับการเปลี่ยนแปลงจากช่องโปรตีนที่มีการดักจับน้ำตาลไปสู่สถานะที่ช่องโปรตีนว่างมีการเปลี่ยนแปลงตามเวลาซึ่งแสดงให้เห็นว่าการดักจับโมเลกุลน้ำตาลของช่องโปรตีนมีหลายรูปแบบ ในการศึกษาครั้งนี้ได้อธิบายพฤติกรรมของการดักจับโมเลกุลภายในช่องโปรตีนโดยการพัฒนาโมเดลอย่างง่ายโดยให้โมเลกุลน้ำตาลมีการเคลื่อนที่แบบสุ่มภายในช่องโปรตีนในรูปแบบใดรูปแบบหนึ่ง ใช้การศึกษานี้เสนอวิธีการประมาณหาค่าความน่าจะเป็นของเหตุการณ์ที่

ช่องโปรตีนดักจับน้ำตาลจะเป็นเหตุการณ์ที่ช่องโปรตีนสามารถขนส่งน้ำตาลไปยังฝั่งตรงข้ามได้ ความน่าจะเป็นนี้ไม่สามารถวัดค่าได้โดยตรง แต่ก็ยังเป็นคุณสมบัติสำคัญของช่องโปรตีนที่มีประสิทธิภาพ นอกจากนี้ได้วิเคราะห์ผลการทดลองที่ใช้โคโคซานแบบมีประจุซึ่งโมเลกุลมีความคล้ายคลึงกับน้ำตาลโคโคซานแต่ตอบสนองต่อความต่างศักย์ไฟฟ้าภายนอกเพิ่มเติมเพื่อสนับสนุนคำอธิบายและวิธีการประมาณค่าความน่าจะเป็นที่ได้เสนอนี้ แบบจำลองการเคลื่อนที่แบบสุ่มอย่างง่ายสามารถอธิบายผลการทดลองและทำให้เกิดความเข้าใจเกี่ยวกับกระบวนการที่น้ำตาลผ่านช่องโปรตีน ซึ่งวิธีศึกษาและวิธีการประมาณค่าความน่าจะเป็นของการขนส่งน้ำตาลผ่านช่องโปรตีนที่ได้เสนอนี้ควรจะสามารถนำไปประยุกต์ใช้สำหรับการศึกษาการขนส่งน้ำตาลผ่านช่องโปรตีนอื่น ๆ ได้



สาขาวิชาฟิสิกส์
ปีการศึกษา 2561

ลายมือชื่อนักศึกษา

วิรัชกร

ลายมือชื่ออาจารย์ที่ปรึกษา

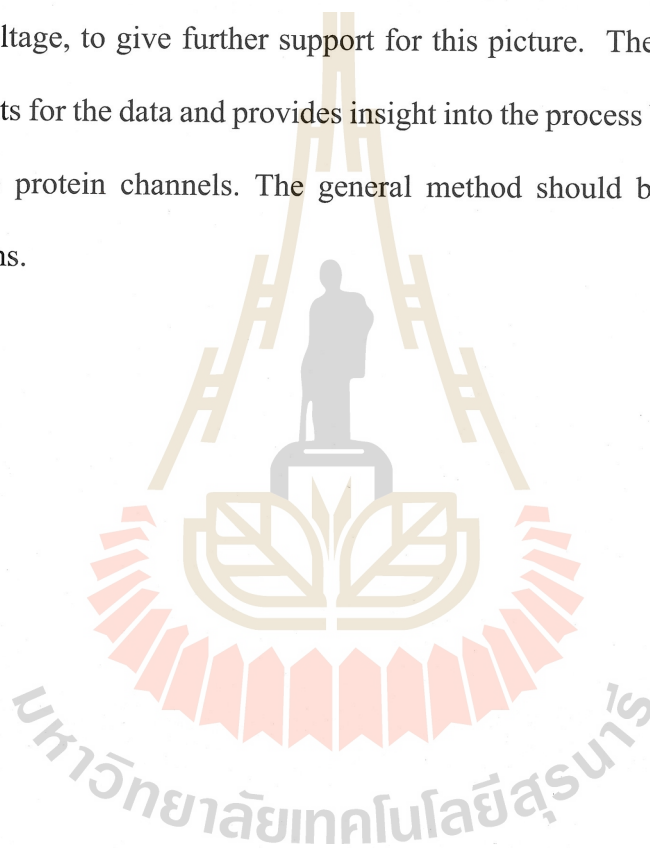
ก. 7. ๕

WATCHARAPORN MOONSAP : SUGAR TRANSLOCATION BY AN
UNEXPRESSED PROTEIN CHANNEL IN *E. COLI* : SINGLE MOLECULE
DYNAMICS. THESIS ADVISOR : ASST. PROF. MICHAEL F. SMITH,
Ph.D. 92 PP.

PROTEIN CHANNEL/TRANSLOCATION PROBABILITY
/CHITOPORIN/SINGLE CHANNEL CURRENT MEASUREMENT

The protein channels buried in outer membrane of bacteria are employed to translocate a substrate, like sugar, between the inside and outside of the cell. If the environment lacks glucose then *E. coli* bacteria must exploit an alternative sugar. A silent gene, relevant to the development of a channel that is specific to chitosugars (an alternative to glucose), called *EcChiP* is expressed in this situation. We are studying this particular protein channel, rarely found in nature. Particularly, we study sugar permeation through the protein channel using the single channel current measurement. With this technique, a small-ion current through the channel is monitored and abrupt changes in current are seen every time a large sugar molecule enters the channel, blocking the ions, or exits it. The dynamics of single sugar molecules, as they are trapped and escape from the channel, are thus seen. The purposes of this study are , with the sugar translocation probability, to develop a method for using single channel current measurements to study the protein channel more completely, to characterize the properties of *EcChiP* by using the channel current data and to develop simple models for sugar translocation in this and similar system. The data reveal that the trapping rate is independent of time. The de-trapping rate is time dependent, revealing that there are multiple different configurations for a trapped molecule. We explain the behavior by

developing a simple model in which molecules are trapped in one of multiple states in the channel through which they perform random walks. We use this to propose a method for estimating the probability that a sugar molecule translocates through the channel, as opposed to escaping backwards to the side from which it came. This probability cannot be measured directly, but is a key property for an effective channel. We use results on charged chitosan molecules, similar to chitosugars but responsive to an applied voltage, to give further support for this picture. The simple random walk model accounts for the data and provides insight into the process by which sugar passes through these protein channels. The general method should be applicable to other similar systems.



School of Physics

Student's Signature

Academic Year 2018

Advisor's Signature

ACKNOWLEDGEMENTS

This thesis could not complete without these people and organizations. First, I am grateful to my advisor, Asst. Prof. Dr. Michael F. Smith, for support and suggestion with kindness through his knowledge and experience. I appreciate to our collaborators, Prof. Dr. Wipa Suginta and Dr. H. Sasimali M. Soysa for providing me with all of the needed experimental data and information in Biochemistry. I would like to thank the thesis committee for the reviews and guidance. I would like to acknowledge the Institute for the Promotion of Teaching Science and Technology (IPST) for the DPST Scholarship (Development and Promotion of Science and Technology Talents Project) during my master degree program. I would like to thank Mrs. Phenkhae Petchmai and all staffs at the School of Physics, Suranaree University of Technology for their support and help in all problems about the documents. I would like to thank all members of Biophysics group and of the School of Physics who have given me good friendship and help. I would like to thank my lovely friends who have been beside me and helped me in many problems, Mr. Kittipong Wangnok, Mr. Adithep Butraburi, Miss Natthagrittha Nakhonthong and Mr. Kummarin Paiboon. I would like to thank many people whom I do not mention here but they helped me, gave me inspiration and they were in some parts of my life during my study in master degree program. Last but not least, I would like to give special thank to my family members who always support me and stand by my side.

Watcharaporn Moonsap

CONTENTS

	Page
ABSTRACT IN THAI	I
ABSTRACT IN ENGLISH	III
ACKNOWLEDGEMENTS	V
CONTENTS	VI
LIST OF FIGURES	IX
LIST OF ABBREVIATIONS	XII
CHAPTER	
I INTRODUCTION	1
1.1 Overview	1
1.2 The previous studies of sugar translocation through trimeric protein Channel	5
1.3 Properties of monomeric protein channel: <i>EcChiP</i>	7
1.4 The single channel current measurements	8
1.5 Research objectives	10
II THEORY	12
2.1 The trapping and de-trapping functions for trimeric protein channel	12
2.2 The effect of electric field on charged molecule translocation	15
2.3 The Arrhenius law for chitosugar translocation	18
2.4 Random walk theory	22

CONTENTS (Continued)

	Page
III THE PROBABILITY OF TRANSLOCATION	26
3.1 Experimental detection methods	26
3.1.1 Event detection methods	26
3.1.2 Data analysis	29
3.1.3 Probability estimation	31
3.1.3.1 Events and possible interpretation for non-linear behavior of $B(t)$	31
3.1.3.2 Find the equation for translocation probability estimation from $B(t)$ function of long-time events	35
3.2 Model of intramonomer dynamics	36
IV RESULTS AND DISCUSSIONS	38
4.1 Trapping and de-trapping of sugar by chitoporin	38
4.2 Voltage-dependent trapping of charged chitosan	44
4.2.1 The trapping function of charged chitosan	44
4.2.2 The de-trapping function of charged chitosan	46
4.3 The random walk model of intramonomer dynamics	49
4.4 The comparison of the translocation probability from different chitosugars	56
4.4.1 The comparisons of average residence time and trapping rate in different channel samples and different length of sugar molecule.....	56

CONTENTS (Continued)

	Page
4.4.2 The comparison of translocation probability in different channel samples and different length of sugar molecule	59
4.5 Voltage-dependent trapping dynamics for neutral chitohexaose	61
4.6 Discussion	67
V CONCLUSION	70
REFERENCES	73
APPENDIX	79
CURRICULUM VITAE	92

LIST OF FIGURES

Figure	Page
1.1	Simple model of substrate translocation through outer membrane protein channel of gram-negative bacteria 5
1.2	Current signal of <i>EcChiP</i> when applied voltage of 100 mV was applied with sugar addition on <i>cis</i> side 8
1.3	Experimental configuration of black lipid membrane technique and the single channel current measurements 9
1.4	Current signal along the time of experiment of the single channel current measurement of monomeric channel with applied voltage $V = -100$ mV 11
2.1	The experimental results of trapping and de-trapping for chitohexaose translocation through chitoporin channel 15
2.2	Simple model of cationic molecule moving in electric field 17
2.3	A random walk model in one dimension 22
2.4	A random walk model of a protein channel with N trapping sites $\alpha = 0, 1, 2, \dots, N - 1$ from <i>cis</i> to <i>trans</i> sides 24
3.1	Ion current transition from level 1 (closed channel) to level 0 (open channel) occurs for 0.1 ms 28
3.2	Event detection of the experiment data where 40 μ M of chitohexaose inserted in <i>cis</i> chamber at applied voltage of -100mV by pCLAMP v.10.6 software 28

LIST OF FIGURES (Continued)

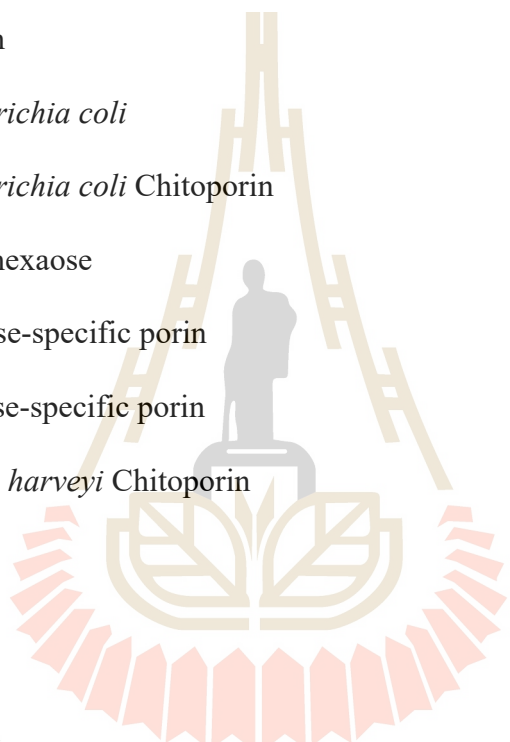
Figure	Page
3.3	The current signal of the experiment data where 100 μM of chitohexaose inserted in <i>cis</i> chamber at applied voltage of -100 mV on pCLAMP v.10.6 software 30
3.4	The relation between $B(t)$ and time t from the experiment results 32
3.5	Possible interpretation for non-linear behavior of $B(t)$ 33
4.1	The linear trapping function $U(t)$ versus time t with $[c]= 1.25, 5, 10, 20, 40$ and $80 \mu\text{M}$ chitohexaose and $V = -100 \text{ mV}$ 41
4.2	The trapping rate $k_{\text{on}}[c]$ derived from $U(t)$ function in figure 4.1 41
4.3	The non-linear de-trapping function $B(t)$ versus time t with $[c]= 1.25, 5, 10, 20, 40$ and $80 \mu\text{M}$ chitohexaose and $V = -100 \text{ mV}$ 43
4.4	The de-trapping function $B(t)$ versus time t with the artificial linear lines for small-time events (line 1) and long-time events (line 2) 43
4.5	The trapping function $U(t)$ versus time t with varying applied voltage $ V = 50, 75, 100$ and 125 mV 45
4.6	The de-trapping function $B(t)$ versus time t with varying applied voltage $ V = 50, 75, 100$ and 125 mV 46
4.7	The translocation probability in various V 48
4.8	The calculations of $B(\tau)$ and $P_T(\tau)$ for $N = 20$ trapping sites 52
4.9	The calculations of P_T (dash lines) and \tilde{P}_T (solid lines) varied with the wedge steepness for an asymmetric wedge potential 55

LIST OF FIGURES (Continued)

Figure	Page
4.10	The inverse of the average time that the channel remains blocked versus the wedge steepness for an asymmetric wedge potential 55
4.11	The average residence time τ_c in different channel samples and in various sugar concentration $[c]$ 57
4.12	The trapping function $U(t)$ from three channel samples with adding 10 μM chitohexaose on <i>cis</i> chamber 57
4.13	The trapping rate $k_{\text{on}}[c]$ in different channel samples and in various sugar concentration $[c]$ 58
4.14	The de-trapping function $B(t)$ versus time t with chitohexaose and chitopentaose addition on <i>cis</i> chamber 60
4.15	The de-trapping function $B(t)$ versus time t with 10 μM chitohexaose addition in three channel samples 60
4.16	The trapping rate $k_{\text{on}}[c]$ versus V 62
4.17	The average residence time τ_c versus V 62
4.18	The de-trapping function $B(t)$ versus time t with 5 μM chitohexaose when $ V = 25, 50, 75, 100, 125$ and 150 mV 64
4.19	The translocation probability \tilde{P}_T versus V 65
4.20	The average current I_0 when an <i>EcChiP</i> channel is unblocked versus applied voltage V 66

LIST OF ABBREVIATIONS

°C	Degree Celsius
ChiP	Chitoporin
Da	Dalton
<i>E. coli</i>	<i>Escherichia coli</i>
<i>EcChiP</i>	<i>Escherichia coli</i> Chitoporin
GlcNAc ₆	Chitohexaose
LamB	Maltose-specific porin
ScrY	Sucrose-specific porin
<i>VhChiP</i>	<i>Vibrio harveyi</i> Chitoporin



มหาวิทยาลัยเทคโนโลยีสุรนารี

CHAPTER I

INTRODUCTION

1.1 Overview

The protein channels embedded in a cell membrane are employed as gates to transport substances between the inside and outside of the cell. In gram-negative bacteria, the membrane is a lipid bilayer membrane. Some protein channels are designed to transport sugar molecules across this membrane (Nikaido, 1993). Studies of sugar transport by outer membrane protein channels can help elucidate the basic properties of the channels and, further, be applied to develop antibiotics (Nikaido, 2003; Richter *et al.*, 2017). For this reason, these studies have been carried out by scientists for decades (Nikaido, 2003). Some examples of topics relevant to this thesis are studies of sugar transport through the protein channel maltoporin (LamB) in *Escherichia coli* bacteria (Benz *et al.*, 1987; Nikaido, 2003), a related channel chitoporin (ChiP) in marine bacteria (Keyhani *et al.*, 2000; Suginta *et al.*, 2013a). Both channels are sugar-specific, i.e. they are designed to transport a particular sugar molecule (Nikaido, 2003). Both channels are also composed of three identical monomers, which act in parallel to transport sugar. When one tries to understand basic properties of such channels, interference between monomers makes it hard to characterize the properties of a single monomer (Schirmer *et al.*, 1995; Dutzler *et al.*, 1996; Wang *et al.*, 1997; Watanabe *et al.*, 1997; Winterhalter, 2001; Hilty and Winterhalter, 2001; Im and Roux, 2002; Suginta and Smith, 2013; Suginta *et al.*, 2016).

Recently, a novel channel (so-called *EcChiP*) has been found in *Escherichia coli* (Mizuno *et al.*, 1984; Guillier *et al.*, 2006; Vogel and Papenfort, 2006). The gene for this channel is normally not expressed. It is a ‘silent’ gene that does not effect the organism. However, if *E. coli* are in the environment that lacks maltodextrin, but instead contains chitooligosaccharides, the silent gene will be expressed (Rasmussen *et al.*, 2009). The result of this gene expression is that the bacteria can access the available nutritional source. The channel is found in *E. coli*, like LamB, but is specific to chitooligosaccharides, making it similar to the ChiP found in marine bacteria. Significantly, it is monomeric channel and forms stable pores in artificial phospholipid membranes (Soysa and Suginta, 2016). Thus, the *EcChiP* channel provides a good opportunity to study the dynamics of sugar transportation and to understand the detailed properties of the channel without inter-monomer interference problems.

In typical studies of sugar transport through a channel, quantities of great interest include the binding constant (deriving from the ratio of on-rate constant and off-rate constant) which indicates the affinity between channel and sugar molecules, the conductance of the channel (obtained from the slope of ion current – applied voltage curve) which is the ability for ion to flow in the channel and others. (Anderson *et al.*, 1995; Hilty and Winterhalter, 2001; Schwarz *et al.*, 2003; Suginta *et al.*, 2013a; Suginta *et al.*, 2013b; Soysa and Suginta, 2016). An important figure of merit for sugar translocation, which is a function of several of these quantities, is the average number of sugar molecules translocated by the channel per second Q_T , which is given by

$$Q_T = \frac{k_{on}[c]}{(1+K)} P_T \quad (1.1)$$

where $K = k_{on}[c]\tau_c$ and $k_{on}[c]$ is the concentration-dependent rate of open-channel events (i.e. the rate at which an empty channel becomes blocked); τ_c is referred to as

the residence time (i.e. the average time that a given channel remains blocked before becoming open again); P_T is the probability of translocation (i.e. the probability that the channel becomes unblocked as a result of sugar molecules proceeding through the membrane from one side to the other). In deriving equation 1.1, one assumes that at most one sugar molecule can occupy the channel at a given time. From the single channel current measurements, described below, we can obtain $k_{on}[c]$ and τ_c directly from the experiments. The number of closed-channel events per second can be counted. This number includes the backwards escape events (sugar molecules move back to the initial side after blocking the channel) and translocation events (sugar molecules move to another side after blocking the channel), but we cannot distinguish these two events since we cannot see, from the data, to which side sugar molecules move upon exiting the channel. For this reason, we cannot obtain P_T directly from the experiments. The determination of Q_T cannot be completed unless we can find some way to estimate P_T .

In previous studies, the researchers have considered the problem of finding the direction sugar molecules escape. For example, in 2003, Schwarz and co-workers claimed to determine the translocation rate successfully in the study of maltodextrin translocation through maltoporin channels (Schwarz *et al.*, 2003). Their estimation was achieved in a trimeric channel study, complicating its theoretical interpretation and obtained from another type of measurement—electrical conductance measurements including current noise analysis. In 2008, to study polyelectrolyte transport through a protein channel in which molecules be charged, the researchers assume that short-time events (in which the channel is briefly blocked) and long-time events (in which the channel remains blocked much longer) are backwards escape and translocation events, respectively (Brun *et al.*, 2008). Our analysis below will lead to a similar conclusion

for sugar molecules and go further in trying to quantify which events are, indeed, translocation. Our study analyzes neutral molecule data and attempts to find a better estimation of Q_T .

In our study, we characterize properties of a specific system, the chitoporin in *E. coli* called *EcChiP*, with regard to sugar translocation and find a way to estimate P_T from the single channel current measurement. (The single channel current measurement is a widely-used technique in the study of substrate transport through protein channels.) The method of translocation probability estimation begins with the consideration that short-time closed-channel events should be backwards escape events and long-time closed-channel events can be either backwards escape or translocation events. In trying to understand the data, we develop a model that assume sugar molecules undergo a one-dimensional random walk through the *EcChiP* channel. Those that just entered the channel, on one end of the random walk, can only escape backwards. Since the model is so simple, it is not specific to this particular system and thus may prove useful in understanding transport more generally.

This thesis report begins with chapter I which consists of an overview, background knowledge in biochemistry/biophysics and research objectives. Chapter II develops the theories which are relevant to our analysis and discussion. In chapter III: the procedure to estimate the probability of translocation is proposed and the model of intramonomer dynamics is presented. Chapter IV gives results and discussion, and chapter V is a conclusion.

1.2 The previous studies of sugar translocation through trimeric protein channel

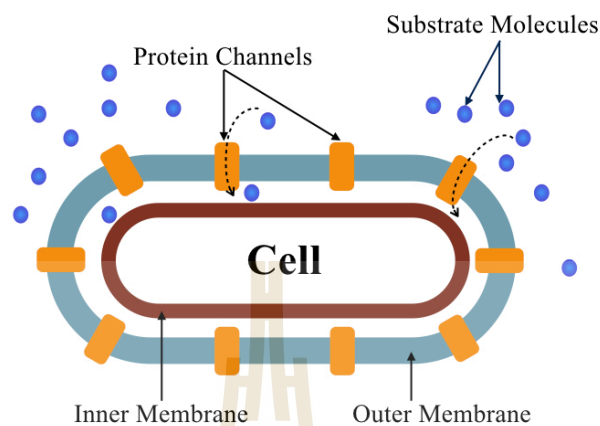


Figure 1.1 Simple model of substrate translocation through outer membrane protein channel of gram-negative bacteria.

Substrate exchange between the environment and the cells of gram-negative bacteria mostly takes place through protein channels embedded in the outer membrane as shown in figure 1.1 (Nikaido, 1993). These channels can be classified as either nonspecific channels or specific channels. Nonspecific channel allows the diffusion of ions and small nutrient molecules while specific channels have specific binding sites that bond certain targeted molecules (Nikaido, 2003). In our study, only specific channels are considered.

Many previous studies of specific channels focus on trimeric channels such as maltoporin (LamB) of *Escherichia coli* which is specific to maltooligosaccharide, chitoporin of *Vibrio harveyi* which is specific to chitooligosaccharide, ScrY of *Salmonella typhimurium* which is specific to sucrose and OprB of *Pseudomonas putida* which is specific to glucose (Anderson *et al.*, 1995; Anderson *et al.*, 1998; Nikaido,

2003; Saravolac, 1991; Schirmer, 1998; Schülein *et al.*, 1991; Suginta *et al.*, 2013b). In these studies, the scientists are interested in, for example, the sugar binding constant, flux through one channel and rate constant which are relevant to the efficiency of substrate translocation through the protein channel (Anderson *et al.*, 1995; Hilty and Winterhalter, 2001; Nikaido, 2003; Schwarz *et al.*, 2003; Suginta *et al.*, 2013a; Soysa and Suginta, 2016). Many of these studies used experimental methods in biochemistry that are difficult for us, from a simplistic modeling perspective, to interpret. Nonetheless, we include them here for completeness. The examples of the experimental techniques in these methods are noise analysis, liposome swelling assay and single-channel current measurement (Anderson *et al.*, 1995; Anderson *et al.*, 1998; Kullman, 2006; Suginta and Smith, 2013; Suginta *et al.*, 2013a; Szelcman, 1975). The noise analysis and single-channel current measurement provides, for example, sugar binding constant, rate constant, the mean time of closed-channel events while liposome swelling assay provides the quality of sugar translocation which identify the specificity of channel (Anderson *et al.*, 1998; Suginta *et al.*, 2013a; Szelcman, 1975). In our study, we focus on single-channel current measurement which is widely used and convenient for the study of sugar translocation.

The average number of sugar molecules translocated through the channel per second Q_T may be used for identifying the effectiveness of sugar translocation. As mentioned above, this quantity cannot be obtained directly from experiment because the probability of translocation is not measured. To obtain Q_T , one must go beyond direct experimental information and attempt to infer the translocation probability using theoretical considerations. Towards this end, it is convenient to study the simplest possible system. The single-channel current data made for a monomeric channel, which

is not susceptible to the intermonomer correlations that affect the current data for a trimeric channel, is thus advantageous.

1.3 Properties of monomeric protein channel: *EcChiP*

The monomeric channel on which we focus our study is the novel monomeric channel in *Escherichia coli* called *EcChiP*. This channel was found to rapidly form stably in artificial membranes and found to be a monomer. An apparent native molecular weight of *EcChiP* is about 50 kDa. Moreover, it was found that *EcChiP* slightly prefers cations and it was found that all molecules with size of 200-300 Da can freely pass through this channel. For the long-chain sugars such as chitooligosaccharides and maltooligosaccharides, the difficulty in permeation of these sugars through *EcChiP* depends on the specificity of this channel to sugars. *EcChiP* is specific to chitooligosaccharides like ChiP found in marine bacteria such as *Vibrio harveyi* but not specific to maltoligosaccharides. This can be seen from the fact that no closed-channel events are observed in the current signal for the single channel current measurement of maltoligosaccharides while two distinct current levels, the lower current being the closed channel event, are clear in measurements of long-chain chitooligosaccharides as shown in figure 1.2 (Soysa and Suginta, 2016).

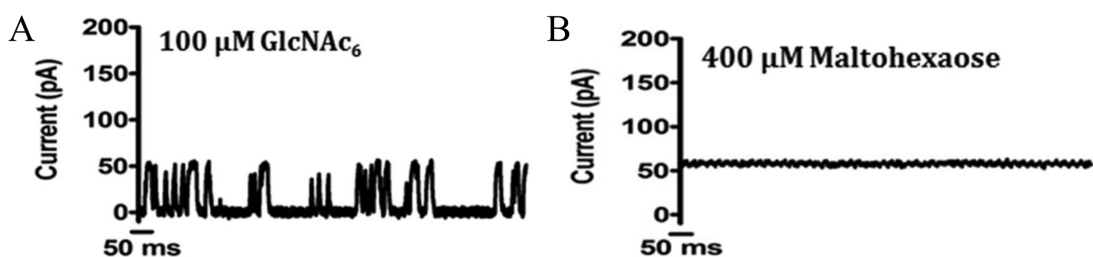


Figure 1.2 Current signal of *EcChiP* when applied voltage of 100 mV was applied with sugar addition on *cis* side. (A) 100 μM of GlcNAc₆ (long-chain chitooligosaccharide) was added on *cis* side. (A) 100 μM of Maltohexaose was added on *cis* side. (Soysa and Suginta, 2016)

1.4 The single channel current measurements

In the single channel current measurements, the sugar trapping by the outer membrane protein channels such as *VhChiP* (trimeric channel in *Vibrio harveyi*) and *EcChiP* (Soysa and Suginta, 2016; Suginta and Smith, 2013; Suginta *et al.*, 2016) were studied by using an artificial membrane from black lipid membrane (BLM) technique and the single channel current measurements.

In this study, the black lipid membrane experiments and the single channel current measurements were achieved by the same methods as seen in Soysa's research paper (Soysa and Suginta, 2016). The small glass box was separated by two chambers by a 25 μm -thick Teflon barrier with a circular aperture 60-100 μm in diameter as shown in figure 1.3. The chambers contained an electrolyte solution, 1 M KCl in 20 mM HEPES pH 7.4, and the voltage was applied to either side and the ion current detected by using Ag/AgCl electrodes where one was connected to the *cis* side of the membrane (ground) and the other was connected to the headstage of the Axopatch 200B amplifier (Axon Instruments, Foster City, CA) on the *trans* side. Black lipid membrane (BLM)

reconstitution were carried out in the electrolyte at room temperature (25°C). Solvent-free bilayer (Montal-Mueller type) formation was performed using 5 mg/mL 1,2-diphytanoyl-sn-glycero-3-phosphatidylcholine (DPhPC; Avanti Polar Lipids, Alabaster, AL) in n-pentane across the aperture by lowering and raising the liquid level. Once the bilayer forms, the observed current is negligible: ions cannot significantly permeate the membrane. After a bilayer has been formed, *EcChiP* was added to the *cis* side of membrane with a potential ± 100 mV and an ion current was observed. A single channel had opened in the membrane—and the *EcChiP* was removed before further channels could form.

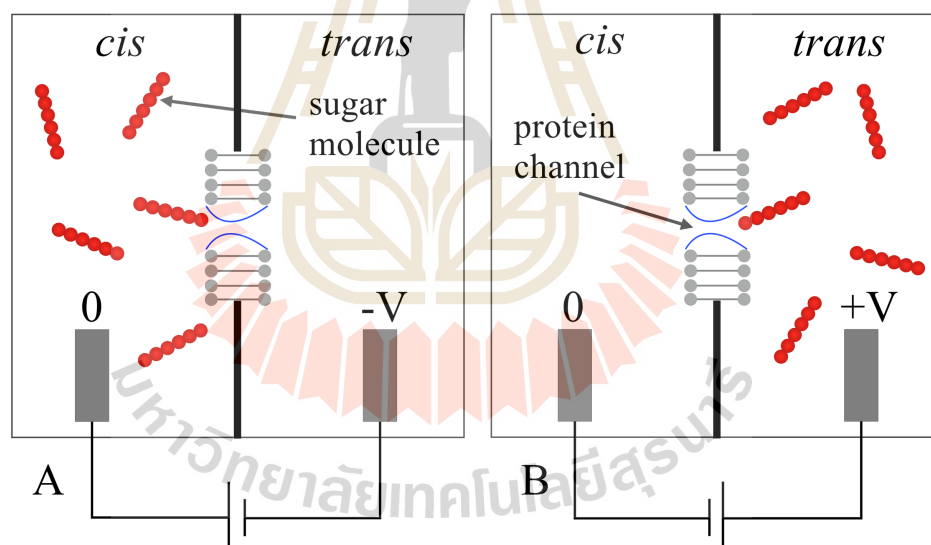


Figure 1.3 Experimental configuration of black lipid membrane technique and the single channel current measurements. (A) Sugar molecules (red 6-circle chains) were added on *cis* side with applied voltage of negative V . Current flows from *cis* side to *trans* side. (B) Sugar molecules were added on *trans* side with applied voltage of positive V . Current flows from *trans* side to *cis* side (Suginta *et al.*, 2016).

The ion current, with the channel open, is given by I_0 as shown in figure 1.4. After sugar solution had been introduced into one chamber, the ion current decreased when the channel was blocked by a sugar molecule. For a monomeric channel, the observed current is either equal to I_0 (when the channel is open) or has a value I_1 that is difficult, in this experimental setup, to distinguish from zero. Evidently, a sugar molecule blocks the ionic current from passing through the channel. For a trimer, with 3 monomers conducting current in parallel, the observed current levels are $I(t) \approx I_n = (3 - n)I_0/3$ with I_3 close to zero where $n=0, 1, 2$ and 3 is the number of trimmers blocked by sugar molecules (Suginta *et al.*, 2016). The ion current signals over 2 minutes were recorded and analyzed by pCLAMP v.10.6 software. This software provides the important data, such as time of each event which the channel is closed or open, the total number of events, the concentration-dependent rate of open-channel events $k_{on}[c]$, average value of current in each level $\langle I_n \rangle$ and mean time of events (τ_{open} , τ_{closed} or τ_c), but does not provide the direct information that classifies events between backwards escape events and translocation events.

1.5 Research objectives

- 1) Develop a method for using single channel current measurements to fully characterize the protein channel, including the sugar translocation probability P_T .
- 2) Construct a simple, general model of sugar transport through protein channels.
- 3) Apply this model to understand a specific channel system: the chitoporin in *E. coli*, called *EcChiP*, which is controlled by a silent gene.

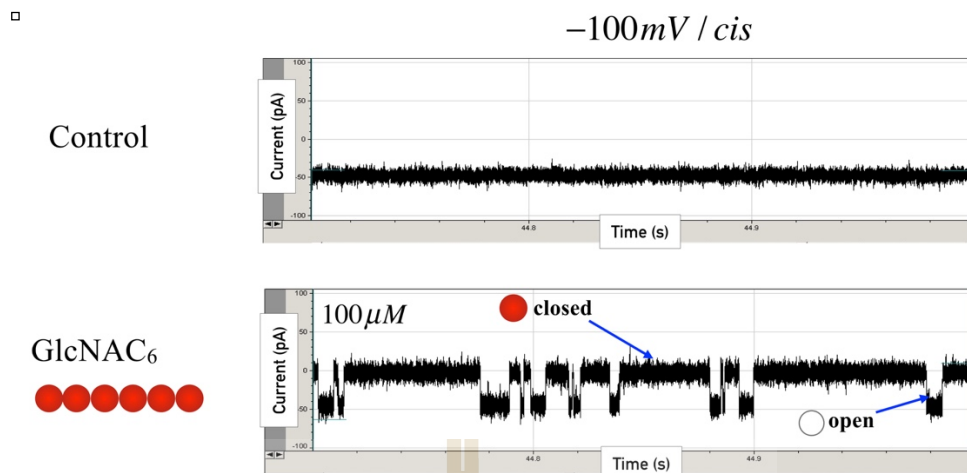


Figure 1.4 Current signal along the time of experiment of the single channel current measurement of monomeric channel with applied voltage $V = -100$ mV. (upper panel) If no sugar is introduced to either chambers then $I(t) \approx I_0 \approx -50$ pA. (lower panel) $100 \mu\text{M}$ of chitohexaose was added into *cis* chamber then $I(t) \approx I_0 \approx -50$ pA when channel was open and $I(t) \approx I_1 \approx 0$ pA when channel was closed.

CHAPTER II

THEORY

In this chapter, relevant theoretical concepts, used the analysis and discussion that follows, are presented. We begin by introducing a trapping function and a de-trapping function. These functions are related to the probability that a channel remains open (this is the trapping function) or closed (the de-trapping function) for a time greater than t . Other theoretical concepts include the effect of electric field on charged molecule translocation through a channel and the well-known Arrhenius law for chitosugar translocation. We also discuss random walk theory.

2.1 The trapping and de-trapping functions for trimeric protein channel

In the studies of *VhChiP* in 2013 and 2016 (Suginta and Smith, 2013; Suginta *et al.*, 2016), the channel consists of three identical monomers. The single-channel current measurements show that the current fluctuates among four levels $I_n = \frac{(3-n)I_0}{3}$, where $I(t) \approx I_n$ with $n = 0, 1, 2,$ or 3 . A current I_n is observed every time n of the three monomers are blocked by a sugar molecule. We keep track of each I_n event, i.e. we measure the time the current remains continuously near I_n for measurable duration. (We say *near* I_n because the instantaneous current $I(t)$ fluctuates rapidly, but remains within a band centered on I_n while the event persists.) Suppose that the j th such event

lasts for a time $t[j]_n$. The average duration over these events is $\tau_n = \langle t[j]_n \rangle$ and the standard deviation of the current during such events is $\sigma_n = \sqrt{\langle t^2[j] \rangle_n - (\langle t[j] \rangle_n)^2}$. Next, we consider probability $f_n(t)$ that an I_n event lasts longer than time t , which is estimated from the fraction of all observed events lasting this long. The function $f_n(t)$ provides detailed information of trapping statistics. This probability is obtained as $f_n(t) \equiv N_n(t)/N_n(0)$ where $N_n(t)$ is the number of times that the current is observed to remain in level I_n for a duration longer than t , and $N_n(0)$ is the total number times that the current was in level I_n (both $N_n(t)$ and $N_n(0)$ are obtained from the pCLAMP event sequences). The mean residence time τ_n is related to this quantity by

$$\tau_n = \int_0^{\infty} dt t \left(-\frac{df_n}{dt} \right) = \int_0^{\infty} dt f_n(t). \quad (2.1)$$

A current level I_n is observed more than a thousand times over several minutes of measurement. We say that each event begins at time $t = 0$ and stays in level n beyond t with probability $f_n(t)$. The probability decays with t because both trapping process and de-trapping process can terminate an I_n state. The rate equation for this system, for trimeric channel, can be written as

$$\frac{df_n}{dt} = -[3 - n]f_n(t)U'_n(t) - nf_n(t)B'_n(t). \quad (2.2)$$

where $U'_n(t) = dU_n/dt$ is the instantaneous rate at which one of the $3 - n$ unblocked monomer becomes blocked and $B'_n(t) = dB_n/dt$ the instantaneous rate at which one of the n blocked monomers becomes unblocked. If it is assumed that all closed-channel events result from the blockade by sugar molecules then $U'_n(t)$ is a sugar trapping rate of an empty monomer and $B'_n(t)$ a sugar de-trapping rate of an occupied monomer. Integration of equation 2.2 gives

$$\ln f_n(t) = -(3 - n)U_n(t) - nB_n(t). \quad (2.3)$$

The trapping function $U_n(t)$ and de-trapping function $B_n(t)$ are obtained from the $I(t)$ data by counting the number of events $N_{n \rightarrow n \pm 1}(t)$ for each level n and using the fact that $f_{n \rightarrow n \pm 1}(t) = N_{n \rightarrow n \pm 1}(t)/N_n(0)$ where “+” and “-” are for trapping and de-trapping, respectively. The expressions of these functions are written as

$$A_n(t) = \frac{1}{a_n} \int_0^t dt \frac{f'_{n \rightarrow n \pm 1}(t)}{f_n(t)} \quad (2.4)$$

where $A = U$ or B and $a_n = (3 - n)$ or n , for trapping (+) or de-trapping (-), respectively. $U_n(t)$ and $B_n(t)$ functions, which are obtained directly from histograms of data and tend to be smooth, are more convenient than $U'_n(t)$ and $B'_n(t)$, which require numerical differentiation and tend to fluctuate wildly. The sample experimental results of trapping and de-trapping functions for the fluctuation of $I(t)$ between level $n = 0$ and $n = 1$ are shown in figure 2.1 for the translocation of $2.5 \mu\text{M}$ chitohexaose in H_2O and in D_2O solutions through chitoporin channel.

In the case that $U'_n(t)$ and $B'_n(t)$ are independent of n and t , the trapping function is linear in time, $U_n(t) = k_{\text{on}}[c]t$, where k_{on} is a constant trapping rate per monomer in 1 molar sugar concentration, and $B_n(t) = k_{\text{off}}t$ where k_{off} is the de-trapping rate of a blocked monomer (Suginta *et al.*, 2016). As seen in figure 2.1, the graph of $U_{1,0}(t)$ versus t are apparently linear, but the graph of $B_{0,1}(t)$ are non-linear. The latter indicates that k_{off} changes with t , such that monomers that have remained blocked for a long time have a smaller k_{off} .

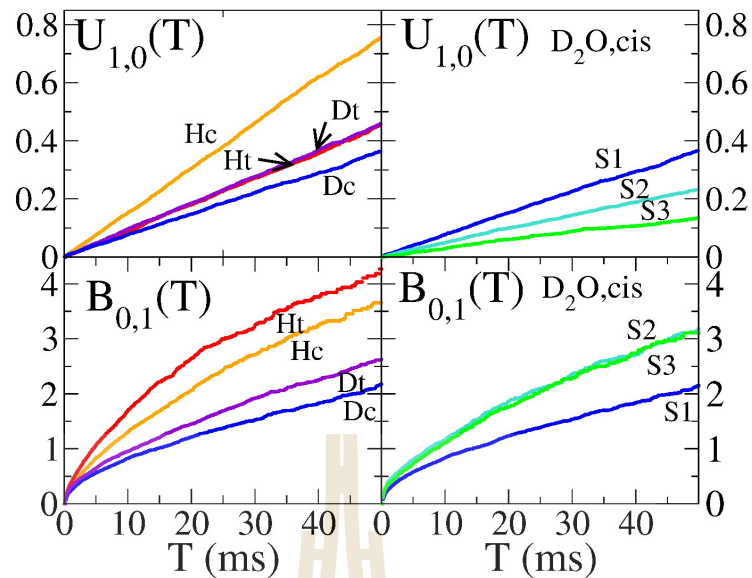


Figure 2.1 The experimental results of trapping and de-trapping functions for chitohexaose translocation through chitoporin channel. The fluctuation of $I(t)$ is between level $n = 0$ and $n = 1$. Given T is time. (left panel) Trapping function $U_{1,0}(T)$ and de-trapping function $B_{0,1}(T)$ obtained in H_2O solution with $2.5 \mu M$ chitohexaose on the *cis* side (Hc) and *trans* side (Ht) of the membrane and in D_2O solution with $2.5 \mu M$ chitohexaose on the *cis* side (Dc) and *trans* side (Dt). (right panel) Trapping function $U_{1,0}(T)$ and de-trapping function $B_{1,0}(T)$ obtained for three different chitoporin channels, i.e. three samples S1, S2, S3, with $2.5 \mu M$ chitohexaose on the *cis* side of the membrane in D_2O solution. (Suginta *et al.*, 2016)

2.2 The effect of electric field on charged molecule translocation

Another phenomenon of interest is charged molecule translocation. Chitosan hexaose is a charged molecule when in low pH solution. Chitosan hexaose is structurally related chitohexaose. Thus, the *EcChiP* can be tricked into thinking it is ingesting chitohexaose sugar when a chitosan hexaose molecule approaches. But the

chitosan hexaose molecules, being charged, can be manipulated with an applied voltage.

The analysis of single-channel current measurements showed that the channel has a high affinity for chitohexaose, but low affinity for chitosan hexaose at neutral pH. At this pH, the chitosan hexose is electrically neutral. However, the chitosan hexaose can be ionized to be cationic charged molecule at pH below 6.7. Thus, we consider the experimental data of chitosan hexaose, done in pH 5.5 solution, in which the chitosan is a cationic molecule.

The single channel current studies of charged molecule translocations help us understand neutral molecule translocation. The probability of translocation for charged molecules depends on voltage, because the electric field pushes the molecule into or away from the channel. Indeed, we can use voltage to control whether the charged molecule is pushed through the channel (translocation) or drawn back out of it (backwards escape).

In the studies of charged molecule translocation, there is an electrolyte solution such as KCl in the chambers. After a voltage has been applied as shown in figure 2.2, ion current flows from the side with higher voltage to the opposite side with lower voltage. The electric force (\vec{F}_i) acting on the charged molecule (i) with the charge q_i in the channel is given by equation 2.5 where \vec{E} is the electric field inside the channel (Gumbart *et al.*, 2012, Suenaga *et al.*, 1998).

$$\vec{F}_i = q_i \vec{E}. \quad (2.5)$$

The study by Gumbart and his team in 2011 demonstrates that constant-field method, which electric field is constant with the position inside the channel and perpendicular to the membrane plane, is a simple and reasonable approach for the explanation of the

membrane potential in molecular dynamics studies of biomolecular system (Gumbart *et al.*, 2011). The electric field is related to the voltage by $\vec{E} = -\vec{\nabla}V$. By assuming that the electric field is constant with the position inside the channel and perpendicular to the membrane plane, the magnitude of electric field changes with applied voltage V as equation 2.6 where a is the length of the channel.

$$|\vec{E}| = V/a . \quad (2.6)$$

Therefore, after the substitution of equation 2.6 into equation 2.5, the magnitude of electric force can be simply calculated by equation 2.7.

$$|\vec{F}| = qV/a . \quad (2.7)$$

A

B

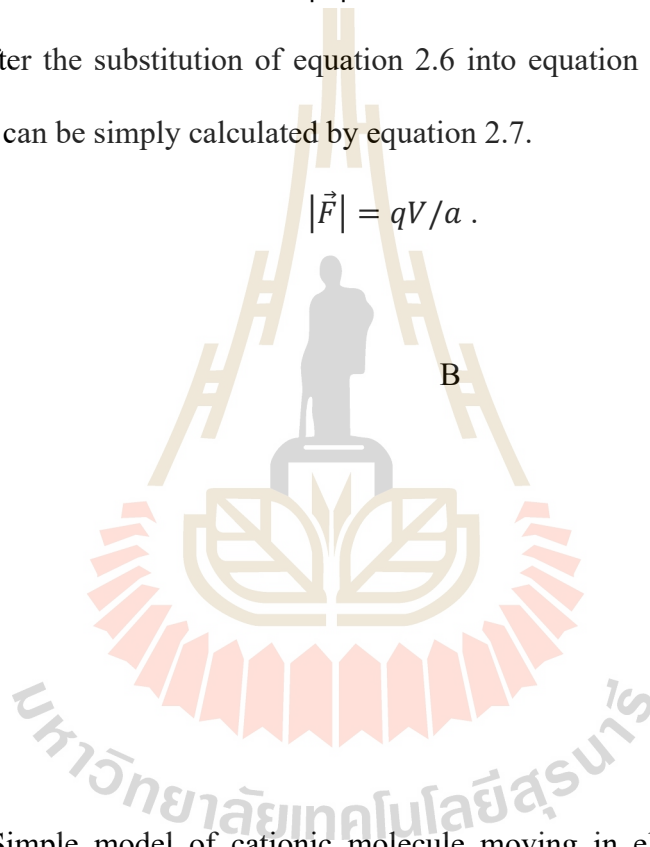


Figure 2.2 Simple model of cationic molecule moving in electric field. (A) The direction of translocation is parallel to electric force acting on cationic molecule. The force drags molecule to the opposite side. (B) The direction of translocation is opposite to electric force acting on cationic molecule. The force prevents molecule from entering the channel.

In case A, sugar molecules are put in the chamber at higher voltage, so the direction that the molecules would move via diffusion is the same as the direction of the electric force. The electric force helps sugar molecule translocation by dragging cationic molecule deeper inside the channel and the probability that the molecule can reach the opposite side increases as shown in figure 2.2A. For example, if voltage on *cis* side is higher than on *trans* side, and sugar molecules are put into *cis* side, then the electric force helps to drag the molecules inside the channel from *cis* side to be deeper to *trans* side. The number of translocation events should increase with the applied voltage.

In case B, if sugar molecules are put into the lower voltage side, the direction of translocation via diffusion is opposite to the direction of electric force. The electric force tries to prevent sugar molecules from entering the channel and, if one manages to enter, pushes them back to the side from which they came, as shown in figure 2.2B.

It is advantageous to be able to use voltage to control the direction of molecular flow in this way. When we compare trapping and de-trapping functions measured for charged molecules to those measured for neutral molecules, we can use the charged case (where we can be confident which way molecules are flowing) to infer what is happening in the neutral case.

2.3 The Arrhenius law for chitosugar translocation

The Arrhenius law gives the rate of a chemical reaction. It assumes there is some energy barrier E_b impeding motion along the reaction coordinate (the reaction coordinate is any convenient quantity that changes when the reaction occurs, but typically is related to an actual position co-ordinate of a molecule that moves during

the reaction). In our case, the change of state from an open to a closed channel proceeds because the sugar molecule enters the channel and becomes bound. To overcome the barrier, the molecule requires thermal energy that is provided, in a stochastic manner, by its surroundings. The probability of receiving a given quantity of energy from its surroundings is proportional to the Boltzmann factor, a function of $k_B T$ where k_B is the Boltzmann constant and T is the temperature. A reaction rate k (units of inverse time or frequency) given by the Arrhenius equation, equation 2.8.

$$k = \nu \exp[-E_b/k_B T] \quad (2.8)$$

where ν is a prefactor with the dimensions of frequency. The prefactor can be conveniently thought of as a natural oscillation frequency for a molecule trapped in a potential well—every time the molecule oscillates it has a chance to overcome the barrier. The exponential factor is the probability that it will be successful. The Arrhenius law is considered below for chitosugar translocation. For the neutral molecule, there is no voltage dependence expected since the neutral particles do not see the electric field.

In our study, chitooligosaccharides, which are neutral, are employed. Surprisingly, the rate of open-channel events ($k_{on}[c]$) and the rate of closed-channel events (k_{off}) in the study of chitohexaose translocations by *EcChiP* by Soysa and co-workers showed a significant voltage dependence (Soysa *et al.*, 2017). The rate depends on applied voltage V in a non-monotonic manner. In their study, the on-rate k_{on} increased with $|V|$ up to 100 mV. For the negative voltage, it remained unchanged from $V = -125$ to -200 mV. At high positive voltages, k_{on} decreased from $V = 125$ mV to 200 mV. In the case of k_{off} , they found that k_{off} increased with $|V|$ from $|V| = 25$ to 100 mV.

We attribute this unexpected voltage-dependence to the dipole character of chitohexaose. The dipole moments may arise due to the existence of the *N*-acetamido (-NHCOCH₃) groups of the multiple GlcNAc units that compose a chitooligosaccharide chain as mentioned in the study of chitooligosaccharide translocation by *VhChiP* (Suginta *et al.*, 2013b).

Since charges are generally not distributed uniformly on various atoms in a molecule, the nonpolar molecule can be polarized by the electric field which leads to induced dipole moment (Jackson, 2006). If the substance consists of nonpolar molecules, the field may induce in each a dipole moment, pointing in the same direction as the field. (If the material is made up of many polar molecules randomly oriented, then the field will cause a torque on each molecule, tending to line them up with the field direction (Griffiths, 1999)). In either case, if the electric field is not too strong, the average polarization is related to the field by

$$\vec{P} = \epsilon_0 \chi \vec{E} \quad (2.9)$$

where χ is the electric susceptibility of the medium which depends on the microscopic structure of the substance, and ϵ_0 is the permittivity of free space.

The external field will polarize the substance and this polarization will produce its own field, which then contributes to the total field; thus, the simplest approach is to begin with the displacement \vec{D} (Griffiths, 1999):

$$\vec{D} = \epsilon_0(1 + \chi)\vec{E}. \quad (2.10)$$

In a dielectric system, the approximate energy per unit volume of the system u_e is

$$u_e \approx \vec{D} \cdot \vec{E} = \epsilon_0(1 + \chi)|\vec{E}|^2. \quad (2.11)$$

For sugar translocation by the protein channel, as mentioned that the electric field can be assumed to be constant with the position inside the channel and perpendicular to the

membrane plane then the magnitude of electric field is $|\vec{E}| \approx V/a$ where a is the length of channel. The electrostatic energy is

$$E \approx u_e \Omega_{\text{eff}} = \varepsilon_0 (1 + \chi) \left(\frac{V}{a}\right)^2 \Omega_{\text{eff}} \quad (2.12)$$

where Ω_{eff} is effective volume. If the polarization of the channel when the channel is open is different from that when the channel is closed, a change in electrostatic energy from closed state to open state will be

$$\Delta E = [\Delta(\chi \Omega_{\text{eff}})] \varepsilon_0 \left(\frac{V}{a}\right)^2. \quad (2.13)$$

Finally, we obtain

$$\Delta E = -\varepsilon_0 \chi_c \left(\frac{V}{a}\right)^2 \Delta \Omega \quad (2.14)$$

where $\Delta \Omega$ is a parameter with the dimension of volume that is used to account for the polarization change occurring when the occupancy of the channel changes (i.e. the sugar molecule comes or goes) and χ_c is the electric susceptibility taken to be the same for both states. (There is some change in the product: $\Delta(\chi \Omega_{\text{eff}}) \approx \chi_c \Delta \Omega$ where we absorbed the change in the susceptibility $\Delta \chi$ into $\Delta \Omega$). Therefore, the Arrhenius equation of the off-rate k_{off} with the change in electrostatic energy ΔE and energy barrier E_b can be written as

$$k_{\text{off}} = \nu \exp[-(E_b - \Delta E)/k_B T]. \quad (2.15)$$

Substitution of equation 2.14 into equation 2.15 gives

$$k_{\text{off}} = B \exp(CV^2/k_B T) \quad (2.16)$$

where B is the zero-voltage rate of open-channel events which is equal to $\nu \exp(-E_b/k_B T)$, and $C = \frac{\varepsilon_0 \chi_c}{a^2} \Delta \Omega$ which is constant with applied voltage. We developed this picture so that it would have a qualitative V -dependence similar to the

experiment. The key point is that the reaction rate depends on V^2 and thus is not sensitive to the sign of the voltage (the direction of the field). We can roughly explain the voltage dependence using this approach.

However, we do not expect quantitative agreement because of the rough estimates made above. For one thing, we think that there are multiple binding states for sugar in the channel, but we developed the Arrhenius equation in equation 2.16 as if there are only two states (closed and open). Indeed, while we are able to account for the voltage dependence of k_{off} , we cannot yet understand the behavior of k_{on} . It is possible that the latter is rate-limited by a different mechanism.

2.4 Random walk theory

A random walk is a mathematical process. For a simple picture of a random walk, suppose that our object is at position $\alpha = 0$ at time $t = 0$ and hops randomly in one dimension to the right side ($\alpha + 1$) or left side ($\alpha - 1$) with probability p and q , respectively after each step of time Δt as shown in figure 2.3.

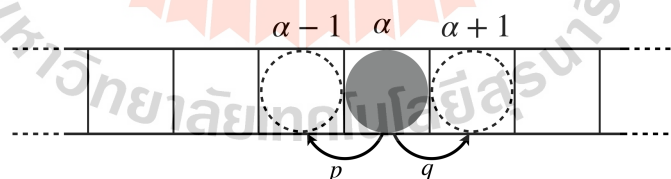


Figure 2.3 A random walk model in one dimension. An object at α hops to the right with the probability p and to the left with the probability q .

After N steps of time, we cannot predict the exact position of the object, but we can predict the probability to find the object at a given position at that time $P(\alpha, N)$. The number of right and left steps are given by n_r and n_l , respectively. For $\alpha < N$,

$n_r = \alpha + n_l$ and $n_r + n_l = N$. Then combining these together, we obtain $n_r = \frac{1}{2}(N + \alpha)$ and $n_l = \frac{1}{2}(N - \alpha)$. The probability for a sequence of left and right hopping is the product of the probabilities of the individual hops

$$p^{n_r} q^{n_l} = p^{\frac{1}{2}(N+\alpha)} q^{\frac{1}{2}(N-\alpha)}. \quad (2.17)$$

This probability must be multiplied by the total number of distinguishable paths $\frac{N!}{n_r!n_l!}$ or $\frac{N!}{(\frac{N+\alpha}{2})!(\frac{N-\alpha}{2})!}$, by substitution of n_r and n_l in terms of α and N . Therefore, the probability of finding an object at position α after N time steps is

$$P(\alpha, N) = \frac{N!}{(\frac{N+\alpha}{2})!(\frac{N-\alpha}{2})!} p^{\frac{1}{2}(N+\alpha)} q^{\frac{1}{2}(N-\alpha)}. \quad (2.18)$$

The random walk is a good model of many physical processes such as the movement of gas particles inside the box. The random walk can occur in one-dimension, two-dimension and three-dimension. In this study, we model the movement of a molecule inside the channel which is a one-dimensional random walk. It can be naturally generalized to include non-zero (or large) probabilities that the object remains in place, with left and right probability rates replacing the simple probabilities mentioned above.

We will crudely model the protein channel as a one-dimensional array of binding sites. The sugar molecule enters the channel and then hops from site to site. In a one-dimensional system of sugar hopping inside a channel, at time t , a molecule at α can move to the left position $\alpha - 1$ and the right position $\alpha + 1$ as shown in figure 2.4. If we suppose only one molecule can occupy the channel in one time, the molecule hops to the right with probability p_α^+ or to the left with probability $p_\alpha^- = 1 - p_\alpha^+$ during a

time interval Δt . The probability of finding a particle being at position α at time $t + \Delta t$ relates to the previous time step as equation 2.19,

$$g_\alpha(t + \Delta t) = g_\alpha(t) - p_\alpha^- g_\alpha(t) - p_\alpha^+ g_\alpha(t) + p_{\alpha-1}^+ g_{\alpha-1}(t) + p_{\alpha+1}^- g_{\alpha+1}(t). \quad (2.19)$$

For the travel of a sugar molecule inside the channel, the event is end when the molecule first reaches a position outside the channel.

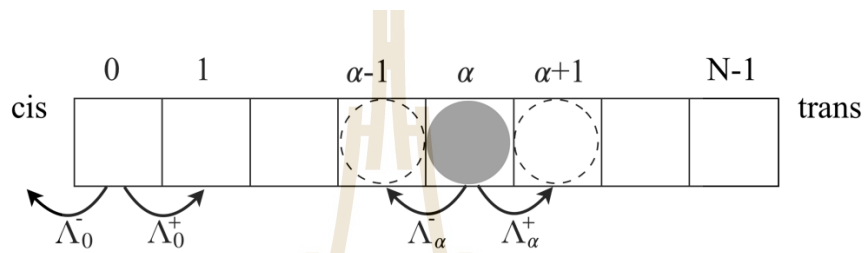


Figure 2.4 A random walk model of a protein channel with N trapping sites $\alpha = 0, 1, 2, \dots, N - 1$ from cis to trans sides. Sugar molecule hops with the rate Λ_α^\pm which depend on potential energy V_α .

In our study, the protein channel is separated to N trapping sites. Each trapping site is labeled as $\alpha = 0, 1, 2, \dots, N - 1$ from cis to trans sides as shown in figure 2.4. There is a dimensionless potential energy V_α which binds the sugar molecule at each trapping site α . Time-independent hopping rates when the sugar molecule at α moves to the left site ($\alpha - 1$) and moves to right site ($\alpha + 1$) are equal to Λ_α^- and Λ_α^+ , respectively. The rates are constant with time which are defined as

$$\Lambda_\alpha^\pm = R \exp(V_\alpha - V_{\alpha \pm 1}) \quad (2.20)$$

where R is the initial rate. The probability of hopping to left or right during the time interval Δt is related to the hopping rate as equation 2.21.

$$p_\alpha^\pm = \Lambda_\alpha^\pm \Delta t. \quad (2.21)$$

Therefore, the probability of finding a particle being at position α at time $t + \Delta t$ can be expressed as equation 2.22,

$$g_{\alpha}(t + \Delta t) = g_{\alpha}(t) - [\Lambda_{\alpha}^{-} + \Lambda_{\alpha}^{+}]g_{\alpha}(t)\Delta t + \Lambda_{\alpha-1}^{+}g_{\alpha-1}(t)\Delta t + \Lambda_{\alpha+1}^{-}g_{\alpha+1}(t)\Delta t. \quad (2.22)$$

The motion which we consider starts at time $t = 0$ when a sugar molecule from one side (i.e. *cis* side) enters the channel at $\alpha = 0$. Thus, $g_0(t = 0) = 1$ and $g_{\alpha \neq 0}(t = 0) = 0$. Next time step Δt , the sugar molecule can move to left or right. At time $t > 0$, the probability of finding the channel still closing at time greater than t is equal to equation 2.23,

$$f_1(t) = \sum_{\alpha} g_{\alpha}(t). \quad (2.23)$$

CHAPTER III

THE PROBABILITY OF TRANSLOCATION

In this chapter, we propose the procedure to estimate the probability of translocation. The procedure begins with detecting events by pCLAMP v.10.6 software, analyzing data, then estimating the probability of translocation by using the extracted de-trapping function. Furthermore, we develop the model of intramonomer dynamics by using random walk theory which may be applicable to similar system.

3.1 Experimental detection methods

3.1.1 Event detection methods

The raw data are analyzed by pCLAMP v.10.6 software. We define the minimum time duration of events t_{\min} to be 0.1 ms and ignore instances where the current remains near I_n for a shorter time. We choose this value because it is of the same scale as the average transition time required for the current to change between levels. An example of the ion current transition of from level 1 to level 0 is shown in figure 3.1. This transition time t_{\min} is much larger than that required for a sugar molecule to move, by diffusion, in or out of the monomer. Thus, the observed transition does not reflect single-molecule dynamics. Rather, when a sugar molecule moves rapidly into the channel and blocks it (or moves out of the channel and unblocks it) it takes time for the measured current to respond to this change. The process can be thought of as the charging or discharging of a capacitor: the blocked channel acts as a

capacitor since a significant amount of ionic charge (of opposite sign) accumulates at its ends. When the sugar molecule escapes the channel, current flow restarts (the capacitor discharges). We have previously analyzed such transitions and found they are well-fit by exponential functions characteristic of RC circuits. They do not give us information about the sugar dynamics, however, since the time for the actual escape is much shorter than the RC time constant. Suffice to say, we simply cannot detect sugar dynamics on a time scale shorter than t_{\min} in our experimental setup because the current would not respond quickly enough to molecular motion. We are limited to those events in which the channel remains blocked or empty for a longer time.

Figure 3.2 shows the event detection by pCLAMP v.10.6 software when the ion current is separated into two levels. The events in level 0 are open channel events for which the current $I(t) \approx I_0$ and the events in level 1 are closed-channel events with $I(t) \approx I_1$. From the data of chitohexaose with $[c] = 40 \mu\text{M}$, $V = -100$ mV at room temperature (25°C) as shown in figure 3.2, $I_0 \approx -45$ pA (electric current flow from *cis* chamber to *trans* chamber) and I_1 is close to zero since the size of sugar molecule is sufficient to fully block the channel.

Such event detections from software provide the number of events in the time duration of experiment and time for each event, as well as the mean and standard deviation of the current over each event.

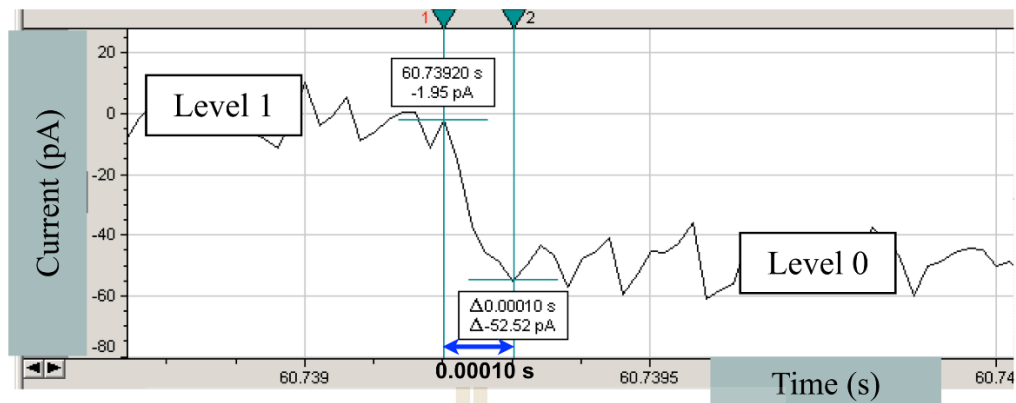


Figure 3.1 Ion current transition from level 1 (closed channel) to level 0 (open channel) occurs for 0.1 ms.

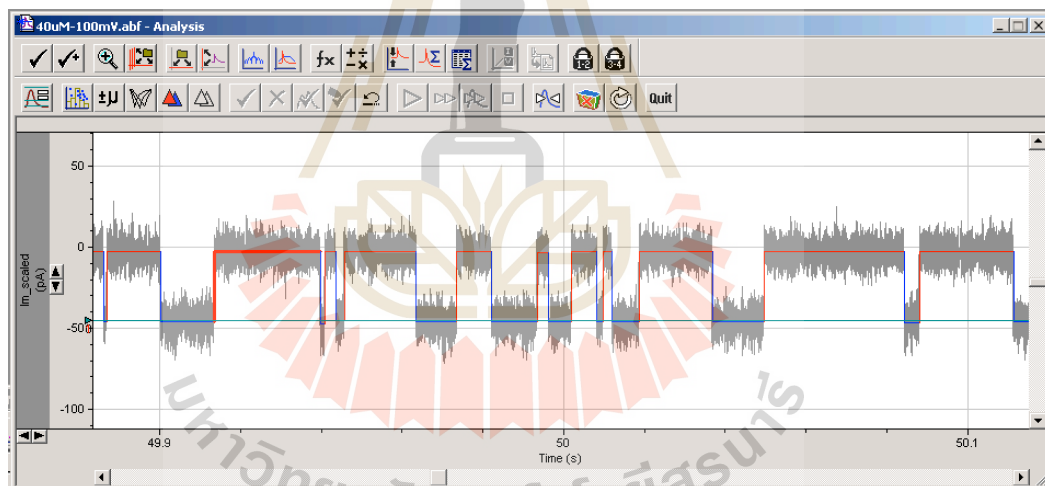


Figure 3.2 Event detection of the experiment data where 40 μM of chitohexaose inserted in *cis* chamber at applied voltage of -100mV by pCLAMP v.10.6 software.

3.1.2 Data analysis

In the simplest case of a time-independent trapping (or de-trapping) rate, probability $f_n(t)$, for the channel to remain in level n with current I_n for time longer than t , changes with time t as equation 3.1 where τ is time constant for level n ,

$$f_n(t) = \exp(-t/\tau). \quad (3.1)$$

The time of the j^{th} event of level n is defined as $t[j]_n$. Figure 3.3 shows the current signal of the experiment which time of closed-channel event starts at $t = 0$ s when the current changes from level 0 to 1 and end when the current changes from level 1 to 0 again. The mean residence time, $\tau_n = \langle t[j]_n \rangle$, is equal to τ which one can prove by equation 3.2 which is mentioned in theory (Suginta *et al.*, 2016).

$$\tau_n = \int_0^{\infty} dt t \left(-\frac{df_n}{dt} \right) = \int_0^{\infty} dt f_n(t) \quad (3.2),$$

where $f_n(\infty) = 0$ and $f_n(0) = 1$.

We generalize the rate equation to cases where the trapping and de-trapping rates need not be constant. We write a rate equation for this probability as

$$\frac{df_n}{dt} = -f_n(t)A'(t) \quad (3.3);$$

so that

$$f_n(t) = \exp(-A(t)) \quad (3.4),$$

and the trapping function is defined by equation 3.5:

$$U(t) = -\ln(f_0(t)) \quad (3.5)$$

while de-trapping function is defined by equation 3.6:

$$B(t) = -\ln(f_1(t)) \quad (3.6)$$

where $A(t)$ is trapping function when $n = 0$ or de-trapping function when $n = 1$.

We note that equation 3.3 amounts to a definition of the trapping and de-trapping function, since any rate equation can be written this way by introducing an unknown function $A'(t)$. The key point is that the argument of the exponential need not be a linear function. This means that the probability, equation 3.4, need not behave as a simple exponential. Consider the case of de-trapping where $B(t)$ is non-linear. We could expand $f_1(t) = \exp(-B(t))$ as a sum over many simple exponentials, with the argument of each corresponding to a different de-trapping rate. This is what we would expect if a sugar molecule can be trapped in many differ configurations, with a different escape rate for each. At short times, all the de-trapping rates are active but, at long times, only the slowest de-trapping rate (the slowest-decaying exponential) would remain.

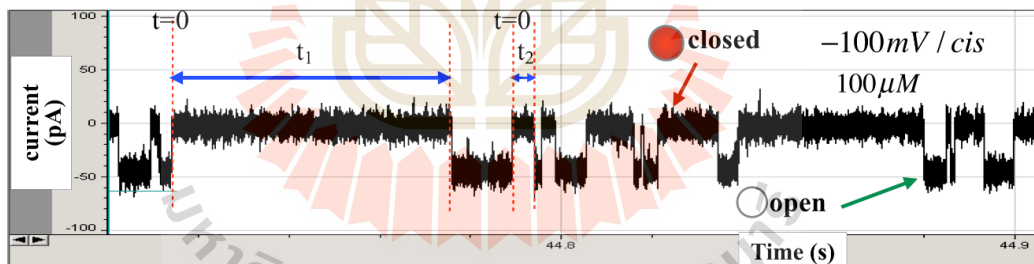


Figure 3.3 The current signal of the experiment data where $100 \mu\text{M}$ of chitohexaose inserted in cis chamber at applied voltage of -100 mV on pCLAMP v.10.6 software. Time of closed-channel events start at $t = 0 \text{ s}$ when the current changes from level 0 to 1 and end when the current changes from level 1 to 0 again.

The probability is obtained from the data via $f_n(t) = \frac{N_n(t)}{N_n(0)}$, and the trapping and de-trapping functions derived from it. In data analysis, we plot $U(t)$ and $B(t)$ functions obtained from measurements on chitopentaose, chitohexaose and charged molecule (chitosan at pH 5.5 which is structurally related to chitohexaose). The experiments were performed, and the data provided, by H. Sasimali M. Soysa.

3.1.3 Probability estimation

In order to estimate the translocation probability, we consider only the de-trapping function which is relevant to closed-channel events. We begin by classifying the events as either short-time or long-time events and considering possible scenarios based on the previous results of trimeric channel (Suginta *et al.*, 2016) and the sample results of *EcChiP* data provided by H. Sasimali M. Soysa. Then, we find the equation for translocation probability estimation from the graph of $B(t)$ versus t by using y-intersection of the linear de-trapping function for long-time events $B_\infty(t)$. The linear $B_\infty(t)$ function is shown in figure 3.4 as line 2.

The basic assumption we are making here is that the long-time events, occurring during the linear regime of $B(t)$, have a good chance to be translocation events, while the short-time events are dominated by backwards escape.

3.1.3.1 Events and possible interpretation for non-linear behavior of $B(t)$. The results of de-trapping function $B(t)$ based on trimeric channel data (Suginta *et al.*, 2016) and the sample results of *EcChiP* data with concentrations $[c]= 5, 40$ and $80 \mu\text{M}$, chitohexaose first contained in *cis* side, $V = -100$ mV at room temperature (25°C) as shown in figure 3.4 exhibit nonlinear relation with time of events. From these results, we consider the events as short-time and long-time events.

Possible interpretation for non-linear behavior of $B(t)$

1) Short-time events should be backwards escape events in which the sugar molecules move back to the initial side after entering the channels as shown in figure 3.5A.

2) Long-time events could be translocation events in which the sugar molecules move toward to the opposite side after entering the channels as shown in figure 3.5B and 3.5C.

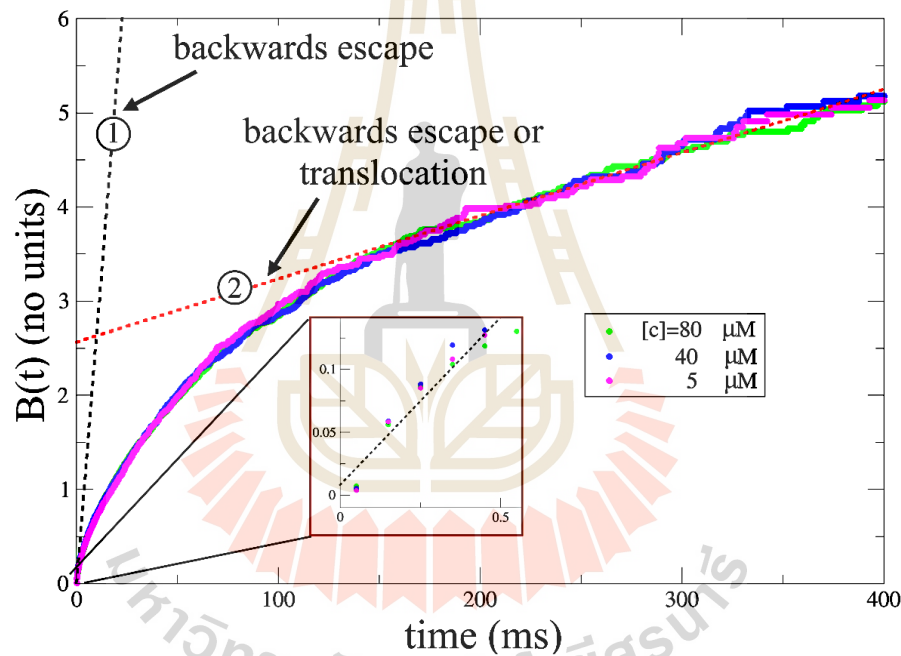


Figure 3.4 The relation between $B(t)$ and time t from the experiment results. Chitohexaose 5, 40 and 80 μM were inserted into cis chamber with $V = -100$ mV at room temperature (25 $^{\circ}\text{C}$) and the linear dash lines are referred to short-time and long-time events.

These two points sound rather hopeful, so let us consider them more carefully. It turns out that this point of view is supported by the simple theoretical model discussed below and by the experimental evidence (particularly that on charged chitosan molecules) discussed in the next chapter.

The first point is rather obvious: it takes time for a sugar molecule to traverse the narrow channel and this is unlikely to occur for the shortest events. The molecule probably got trapped near the entrance then escaped back from whence it came. If the molecule hangs around longer than this, it has a chance to move deeper into the channel, from which it may either be translocated through the channel or make a long backwards escape.

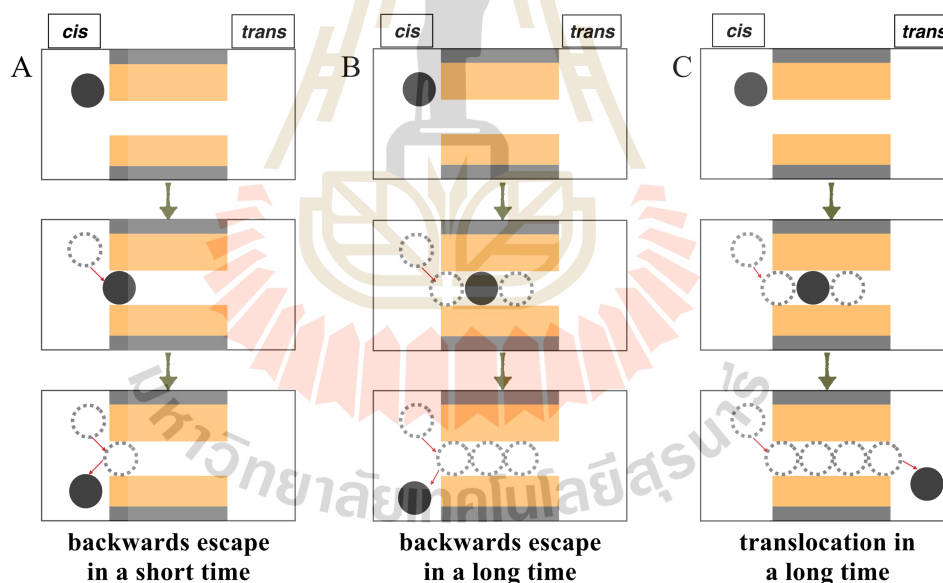


Figure 3.5 Possible interpretation for non-linear behavior of $B(t)$. (A) Sugar molecule moves backwards to *cis* chamber after blocking the channel for a short time. (B) Sugar molecule moves backwards to *cis* chamber after staying in some trapping sites (dash circle) inside the channel for a long time. (C) Sugar molecule is translocated to *trans* chamber after staying in all trapping sites inside the channel for a long time.

When there are many possible escape (i.e. de-trapping) mechanisms, the linear behavior of $B(t)$ that occurs at large times has a slope given by the slowest of all these escape rates. Moreover, $B(t)$ is the integral of a probability rate, as evident from its definition above. So, when we obtain the intercept of $B_{\infty}(t)$, we are finding the fraction of all escape events that utilized the slowest escape mechanism available. Our assumption that this intercept reflects the translocation probability is equivalent to saying that escape via translocation is slower than any other mechanism of escape. In other words, the fraction of molecules that escape slowly is a good estimate of the fraction of molecules that escape correctly into the opposite side of the channel. Of course, this is not a perfect estimate (some mechanism of translocation may proceed more rapidly than certain mechanisms of back-escape) but it is a plausible approach.

Short-time events: the events with the time of events are in a few milliseconds

At very small t , we can approximate de-trapping function $B(t)$ as equation 3.7

$$B(t) \approx B_0(t) = B'(0)(t - t_{\min}) \quad (3.7)$$

where $B'(0)$ is the initial slope which is roughly obtained from first two data point above t_{\min} . The exact value of $B'(0)$ is not significant, thus we consider only order of magnitude. Also, note that there may be many escape events that are even shorter than these, but that are unobservable in our experiment because of the slow response-time of the ionic current. However, if we think the shortest observable events are too short to allow translocation, then not of the unobservable (even shorter) events would allow translocation either. Thus, for the purposes of finding translocation probability among observable events, we are not missing anything.

Long-time events: the events with the time of events are large.

At long- t , we express the linear equation of de-trapping function for long-time events $B_\infty(t)$ as equation 3.8,

$$B(t) \approx B_\infty(t) = \lambda_{\min}t + B_\infty(0) \quad (3.8)$$

where λ_{\min} is the slope of line 2 in the graph shown in figure 3.4; t is time; and $B_\infty(0)$ is the extrapolated intercept for long-time regime.

3.1.3.2 Find the equation for translocation probability estimation from $B(t)$ function of long-time events. As mentioned in equation 3.4, we have the probability that monomer remains blocked for time greater than t is

$$f_1(t) = \exp(-B(t)). \quad (3.9)$$

In order to estimate probability of translocation, we consider only long-time events.

In this case, the probability of translocation is

$$P_T \approx \eta \cdot f_1(t^*) \quad (3.10)$$

where t^* is the smallest considered time for long-time events and parameter η is the ratio of the number of translocation events to the number of all long-time events which is placed for the possible situations that long-time events can be either backwards escape or translocation events.

Substitution of equation 3.9 into equation 3.10 gives

$$P_T \approx \eta \exp(-B_\infty(t^*)). \quad (3.11)$$

Since $B_\infty(0) > \lambda_{\min}t^*$, we obtain from equation 3.8 that $B_\infty(t^*) \approx B_\infty(0)$.

Therefore, in general, the translocation probability can be estimated by

$$P_T \approx \eta \exp(-B_\infty(0)). \quad (3.12)$$

In the case that all long-time events are translocation: $\eta = 1$. The translocation probability can be estimated by

$$\tilde{P}_T \approx \exp(-B_\infty(0)). \quad (3.13)$$

In this part, we analyze the experimental data of chitohexaose in various applied voltages and various concentrations, and the experimental data of chitopentaose in various concentrations and estimate the probability of translocation by using equation 3.13. In order to know the effects of charge of sugar molecules on the results of experiments, we also analyze the experimental data of cationic chitosan hexaose at pH 5.5 which is structurally related to chitohexaose in various applied voltages.

3.2 Model of intramonomer dynamics

In our study, the protein channel is separated to N trapping sites. Each trapping site is labeled as $\alpha = 0, 1, 2, \dots, N-1$ from cis to trans sides. At $t = 0$, the probability of finding the channel still closing at time greater than t is equal to $f_1(0) = 1$ and the backwards escape rate into the cis side is equal to Λ_0^- . This determines the initial slope which is $\Lambda_0^- = -f_1'(0) = B'(0)$. A dimensionless time variable τ is defined by

$$\tau \equiv B'(0)t. \quad (3.14)$$

Hopping rates are expressed in units of $B'(0)$, so all Λ_α^\pm are dimensionless and $\Lambda_0^- \equiv 1$.

In order to find $B(\tau)$, we consider equation 3.15:

$$f_1(\tau) = \exp(-B(\tau)) = \sum_{\alpha} g_{\alpha}(\tau). \quad (3.15)$$

Thus,

$$B(\tau) = -\ln\left(\sum_{\alpha} g_{\alpha}(\tau)\right). \quad (3.16)$$

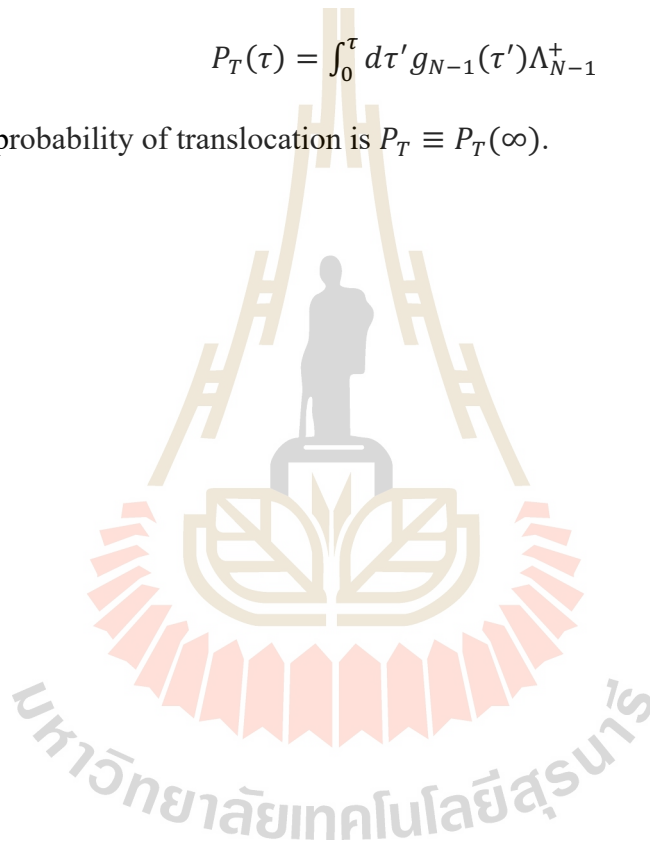
In our simulation, we input V_α and calculate Λ_α^\pm from equation 2.20 where all Λ_α^\pm are expressed in units of initial slope $R = B'(0)$, find $g_\alpha(\tau)$ from equation 2.22 in theory then calculate $B(\tau)$ from equation 3.16 and further calculate \tilde{P}_T from equation 3.17.

$$\tilde{P}_T = \exp [-B_\infty(0)]. \quad (3.17)$$

Moreover, we calculate the probability of translocation $P_T(\tau)$ occurring before time τ from

$$P_T(\tau) = \int_0^\tau d\tau' g_{N-1}(\tau') \Lambda_{N-1}^+ \quad (3.18),$$

and the total probability of translocation is $P_T \equiv P_T(\infty)$.



CHAPTER IV

RESULTS AND DISCUSSIONS

In this chapter, we begin with the results of the trapping function $U(t)$ and de-trapping function $B(t)$ in various chitohexaose concentrations and try to explain the behaviors of these functions. $U(t)$ is derived from the probability that a channel remains open for time greater than t , $f_0(t)$, as $U(t) = -\ln(f_0(t))$ and $B(t)$ is derived from the probability that a channel remains closed for time greater than t , $f_1(t)$, as $B(t) = -\ln(f_1(t))$. In order to explain the physical processes that affect the behavior of $B(t)$ and to validate our claims below about translocation probability, we investigate the voltage-dependence of charged chitosan translocation. We then apply the random walk model of intramonomer dynamics to try to interpret these data. Since this model appears to provide a good framework for understanding the experiments, we use it further to interpret experimental results for different sizes of chitosugar and the voltage dependence of the dynamics for neutral chitohexaose translocated by *EcChiP* channel.

4.1 Trapping and de-trapping of sugar by chitoporin

The trapping functions $U(t)$, shown in figure 4.1A and 4.1B, were obtained with an applied voltage $V = -100$ mV and varying chitohexaose concentration $[c]$ introduced to *cis* and *trans* chambers, respectively. The graphs show that the slope of $U(t)$ is independent of time and increases linearly with sugar concentration. The results indicate that the slope $U'(t)$ may be associated with single constant trapping rate that

increases with sugar concentration. Thus, $U(t) = U'(t)t \approx k_{on}[c]t$ where the slope $k_{on}[c]$ increases with sugar concentration $[c]$ with the rate constant k_{on} .

The results in figure 4.1 provide $k_{on}[c]$ as shown in figure 4.2. By linear graph fitting, we see that k_{on} for a sugar molecule entering the channel from the *cis* chamber is about $3 \times 10^6 \text{ M}^{-1}\text{s}^{-1}$ and that from the *trans* chamber is about $2 \times 10^6 \text{ M}^{-1}\text{s}^{-1}$. We observe that k_{on} obtained from a slope of $U(t)$ is about the same as $1/\tau_{on}$ where τ_{on} is the average duration that a channel remains unblocked (the two may not exactly coincide because small deviations from linearity occur more at large times).

The experimental results of the de-trapping function $B(t)$, shown in figure 4.3, were obtained with chitohexaose on the *cis* and *trans* chambers when $V = -100 \text{ mV}$ was applied. The graph shows that $B(t)$ is roughly independent of concentration and changes non-linearly with time.

As noted above, the non-linear $B(t)$ function with a slope that changes with time describes a system with many different escape mechanisms possible for trapped molecules. This description is well suited to a 'hidden Markov model'. Basically, this is a model of a system that has many states, with random transitions between them, but some states are hidden, i.e. unobservable. For example, if there are many binding sites inside the channel then a sugar molecule can move from one site to another and the channel would remain blocked, with no observable change in current. Our proposed random walk model is an example of a hidden Markov model.

There are many different escape rates $B'(t)$ that appear to decrease with t and come close to constant at large time. This is exactly what ones expect in the hidden Markov picture. After a long time, only the single slowest escape process is occurring because all other, faster, escape processes have already completed their work. We can

crudely break up the plot into two regions of the graph as shown in figure 4.4. In the small t region, $B(t)$ increases rapidly whereas, in the long t region, $B(t)$ increases slowly with a small rate $\lambda_1 =$ the slope of line 2. Again, according to the model language, many different escape mechanisms are occurring during the small t region while only the slowest one of all happens at large t .

In the small-time region, if we zoom at small time t ,

$$B(t) \approx B_0(t) = B'(0)(t - t_{\min}) \quad (4.1)$$

where $B'(0)$ is the initial slope. The initial, and largest, value of the slope occurs at $t = t_{\min}$. The slope at t_{\min} ($B'(t = t_{\min}) = 600 \text{ s}^{-1}$) is two orders of magnitude larger than the slope in the long-time region ($B'(t = \text{large } t) = 7.6 \text{ s}^{-1}$). Thus, there are some escape processes that are a hundred times faster than others. (Again, even faster processes are presumably occurring for $t < t_{\min}$, but we cannot see these because of the slow current response time in the experiment.) Our central assumption is that the majority of the rapid escape process, occurring in the small-time regime, are backwards escapes of sugar molecules. Translocation takes longer than this. The large t region describes molecules that are bound in the channel for an extended time before escaping. These could be translocations or highly ineffective backwards escapes.

A

B

Figure 4.1 The linear trapping function $U(t)$ versus time t with $[c]= 1.25, 5, 10, 20, 40$ and $80 \mu\text{M}$ chitohexaose and $V = -100 \text{ mV}$. (A) The chitohexaose was introduced to *cis* chamber. (B) The chitohexaose was introduced to *trans* chamber.

A

B

Figure 4.2 The trapping rate $k_{\text{on}}[c]$ derived from $U(t)$ function in figure 4.1. $[c]$ of chitohexaose = 1.25, 5, 10, 20, 40 and $80 \mu\text{M}$ chitohexaose and $V = -100 \text{ mV}$. (A) and (B) The chitohexaose was introduced to *cis* chamber and *trans* chamber, respectively. Graphs are fitted with the linear equation $y = mx + c$ where m and c are constant. Case A: $m = 3 \times 10^6 \text{ M}^{-1}\text{s}^{-1}$ and $c = 1.7 \text{ s}^{-1}$. Case B: $m = 2 \times 10^6 \text{ M}^{-1}\text{s}^{-1}$ and $c = -3.3 \text{ s}^{-1}$. The values of c from both cases are very small when compared to y -scale then we can approximate c to be zero as expected that the rate $k_{\text{on}}[c]$ should be zero if there is no sugar molecule.

In the long-time region, the slope is nearly constant and the de-trapping function can be approximated by equation 4.2:

$$B(t) \approx B_\infty(t) = \lambda_1 t + B_\infty(0). \quad (4.2)$$

From the $B(t)$ function, the quantity \tilde{P}_T , which should be a reasonable estimate of translocation probability, is obtained from

$$\tilde{P}_T \equiv \exp(-B_\infty(0)). \quad (4.3)$$

According to the model description, what \tilde{P}_T really tells us is the probability that the sugar molecule escapes via the slowest of all escape rates, as opposed to via any faster rate. (The extrapolated intercept is the correct way to determine this: we are describing the escape rate as a probability rate, a probability per unit time of escaping. The slowest escape rate proceeds more slowly than others but still enjoys some probability of an escape occurring at small times, and such instances are rightly included when we use the extrapolated intercept.) The long-time region linear fitting of the experimental data in figure 4.3 with chitohexaose on *cis* and *trans* chambers and $V = -100$ mV gives $B_\infty(0) = 2.35$ and 2.94 , respectively. This translates to $\tilde{P}_T = 0.1$ and 0.05 for sugar addition on *cis* and *trans* chambers, respectively.

Sugar addition on either the *cis* and *trans* chambers shows the same behavior in its $B(t)$ function. Next we consider the behavior of $B(t)$ in charged chitosan in order to test our claim that the observable parameter \tilde{P}_T is an estimate of the key property P_T .

A

B

Figure 4.3 The non-linear de-trapping function $B(t)$ versus time t with $[c]= 1.25, 5, 10, 20, 40$ and $80 \mu\text{M}$ chitohexaose and $V = -100 \text{ mV}$. (A) The chitohexaose was introduced to *cis* chamber. (B) The chitohexaose was introduced to *trans* chamber.

A

B

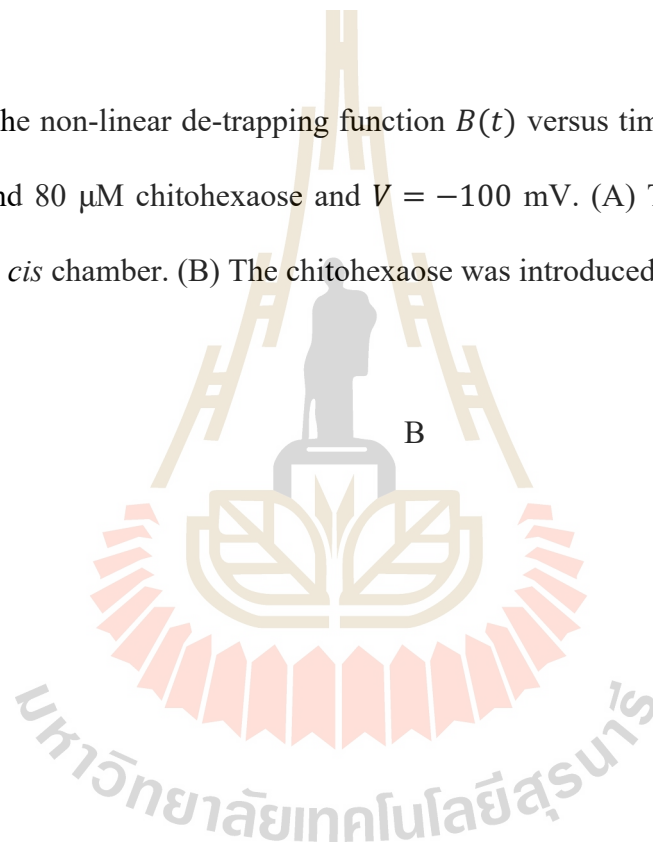


Figure 4.4 The de-trapping function $B(t)$ versus time t with the artificial linear lines for small-time events (line 1) and long-time events (line 2). $5 \mu\text{M}$ chitohexaose was introduced to *cis* chamber and $V=-100 \text{ mV}$. Line 2 intersects y-axis at $y = B_{\infty}(0) = 2.35$ and the slope of line 1 and line 2 are 7.6 s^{-1} and 600 s^{-1} , respectively. (A) The full view of the graph. (B) The zoom-view at small time t .

4.2 Voltage-dependent trapping of charged chitosan

Charged chitosan hexaose is used in our study because we can control the direction of charged sugar current by using the applied voltage V . We can observe the changes in $B(t)$ and $U(t)$ and, knowing the effect of the voltage, better interpret these changes. In our analysis, the experimental data are from the single-channel measurement of chitosan hexaose translocated through *EcChiP* in pH 5.5 electrolyte solution where the chitosan molecule acts as cationic charged molecule. The results show that the trapping of chitosan hexaose is strongly voltage dependent, which is obvious since V influences the charged molecule. We can exploit this dependence to confirm that the small- t behavior of $B(t)$ is dominated by backwards escape.

4.2.1 The trapping function of charged chitosan

Figure 4.5A and 4.5B show the plots of the $U(t)$ function for cationic chitosan on the *cis* chamber with $V = -50, -75, -100$ and -125 mV and on the *trans* chamber with $V = 50, 75, 100$ and 125 mV. For all these cases, the electric field is acting in the same direction as the molecular diffusion current. That is, this is a forward bias that encourages translocation. $U(t)$ function is linear in time with a slope $k_{\text{on}}[c]$ increasing with $|V|$. In contrast, figure 4.5C and 4.5D show results with opposite polarity, so the electric field is opposite to the diffusion currents. This is a reverse bias that is acting to prevent chitosan molecules from reaching the channel. Those few molecules lucky enough to arrive at the channel and become trapped in it will be dragged back to the side from which they entered by the electric field. The resulting $U(t)$ function is noisy and does not exhibit a systematic $|V|$ dependence. This is because closed-channel events rarely occur, and the resulting statistical noise is large. The number of events is about 6-10% of previous cases. (Note, the gradient in chitosan

concentration, large because one chamber contains the given concentration and the other essentially none, drives the diffusion current and this persists despite the reverse bias, so the number of channel blocking events is not zero.) It is natural that $k_{\text{on}}[c]$ increases with $|V|$ for forward bias. The probability of translocation should vary likewise. For reverse bias $k_{\text{on}}[c]$ is understandably small (it should decrease further with $|V|$ but this effect might be lost in the noise) and backwards escape dominant.

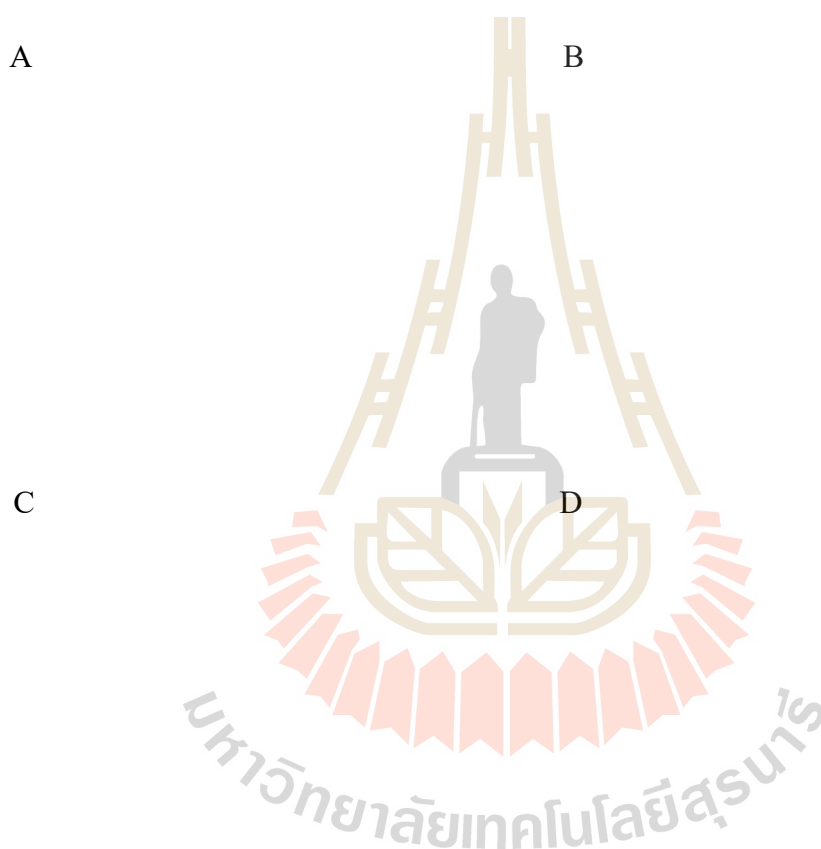


Figure 4.5 The trapping function $U(t)$ versus time t with varying applied voltage $|V|$ = 50, 75, 100 and 125 mV. (A) and (B) The cationic chitosan hexaose was introduced to *cis* and *trans* chambers, respectively. The molecular diffusion current flows in the same direction to the ion current. (C) and (D) The cationic chitosan hexaose was introduced to *cis* and *trans* chambers, respectively. The molecular diffusion current flows in the opposite direction to the ion current.

4.2.2 The de-trapping function of charged chitosan

The plots in figure 4.6A and 4.6B are for cationic chitosan added to the *cis* side with negative applied voltage and *trans* side with positive applied voltage, $|V| = 50, 75, 100$ and 125 mV. This is forward bias, the ion current is in the same direction as the chitosan diffusion current. The results show the nonlinear t -dependence of the $B(t)$ function that we have come to expect. (In the case of the reverse bias, only a small number of brief closed channel events are seen, with all events lasting less than 2 ms, so we cannot see much from the de-trapping function.)

A

B

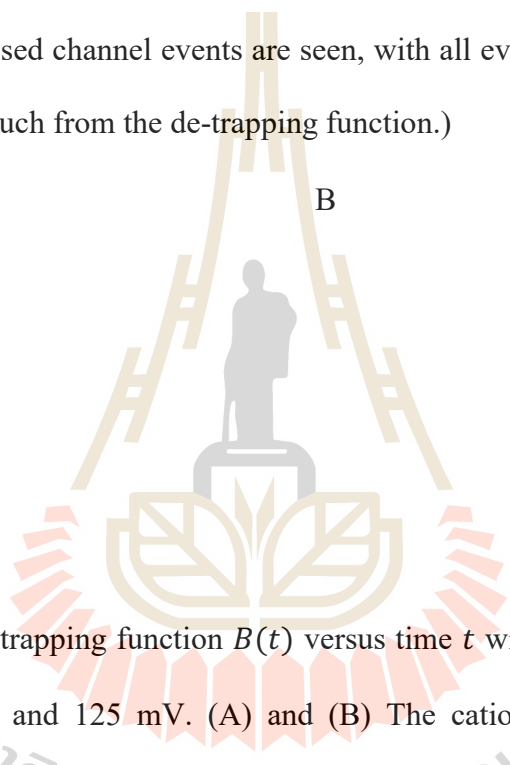


Figure 4.6 The de-trapping function $B(t)$ versus time t with varying applied voltage $|V| = 50, 75, 100$ and 125 mV. (A) and (B) The cationic chitosan hexaose was introduced to *cis* and *trans* chambers, respectively. The molecular diffusion current flows in the same direction to the ion current.

In the small- t region, the results show that the slope $B'(t)$ decreases with the applied voltage $|V|$. That is, increasing the forward bias reduces the rate of escape during the small-time region. This is an obvious indication that the escape occurring at small time is backwards escape. If it was translocation then the forward bias would help push molecules through rapidly and thus the trend would be opposite. The increase in

$|V|$ makes back-escape slower and less common because molecules have to overcome the bias in order to make their retreat. Along with this, we must have a complementary increase in the probability of translocation (there are only two options: translocation and backwards escape). For chitosan, $B(t)$ must be dominated by backwards escape for $t < 1$ ms.

In the long- t regime, we fit $B(t)$ graphs with $B(t) \approx B_\infty(0) + \lambda_1 t$. In the case of forward bias, the intercept of $B_\infty(0)$ gets smaller as $|V|$ increases. The slope does not change much. The former is the required result of having a smaller number of events during the small-time region. The value of \tilde{P}_T increases rapidly with $|V|$ as shown in figure 4.7 (The error bars were obtained by selecting various possible high- t ranges to perform linear graph fitting.). At the same time, we know that the translocation probability P_T , though it cannot be observed in the experiment, must be increasing. The applied voltage is pushing the chitosan through the channel. In equilibrium, for a model with a single trapping site in the middle of the channel (i.e. a symmetric situation), a molecule with charge q is more likely to escape to the side with lower voltage V by a factor $\exp(q|V|/kT)$ after being trapped. This factor is large, from 7 to 400 for $|V|$ from 50 to 150 mV. Of course, in the model we consider below that has many trapping sites, those molecules that just entered one channel end must proceed through a series of other sites before achieving translocation. This gives a large statistical advantage to back escape, an advantage that the forward bias can only partly overcome.

A

B

Figure 4.7 The translocation probability in various V . (A) and (B) The cationic chitosan hexaose was introduced to *cis* and *trans* chambers, respectively. The molecular diffusion current flows in the same direction to the ion current.

The discussion about the $B(t)$ function above reveals that the physics of rapid escape processes in the small time regime is different from that of slow escape processes in long-time regime. The former rates are strongly voltage dependent, decreasing with the strength of the forward bias, the latter are nearly independent of voltage. The former events occur less often with an increased forward bias, the latter occur more often. We can be reasonably sure that the small-time processes are backwards escape. The long-time processes are thus either translocation or a form of backwards escape that differs dramatically, and for an unknown reason, from backwards escape seen at earlier times. Obviously, translocations seem a much more likely explanation.

The rapid change of $B(t)$ at small time regime of chitosan hexaose data is mostly from backwards escape. The $B(t)$ function of neutral chitohexaose is qualitatively similar to that of chitosan hexaose, so it is reasonable to attribute the small-time behavior of chitohexaose to backwards escape as well. The biological function of the channel is the translocation of chitohexaose. So, while the single channel current

measurement provides no direct evidence of translocation (it cannot distinguish it from backwards escape) we may presume that translocation does happen. The small time regime is dominated by backwards escape, so translocation can only occur in the long-time regime. From the $B(t)$ behavior of chitosan hexaose data, it is now more reasonable to claim that $\bar{P}_T \gtrsim P_T$ for neutral chitohexaose as well.

4.3 Random walk model of intramonomer dynamics

For the random walk model of molecular dynamics in the molecule, we first suppose that a molecule that just entered the channel on one end has certain rate of escape backwards. We use the inverse of this initial backwards escape rate as a unit of time, and measured in this unit, time τ is dimensionless. At $\tau = 0$, a sugar molecule is bound at position $\alpha = 0$, so the initial probability of finding the molecule at position α is $g_\alpha(0) = \delta_0^\alpha$. This probability will change with time. To track this change and predict the resulting behavior of $B(\tau)$, we solve the rate equation, expressed in matrix form as:

$$d\mathbf{g}/d\tau = \mathbf{\Lambda}\mathbf{g} \quad (4.4),$$

where $\mathbf{g}(\tau)$ is a vector with components $g_\alpha(\tau)$ and $\mathbf{\Lambda}$ is a matrix with all elements equal zero except $\Lambda_{\alpha,\alpha} = -\Lambda_\alpha^+ - \Lambda_\alpha^-$ and $\Lambda_{\alpha,\alpha\pm 1} = \Lambda_{\alpha\pm 1}^\mp$ (that is, we assume a molecule can only move into adjacent sites, without skipping any). The solution of equation 4.4 is $\mathbf{g}(\tau) = \exp(\mathbf{\Lambda}\tau)\mathbf{g}(0)$, where the exponential of the matrix is shorthand for the Taylor series

$$\exp(\mathbf{\Lambda}\tau) \equiv \mathbf{1} + \mathbf{\Lambda}\tau + \mathbf{\Lambda} \cdot \mathbf{\Lambda} \frac{\tau^2}{2} + \dots \quad (4.5)$$

and $\mathbf{1}$ is the $N \times N$ unit matrix.

At small time τ , the behavior of $B(\tau)$ is obtained from the first few terms of the Taylor series, which gives

$$B(\tau) \approx \tau - \Lambda_0^+ \frac{\tau^2}{2} + \Lambda_0^+ (\Lambda_0^+ + \Lambda_1^- - 1) \frac{\tau^3}{6} + \dots \quad (\text{small } \tau). \quad (4.6)$$

The first term describes molecules that escape backwards to the *cis* chamber immediately after entering the channel and trapping at $\alpha = 0$. The next few terms explain molecules that undergo short walks in the channel, taking a few steps in before eventually escaping backwards. There is no translocation possible at small time τ . Indeed, if there are N trapping sites, arranged in series, then one does not see any translocation until the N th term in the Taylor series. This means the effect of translocation on $B(\tau)$, which is described by terms τ^n with $n \geq N$, is negligible at small τ .

The solution can be written more generally as $g_\alpha(\tau) = \sum_n u_{n,\alpha} u_{n,0} \exp(-\lambda_n \tau)$ with $B(\tau) = -\ln f_1(\tau)$ where $f_1(\tau) = \sum_{n=1}^N p_n \exp(-\lambda_n \tau)$ and $p_n = (\Lambda_0^- u_{n,0} + \Lambda_{N-1}^+ u_{n,N-1}) u_{n,0} \lambda_n^{-1}$ where each λ_n is an eigenvalue of $\mathbf{\Lambda}$ and $u_{n,\alpha}$ is the α th component of the corresponding eigenvector. These eigenvalues satisfy $\sum \lambda_n p_n = \Lambda_0^-$.

At long time τ , the sum of exponentials is dominated by the term with the smallest positive eigenvalue, which is denoted by λ_1 . This gives

$$B(\tau) \approx B_\infty(\tau) = B_\infty(0) + \lambda_1 \tau + \dots \quad (\text{large } \tau) \quad (4.7),$$

with $\tilde{P}_T = \exp(-B_\infty(0)) = p_1$.

Sample numerical calculations of $B(\tau)$ and $P_T(\tau)$ shown in figure 4.8 are for an arbitrary channel size $N = 20$. There are four patterns of a dimensionless potential energy V_α with zero potential outside the channel shown in this figure. These potentials

determine the hopping rates Λ_{α}^{\pm} . Pattern 1: $V_{\alpha} = 0$, so all $\Lambda_{\alpha}^{\pm} = 1$. (This one can be solved analytically.) Pattern 2: $V_{\alpha} = -1$, giving fast intramonomer hopping with slower escape at each end of the channel. Pattern 3: a symmetric wedge potential with $V_{\alpha} = -0.1(\alpha + 1)$ for $\alpha < N/2$. Pattern 4: an asymmetric wedge potential $V_{\alpha} = -0.1(\alpha + 1)$ for all α . Figure 4.8A, 4.8C, 4.8E and 4.8G are $B(\tau)$ functions for pattern 1 to 4, respectively. Figure 4.8B, 4.8D, 4.8F and 4.8H are $P_T(\tau)$ results for pattern 1 to 4, respectively.

The results show that the behavior of $B(\tau)$ function from the calculation shown in figure 4.8 is similar to the behavior of $B(t)$ function from the experimental data shown in figure 4.3. $B(\tau)$ changes rapidly at small τ then flattens out, eventually increasing linearly with time at long τ . The graphs in figure 4.8 show that $P_T(\tau)$ is negligible at small τ then starts to increase at long τ which is in the same τ when $B(\tau)$ changes linearly. This can be implied that, at small τ , the translocation does not occur and $B(\tau)$ accounts for only backwards escape.

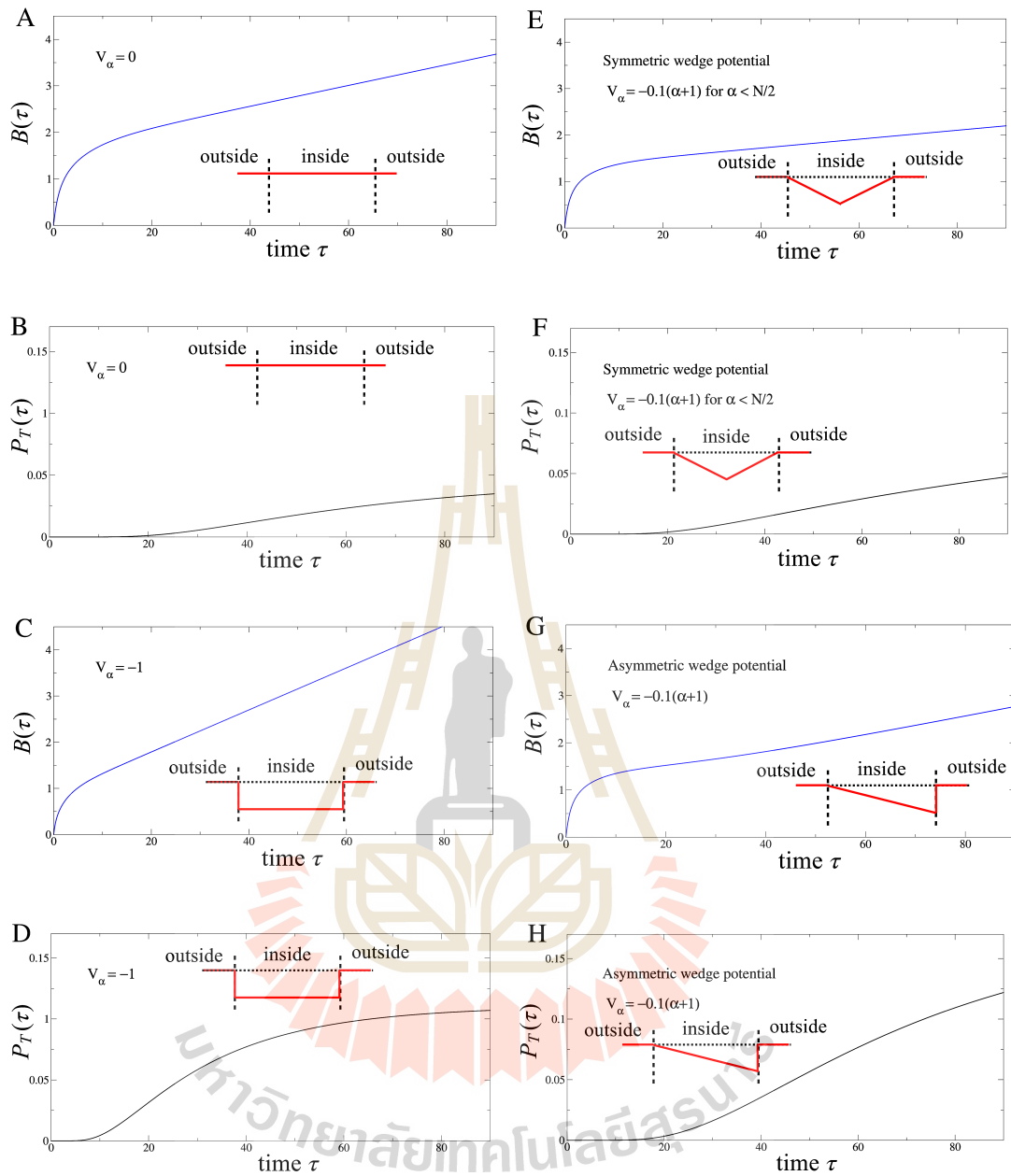


Figure 4.8 The calculations of $B(\tau)$ and $P_T(\tau)$ for $N = 20$ trapping sites. A, C, E and G are $B(\tau)$, and B, D, F and H are $P_T(\tau)$ in different patterns of effective potential V_α (red lines).

Figure 4.9 is the comparison between P_T and \tilde{P}_T for the asymmetric wedge potential when $N = 5, 10$ and 20 . These two functions follow the same trend when varied with the wedge steepness ΔV . In the difference of N , the value of P_T is higher when N is small at small ΔV then increasing to one value ($P_T \approx 0.6$) at large ΔV for all N . This trend is the same for \tilde{P}_T but the maximum value of \tilde{P}_T approaches 1 at large ΔV . (This means that, for this wedged model at large steepness, all escape proceeds via the slowest rate but only 60% of these processes are translocation events, the rest are highly inefficient backwards escape.) The average time that the channel remains blocked τ_c increases rapidly with ΔV . Figure 4.10 shows the rapid decrease of $1/\tau_c$ for $N = 5, 10$ and 20 .

The results in figure 4.9 gives the obvious evidence for the connection between P_T and \tilde{P}_T . Both $f_1(\tau)$ and P_T are given by sums over eigenvalue n . If we approximate $f_1(\tau)$ and P_T by giving $n = 1$ term which is relevant to smallest eigenvalue, then

$$\tilde{P}_T = \left(\frac{1}{\lambda_1}\right) (u_{1,0}^2 \Lambda_0^- + u_{1,0} u_{1,N-1} \Lambda_{N-1}^+) \quad (4.8)$$

where the first term explains backwards escape to *cis* chamber in long-time τ and the second term explains translocation in long-time τ ,

and

$$P_T \approx \left(\frac{1}{\lambda_1}\right) u_{1,0} u_{1,N-1} \Lambda_{N-1}^+ \quad (4.9)$$

which is same as the second term in equation 4.8. These predictions for \tilde{P}_T and P_T are equal if we make the assumptions that (i) the second term in equation 4.8 dominates over the first term and (ii) the sum over n that determines P_T is well approximated by its $n = 1$ term. These two assumptions are seen below to be valid when V_α is reasonable.

If $V_\alpha = 0$ and all hopping rates Λ_α^\pm are equal to one, we can solve the equations analytically. The eigenvalues are

$$\lambda_n = 2 - 2 \cos \left[\frac{n\pi}{N+1} \right] \quad (4.10)$$

with $n = 1, 2, \dots, N + 1$ varying over a range of order $1/N^2$ and producing $f_1(t)$ function with the same qualitative behavior as the data when N is large. The weights p_n are

$$p_n = \cos^2 \left(\frac{n\pi}{2(N+1)} \right) [1 - (-1)^n]. \quad (4.11)$$

From the analytic calculation, the result is $P_T = 1/(N + 1)$ and $\tilde{P}_T = 4/(N + 1)$ when assuming $N \gg 1$. The first and the second terms in equation 4.8 are equal and the $n = 1$ term is twice as large as the full series giving P_T . By combining the errors in both assumptions, \tilde{P}_T overestimates P_T by a factor of 4. As shown in figure 4.9, \tilde{P}_T overestimates P_T by a factor of 4, 2.6 and 2.2 when $V_\alpha = 0$. The estimate is more accurate when the steepness of asymmetric wedge potential ΔV increases. The value of \tilde{P}_T overestimates (slightly) that of P_T because all translocation are slow events but not all slow events are translocation.

\tilde{P}_T generally provides the probability that a sugar molecule occupies the channel for a time much greater than that which is required for initial backwards escape. This parameter does not indicate whether a molecule will be translocated. In fact, if we make extreme choices for the potential V_α then we can produce a large difference between \tilde{P}_T and P_T . It happens that $\tilde{P}_T \gg P_T$ and $P_T \ll 1$ for the effective potentials V_α that pose large barriers for translocation. However, if we consider the biological function of the protein channel, which is designed to transfer sugar molecules, it seems unlikely that translocation would be prevented by a large energy barrier. Rather, if the potential V_α

is chosen reasonably, then $\tilde{P}_T \gtrsim P_T$ are in good agreement. This can support our claim that the probability of translocation can be found from \tilde{P}_T .

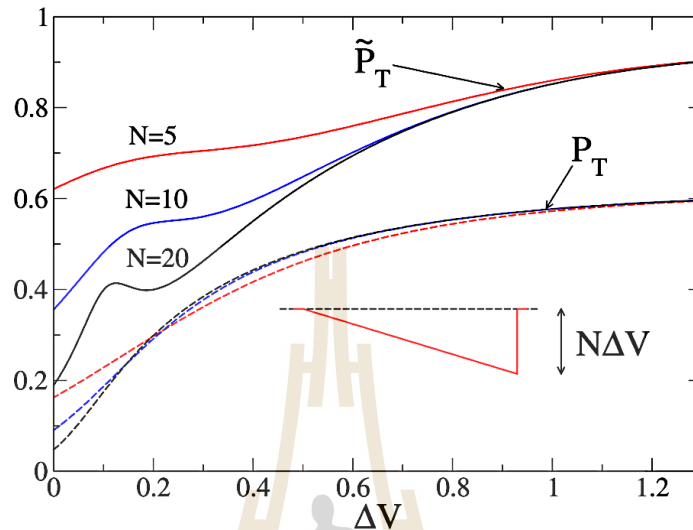


Figure 4.9 The calculations of P_T (dash lines) and \tilde{P}_T (solid lines) varied with the wedge steepness for an asymmetric wedge potential when $N = 5, 10$ and 20 (from top to bottom lines).

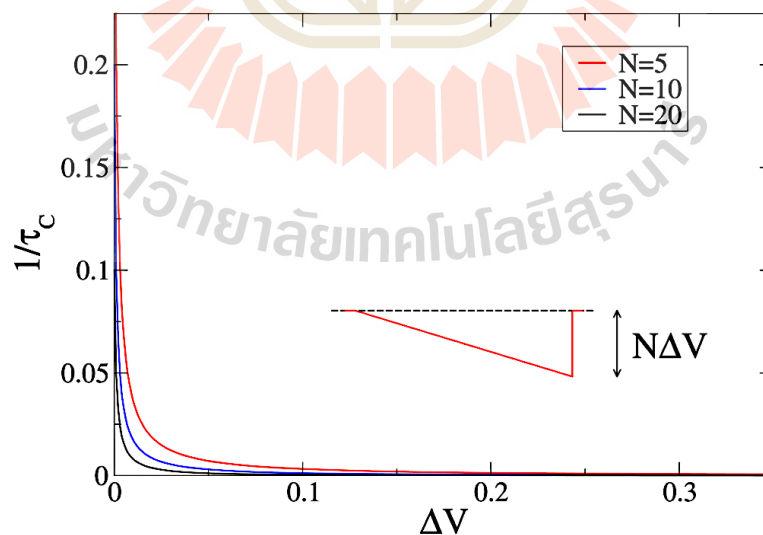


Figure 4.10 The inverse of the average time that the channel remains blocked versus the wedge steepness for an asymmetric wedge potential. $N = 5, 10, 20$ (from top to bottom line).

4.4 The comparison of the translocation probability from different chitosugars

In this section, the results of $k_{\text{on}}[c]$, τ_C and \bar{P}_T in different *EcChiP* channel samples are discussed and the single-molecule dynamics is compared for different-sized sugar molecules—namely chitohexaose and chitopentaose. The results of τ_C , $U(t)$ and $k_{\text{on}}[c]$ are shown in figure 4.11, 4.12 and 4.13, respectively and the de-trapping function $B(t)$ results are shown in figure 4.14 and 4.15. The results were obtained by introducing either chitohexaose and chitopentaose to one chamber with $|V| = 100$ mV.

4.4.1 The comparisons of average residence time and trapping rate in different channel samples and different lengths of sugar molecule

The residence time τ_C , found by linear fitting for one sample, is approximately independent of sugar concentration $[c]$. The value of τ_C for chitohexaose is around five times larger than for chitopentaose. Also, τ_C is slightly larger when sugar is added to the *cis* chamber. By comparing three *EcChiP* channels, the results are qualitatively the same ($[c]$ -independent) but differ over a range of about 30%. This is not surprising, the channels are extremely large molecules embedded in the lipid membrane, so channel characteristics are expected to vary for different channel insertions. The trapping rates $k_{\text{on}}[c]$ for the three samples differ by about 30% (at the same concentration) with sugar in the *cis* chamber and by even more with sugar in the *trans* chamber. Also, $k_{\text{on}}[c]$ changes linearly with $[c]$ as expected. The values of $k_{\text{on}}[c]$ for chitohexaose and chitopentaose are not significantly different. These results show that the difference in the channel samples is the largest source of uncertainty in trying

A

B

C

D

Figure 4.11 The average residence time τ_c in different channel samples and in various sugar concentration $[c]$. (A) and (B) The chitopentaose was introduced to *cis* and *trans* chambers, respectively. (C) and (D) The chitohexaose was introduced to *cis* and *trans* chambers, respectively.

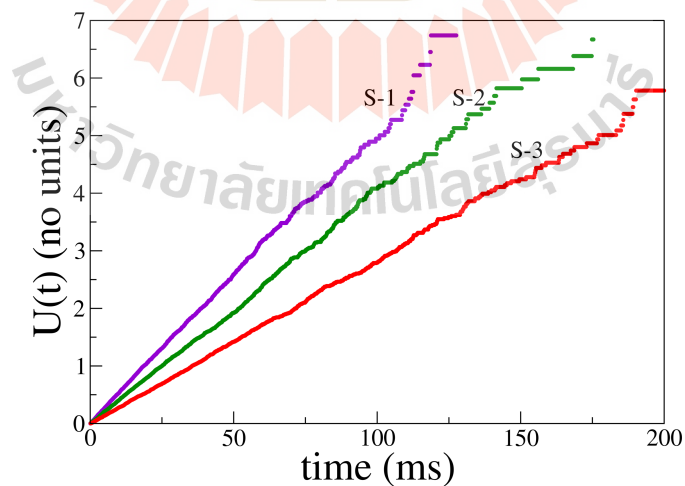


Figure 4.12 The trapping function $U(t)$ from three channel samples with adding 10 μM chitohexaose on *cis* chamber.

A

B

C

D

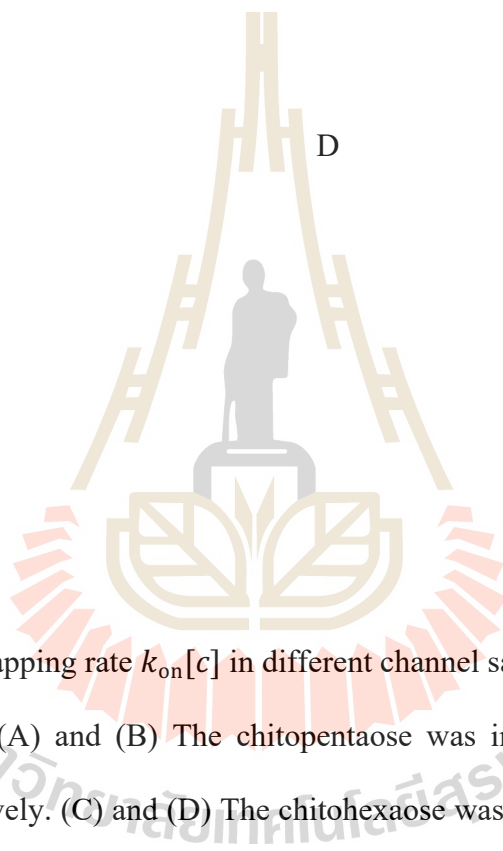


Figure 4.13 The trapping rate $k_{\text{on}}[c]$ in different channel samples and in various sugar concentration $[c]$. (A) and (B) The chitopentaose was introduced to *cis* and *trans* chambers, respectively. (C) and (D) The chitohexaose was introduced to *cis* and *trans* chambers, respectively.

to understand the characteristics of a given channel. Also, they show that the channel is approximately equally effective at trapping chitohexaose and chitopentaose.

4.4.2 The comparison of translocation probability in different channel samples and different length of sugar molecule

The de-trapping function $B(t)$ with chitohexaose added to the *cis* chamber and the de-trapping function with chitopentaose added to the *cis* chamber, both at $|V| = 100$ mV, are compared in figure 4.14. The de-trapping functions are approximately $[c]$ -independent, so we chose $[c]$ values that give largest useable time-ranges for these functions and the least noisy data. The probability $f_1(t)$ decreases rapidly at low $[c]$, when the total sample size of events is small, so higher $[c]$ is more convenient. The results for high $[c]$ are shown in figure 4.14B. There are clear differences in the plots for sugar introduced to different chambers and for different channel samples. But, qualitatively, the results are the same regardless of these details.

The slope of $B(t)$ in the long-time region is similar for chitohexaose and chitopentaose. In the small-time regime, the $B(t)$ function increases much more rapidly for chitopentaose than it does for chitohexaose. This results in \bar{P}_T being much larger for chitohexaose compared to chitopentaose. From the results shown in figure 4.14B, $B_\infty(0)$ of chitohexaose and chitopentaose are about 1.6 and 3.8, respectively. So \bar{P}_T of chitohexaose and chitopentaose are approximated to be 0.2 and 0.02, respectively.

The rapid escape probability of chitopentaose is high when it is trapped within the *EcChiP* channel. The chitohexaose molecules are less likely to escape so rapidly and have a high probability to occupy the channel for a time longer than 10 ms or so. Under the assumption $P_T \approx \bar{P}_T$, chitohexaose is expected to be transported through the channel ten times more rapidly at low $[c]$ according to $Q_T = k_{\text{on}}[c]P_T/(1 +$

K). It is noteworthy that, within this picture, the *EcChiP* channel transports chitohexaose more effectively because it permits less chitohexaose molecules to escape (rapidly) backwards.

A

B

Figure 4.14 The de-trapping function $B(t)$ versus time t with chitohexaose and chitopentaose addition on *cis* chamber. (A) Sugar concentration $[c] = 2.5, 5$ and $10 \mu\text{M}$. (B) Sugar concentration $[c] = 10 \mu\text{M}$.

A

B

มหาวิทยาลัยเทคโนโลยีสุรนารี

Figure 4.15 The de-trapping function $B(t)$ versus time t with $10 \mu\text{M}$ chitohexaose addition in three channel samples. (A) Chitohexaose was added on *cis* chamber. (B) Chitohexaose was added on *trans* chamber.

4.5 Voltage-dependent trapping dynamics for neutral chitohexaose

Chitohexaose is not a charged molecule; however, the measured $B(t)$ function is dependent on applied voltage. The voltage dependence is different to that seen for the charged chitosan hexaose molecule. Indeed, the de-trapping function for the neutral molecule appears to be sensitive to the magnitude of the applied voltage but not its sign (i.e. polarity). This voltage dependence of chitohexaose translocation came as a surprise, since we expected the neutral molecule to be little affected by the voltage. To interpret the $|V|$ -dependence, we developed the theoretical picture that was discussed briefly in a previous chapter. We consider the V -dependence of chitohexaose translocation here in more detail.

The plot of the data, with sugar on either the *cis* and *trans* chamber, is shown in figure 4.16. The plots appear to exhibit a rough mirror symmetry in the $k_{\text{on}}[c]$ qualitative results dependence. Recalling that changing sugar from the *cis* to *trans* sides is equivalent to switching the polarity of the applied voltage, it appears that the trapping depends on $|V|$, the magnitude of the voltage. While the data is rough, it looks like the trapping rate would have its smallest value at zero voltage. (We cannot do the measurement at zero voltage since we are detecting changes in the ion current—but the extrapolation of our finite- V results gives this impression.) Moreover, $k_{\text{on}}[c]$ has its largest value when the electric field is large and in the same direction as the molecular diffusion current ($V < 0$ for sugar in the *cis* chamber and $V > 0$ for sugar in the *trans* chamber). The results in figure 4.17 shows that τ_c decreases with $|V|$.

A

B

Figure 4.16 The trapping rate $k_{\text{on}}[c]$ versus V . In (A) and (B) $5 \mu\text{M}$ chitohexaose was introduced to *cis* chamber and *trans* chamber, respectively.

A

B

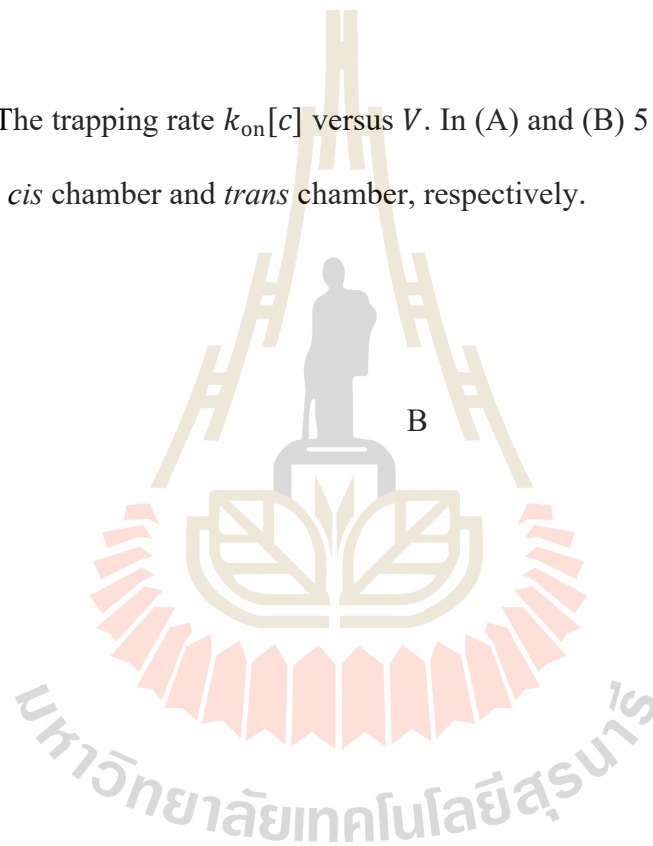


Figure 4.17 The average residence time τ_c versus V . In (A) and (B) $5 \mu\text{M}$ chitohexaose was introduced to *cis* chamber and *trans* chamber, respectively.

The experimental data obtained with chitohexaose on the *cis* side and that with it on the *trans* side, for an applied voltage $\pm 25, \pm 50, \pm 75, \pm 100, \pm 125$ and ± 150 mV were analyzed. The results of the de-trapping function $B(t)$ are shown in figure 4.18. From the plots, the $B(t)$ curves are dependent on applied voltage but the escape rate $B'(t)$ in the long-time region is approximately independent of voltage. The dependence occurs at small times. $B'(t)$ at small times increases with the magnitude of the applied voltage. Consequently, \bar{P}_T decreases with $|V|$ when $\bar{P}_T = \exp[-B_\infty(0)]$ as shown in figure 4.19.

For chitohexaose translocation, the dependence of $B'(0)$ on $|V|$ in small-time regime suggests an induced polarization effect. The electric field in the channel with the length $a \approx 4$ nm is supposed to be large and constant: $|\vec{E}| \approx V/a$, so we suppose that it results in some average polarization density $P = \epsilon_0 \chi E$ within the channel. If the polarization of a channel blocked by a sugar molecule is different from an open channel, then there will be a change in electrostatic energy is when the channel becomes unblocked, given by

$$\Delta E = -\epsilon_0 \chi_c \left(\frac{V}{a}\right)^2 \Delta \Omega \quad (4.12)$$

where $\Delta \Omega$ is a parameter with the dimension of volume that is used to account for the polarization change. (Any change in the susceptibility $\Delta \chi$ can be absorbed into $\Delta \Omega$ then $\Delta \chi \approx \chi_c \Delta \Omega$ where χ_c is the electric susceptibility for closed-channel state).

The reaction rate $B'(0)$ of changing the state from a closed to channel is determined, according to reaction-rate theory, by a Boltzmann factor dependent on the energy difference between these states. That is, we expect the reaction rate to be given by the Arrhenius equation as given in equation 4.13.

$$B'(0)|_V \approx B'(0)|_{V=0} \exp\left(\frac{CV^2}{k_B T}\right) \quad (4.13)$$

where $C = \frac{\epsilon_0 \chi_c}{a^2} \Delta\Omega$ is a constant. For positive $\Delta\Omega$ values, equation 4.13 predicts that the rapid escape rate $B'(0)|_V$ will increase with $|V|$.

A

B

C

D

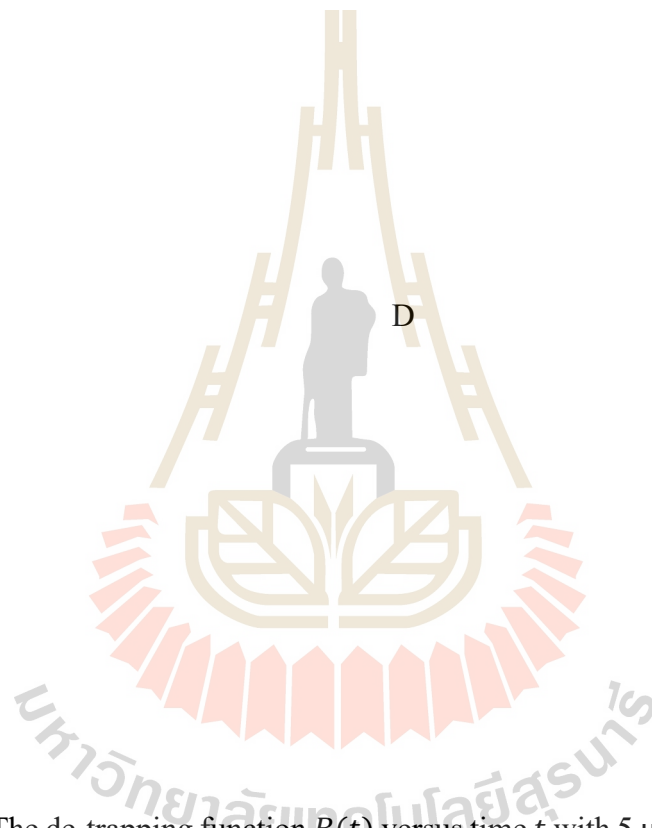


Figure 4.18 The de-trapping function $B(t)$ versus time t with $5 \mu\text{M}$ chitohexaose when $|V| = 25, 50, 75, 100, 125$ and 150 . (A) The chitohexaose was introduced to *cis* chamber when $V > 0$ mV. (B) Same as (A) but $V < 0$ mV. (C) and (D) are same as (A) and (B), respectively but the chitohexaose was introduced to *trans* chamber.

A

B

Figure 4.19 The translocation probability \tilde{P}_T versus V . (A) 5 μM chitohexaose was introduced to *cis* chamber. (B) 5 μM chitohexaose was introduced to *trans* chamber

It is suggested by Schwarz and his team that a V -dependent τ_c of sugar translocation by LamB may be from a transition of an open monomer to a different configuration with a reduced sugar-binding affinity (i.e., a gating transition) in addition to a dipole energy effect (Schwarz *et al.*, 2003). If the ion conductance of different configurations is different, then the ion current would not follow the Ohm's law. This is not consistent with our results, since the ion current does obey Ohm's law as shown in figure 4.20, so our results do not appear compatible with this suggestion.

At long-time regime, the escape rate λ_1 (the slope of $B(t)$ function) is approximately independent of $|V|$. When a sugar molecule moves deeper inside the channel, it is not susceptible to backwards escape anymore. If the molecule travels to the opposite chamber, then the final escape rate would be enhanced by $|V|$. However, if the passage through the channel on the way to translocation (as opposed to the final escape from the far end of the channel) is rate-limiting, then the escape rate λ_1 would be independent of voltage. Thus, the results appear to be compatible with this rough theoretical picture. (One might also consider that a molecule that just entered the channel could be ‘hanging out’ of the channel into the ambient solution, and thus susceptible to different electrostatic considerations than a molecule deep within the channel.)

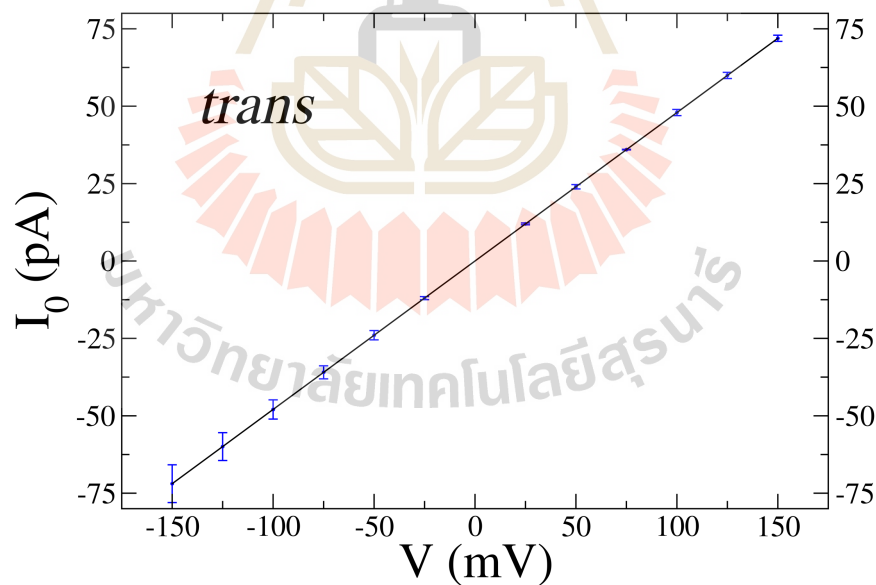


Figure 4.20 The average current I_0 when an *EcChiP* channel is unblocked versus applied voltage V . $2.5 \mu\text{M}$ of Chitohexaose is added on *trans* chamber. The plot follows Ohm's law that $I = GV$ where G is conductance. The graph fitting gives G is equal to 0.48 nS .

4.6 Discussion

The trapping function $U(t)$ is derived from the probability that a channel remains open for time greater than t , $f_0(t)$, as $U(t) = -\ln(f_0(t))$. Our results of chitohexaose translocation show that this function changes linearly with t , so $f_0(t)$ is a single exponential and the statistics of trapping can be characterized by a single value. A slope of $U(t)$ versus t is $U'(t) = k_{\text{on}}[c]$ which is a $[c]$ -dependent trapping rate and k_{on} is approximately constant with varying $[c]$. This rate depends on the applied voltage V but it is roughly the same whether sugar addition is on *cis* or *trans* sides. The value of k_{on} is of order $2 \times 10^5 \text{ M}^{-1}\text{s}^{-1}$ for $V = 100 \text{ mV}$. This value is close k_{on} for one monomer of *VhChiP*.

The de-trapping function $B(t)$ is derived from the probability that a channel remains close for time greater than t , $B(t) = -\ln f_1(t)$, and behaves very differently than $U(t)$. The slope of $B(t)$ is not constant with t , so $B(t)$ is not linear and $f_1(t)$ is not a single exponential. This means the statistics of escaping requires more than one parameter (the value of τ_C or its inverse $k_{\text{off}} = 1/\tau_C$ is not sufficient) to characterize it. The shortest duration of events that can be measured in our setup is t_{min} . The escape rate for a molecule trapped for only t_{min} is of order 1 ms^{-1} . A molecule that has already been in the channel for tens of milliseconds exhibits a much slower escape rate of $\lambda_1 \approx 10 \text{ s}^{-1}$.

The average time that a chitohexaose molecule remains bound τ_C varies from sample to sample. Our results show that τ_C depends on applied voltage V . For $V = -100 \text{ mV}$, τ_C is of order 20 ms. The results are not much different between sugar added on the *cis* and *trans* sides. When τ_C is combined with k_{on} as $k_{\text{on}}\tau_C$, the value of $k_{\text{on}}\tau_C$ is of order 10^5 M^{-1} .

The results of $B(t)$ provide that $f_1(t)$ is not a single exponential function. This means that a model of the channel with a single trapping configuration is not sufficient to account for the behavior. We had to consider models with multiple trapping configurations. These are hidden-Markov models because we cannot see, by measuring the current, which configuration the system is in. We see only that the channel is blocked.

As a model capable of explaining the non-linear $B(t)$ function, we used a one dimensional lattice of trapping sites that a sugar molecule encounters in series. The molecule makes a random walk through this series of trapping sites. We suppose that there are N trapping sites located along the channel length. Solving the mathematical model, we find N different escape rates (these escape rates are eigenvalues of the corresponding rate equation—they correspond to particular walks involving moving in and out of individual trapping sites). Thus the probability $f_1(t)$ can be written as a weighted sum over many N exponentials, each with a different decay rate. The de-trapping function $B(t)$ is non-linear and, in fact, in qualitative agreement with the experimental data. At small t , $B(t)$ increases rapidly since the immediate backwards escape rate is high. For longer t , a molecule moves deeper into the channel, so it is more difficult to escape. This causes the reduction of the escape rate. However, the molecule can move to both *cis* and *trans* chambers. At long- t , $B(t)$ shows the linear relation with t . Therefore, $f_1(t)$ in this t regime is a single exponential with the escape rate λ_1 . If this one-dimensional model is applicable, we can possibly estimate the probability of translocation from $B(t)$ versus t graph.

We mention that the transition probability P_T cannot be directly obtained from the current data; however, P_T can be inferred from $I(t)$ data based on these three points.

(i) $B(t)$ is dependent on t and the behavior of $B(t)$ is consistent with the multiple trapping configuration model that predicts backwards escape at small t and translocation at long t . (ii) $B(t)$ from charged chitosan hexaose experiments is also dependent on t in the same way as seen in the neutral chitohexaose experiments—but for the charged molecules we can control which way molecules move using the applied potential. The small- t behavior of $B(t)$ for charged chitosan is dominated by backwards escape. It is plausible, then, that a similar interpretation for the neutral chitohexaose is correct. (iii) An *EcChiP* channel in *E. coli* can be expressed when it is surrounded by the environment lacking any nutritional source but chitosugar. The average binding characteristics k_{on} and τ_C of this channel are similar to these parameters of other chitosugar transport, so it is likely that the translocation of chitohexaose occurs with the reasonable efficiency. By combining these points, we imply that there is translocation happening only at long t and the translocation probability P_T is similar to the parameter \tilde{P}_T , which can be obtained from the experimental data.

CHAPTER V

CONCLUSION

In this study, we looked at properties of the *EcChiP* channel, which is a monomeric protein channel used by bacteria to translocate chitosugars inside their cell bodies from the environment. This particular channel is associated with a gene that is usually silent in *E. coli*. Under normal circumstances, the *E. coli*. rely on glucose in their environment and use glucose-specific channels to uptake this sugar. But in a bacteria population deprived of glucose, the silent gene for *EcChiP* will be expressed and the bacteria will start to use this channel to uptake chitosugars, an alternative nutritional source.

We looked at the electric current $I(t)$ carried by ions in solution that flowed through a single *EcChiP* channel in an artificial cell membrane. With chitosugars in the solution, the current $I(t)$ reveals the motion of single sugar molecules: when a molecule becomes trapped in the channel the current drops and when the molecule escapes, i.e. is 'de-trapped', from the channel the current is recovered.

To interpret the $I(t)$ data we introduced a trapping function, $U(t)$ and de-trapping function $B(t)$. The trapping function is the logarithm of the probability that the channel remains open (and the current large) for longer than time t while the de-trapping function is the logarithm of the probability that the channel remains blocked longer than t . The slope $dU(t)/dt$ is the rate at which a channel that has been unblocked for time t will trap a sugar molecule, while $dB(t)/dt$ is the rate at which a channel blocked for

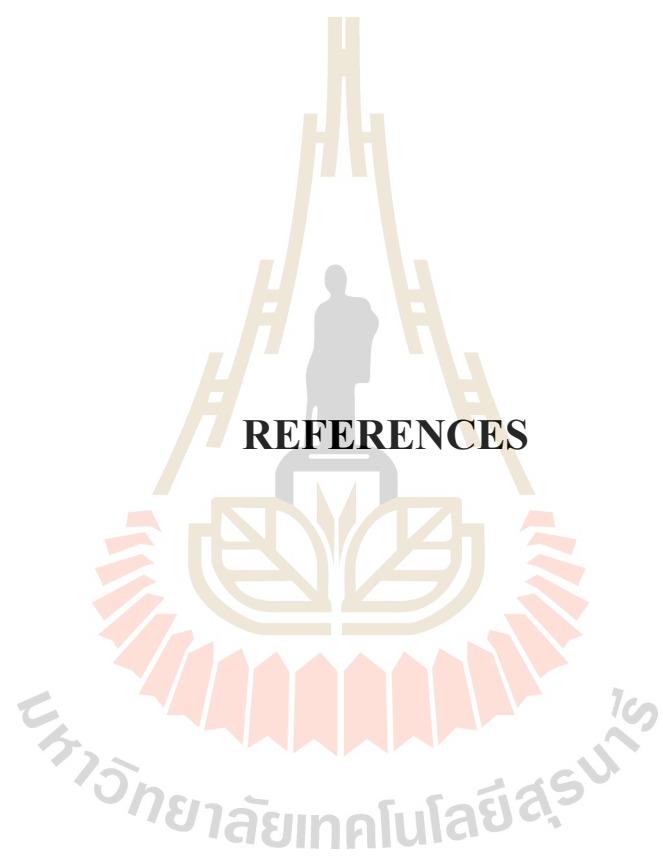
time t will de-trap the molecule.

We found that $U(t)$ is linear in time, so there is a single trapping rate $U'(t) = k_{on}[c]$ that increases with sugar concentration $[c]$. The trapping rate we found is similar to that observed in comparable channels. The de-trapping function $B(t)$ is non-linear: it increases rapidly at small times then flattens out, becoming linear with a relatively small slope λ_1 at long times. This means that there are many different de-trapping rates $B'(t)$, the slowest among them being λ_1 . The rate at which a sugar molecule escapes decreases with time (i.e. molecules long held captive have the lowest escape rate).

In trying to understand the $B(t)$ behavior, especially that obtained for charged chitosan molecules where the motion of the sugar can be controlled by an applied voltage, we suggested that the rapid increase of $B(t)$ at small- t is dominated by backwards escape processes: the sugar retreats to the side of the channel from which it entered. Translocation events, where the sugar properly moves from one channel end to the other, likely occur at long- t with an associated rate λ_1 .

This picture is supported not only by the data itself (e.g. an applied forward bias pushing charged sugar molecules through the channel resulted in a *decrease* in the small-time escape rate, which is only possible if the latter was mainly backwards escape) but by the results of a random-walk simulation, in which the channel is modeled as a 1D series of trapping sites through which a sugar molecule moves. Its significance is that it means it is possible to obtain an indirect experimental measure of P_T , the probability that sugar translocates through the channel rather than escaping backwards, from the current data. This parameter is a key property determining the efficacy of the channel, i.e. the rate Q_T of sugar transport through the channel, which is not directly observable in the experiment.

Our proposal is that the extrapolated linear intercept of the $B(t)$ curve provides a reasonable probability of the translocation probability P_T . In the context of model calculations, the intercept actually tells us the probability that a sugar molecule will escape the channel via the slowest of all escape processes (as opposed to escaping via a faster mechanism). But the data on charged chitosan, along with plausible assumptions about the channel itself, make it clear that backward-escape processes are faster than translocation. Backwards escape can occur immediately after trapping, whereas translocation is delayed by the time required for passage through the long narrow channel. Thus, slow escape is suggestive of successful escape, i.e. translocation. We used this line of reasoning to study various properties of the exotic channel *EcChiP*, including its specificity to different-sized chitosugars and its dependence on applied potential. Moreover, our analysis is quite general, being based on extremely simple models, with a minimal number of assumptions. It can likely be applied to understand other problems in channel transport.



REFERENCES

REFERENCES

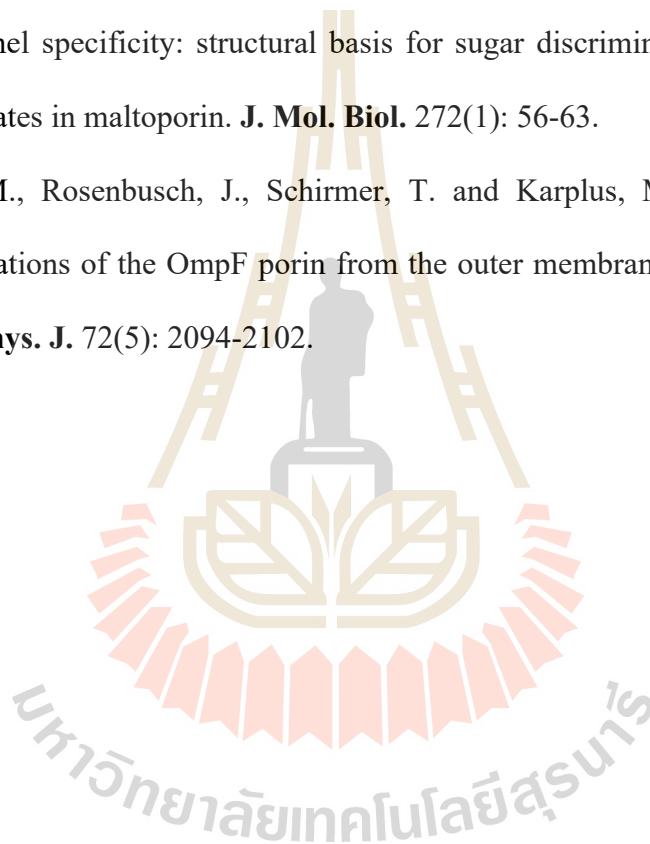
- Andersen, C., Cseh, R., Schülein, K. and Benz, R. (1998). Study of sugar binding to the sucrose-specific ScrY channel of enteric bacteria using current noise analysis. **J. Membr. Biol.** 164(3): 263-274.
- Andersen, C., Jordy, M. and Benz, R. (1995). Evaluation of the rate constants of sugar transport through maltoporin (LamB) of *Escherichia coli* from the sugar-induced current noise. **J. Gen. Physiol.** 105(3): 385.
- Benz, R., Schmid, A. and Vos-Scheperkeuter, G. H. (1987). Mechanism of sugar transport through the sugar-specific LamB channel of *Escherichia coli* outer membrane. **J. Membr. Biol.** 100(1): 21-29.
- Brun, L., Pastoriza-Gallego, M., Oukhaled, G., Mathe, J., Bacri, L., Auvray, L. and Pelta, J. (2008). Dynamics of polyelectrolyte transport through a protein channel as a function of applied voltage. **Phys. Rev. Lett.** 100(15): 158302.
- Dutzler, R., Wang, Y. F., Rizkallah, P. J., Rosenbusch, J. P. and Schirmer, T. (1996). Crystal structures of various maltooligosaccharides bound to maltoporin reveal a specific sugar translocation pathway. **Structure** 4(2): 127-134.
- Griffiths, D. J. (1999). **Introduction to electrodynamics**. 3rd ed. New Jersey: Prentice Hall.
- Guillier, M., Gottesman, S. and Storz, G. (2006). Modulating the outer membrane with small RNAs. **Genes Dev.** 20(17): 2338-2348.

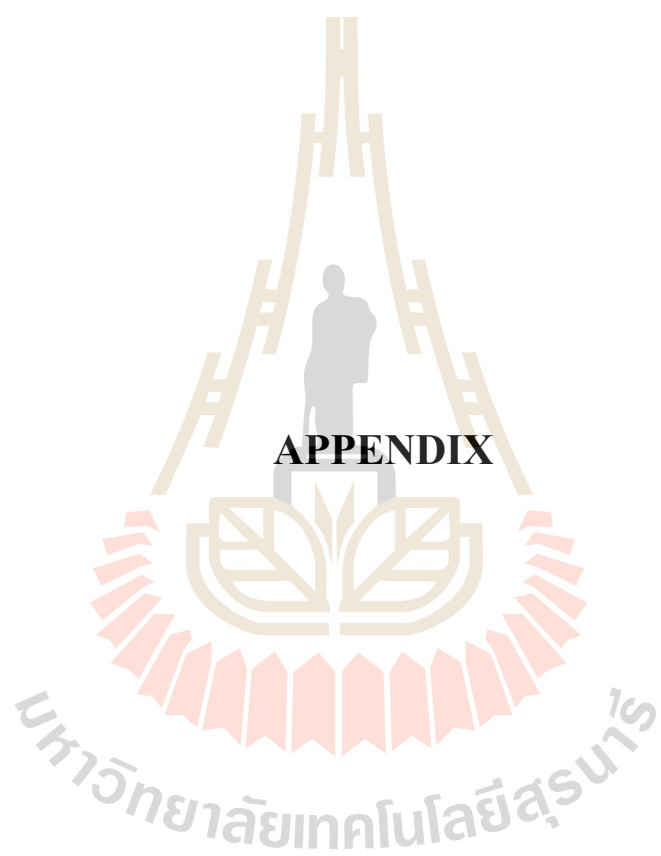
- Gumbart, J., Khalili-Araghi, F., Sotomayor, M. and Roux, B. (2012). Constant electric field simulations of the membrane potential illustrated with simple systems. **Biochim. Biophys. Acta.** 1818(2): 294-302.
- Hänggi, P., Talkner, P. and Borkovec, M. (1990). Reaction-rate theory: fifty years after Kramers. **Reviews of Modern Physics** 62(2): 251-341.
- Hilty, C. and Winterhalter, M. (2001). Facilitated substrate transport through membrane proteins. **Phys. Rev. Lett.** 86(24): 5624-5627.
- Im, W. and Roux, B. (2002). Ion permeation and selectivity of OmpF porin: a theoretical study based on molecular dynamics, brownian dynamics, and continuum electrodiffusion theory. **J. Mol. Biol.** 322(4): 851-869.
- Jackson, M. B. (2006). **Molecular and Cellular Biophysics**. Cambridge: Cambridge University Press.
- Kasianowicz, J. J., Brandin, E., Branton, D. and Deamer, D. W. (1996). Characterization of individual polynucleotide molecules using a membrane channel. **Proceedings of the National Academy of Sciences** 93(24): 13770-13773.
- Keyhani, N. O., Li, X. B. and Roseman, S. (2000). Chitin catabolism in the marine bacterium *Vibrio furnissii*. **J. Biol. Chem.** 275(42): 33068-33076.
- Kullman, L., Gurnev, P. A., Winterhalter, M. and Bezrukov, S. M. (2006). Functional subconformations in protein folding: evidence from single-channel experiments. **Phys. Rev. Lett.** 96(3): 038101.
- Mizuno, T., Chou, M. Y. and Inouye, M. (1984). A unique mechanism regulating gene expression: translational inhibition by a complementary RNA transcript

- (micRNA). **Proceedings of the National Academy of Sciences of the United States of America** 81(7): 1966-1970.
- Nikaido, H. (1993). Transport across the bacterial outer membrane. **J. Bioenerg. Biomembr.** 25(6): 581-589.
- Nikaido, H. (2003). Molecular basis of bacterial outer membrane permeability revisited. **Microbiol. Mol. Biol. Rev.** 67(4): 593-656.
- Rasmussen, A. A., Johansen, J., Nielsen, J. S., Overgaard, M., Kallipolitis, B. and Valentin-Hansen, P. (2009). A conserved small RNA promotes silencing of the outer membrane protein YbfM. **Mol. Microbiol.** 72(3): 566-577.
- Richter, M. F., Drown, B. S., Riley, A. P., Garcia, A., Shirai, T., Svec, R. L. and Hergenrother, R. L. (2017). Predictive compound accumulation rules yield a broad-spectrum antibiotic. **Nature** 545(7654): 299-304.
- Saravolac, E. G., Taylor, R. L., Benz, R. and Hancock, R. E. (1991). Purification of glucose-inducible outer membrane protein OprB of *Pseudomonas putida* and reconstitution of glucose-specific pores. **J. Bacteriol.** 173(16): 4970-4976.
- Schirmer, T. (1998). General and specific porins from bacterial outer membranes. **J. Struct. Biol.** 121(2): 101-109.
- Schirmer, T., Keller, R. E., Wang, Y. F. and Rosenbusch, J. P. (1995). Structural basis for sugar translocation through maltoporin channels at 3.1 Å resolution. **Science** 267(5197): 512.
- Schüleln, K., Schmid, K. and Benzl, R. (1991). The sugar-specific outer membrane channel ScrY contains functional characteristics of general diffusion pores and substrate-specific porins. **Mol. Microbiol.** 5(9): 2233-2241.

- Schwarz, G., Danelon, C. and Winterhalter, M. (2003). On translocation through a membrane channel via an internal binding site: kinetics and voltage dependence. **Biophys. J.** 84(5): 2990-2998.
- Soysa, H. S. M. and Suginta, W. (2016). Identification and functional characterization of a novel OprD-like chitin uptake channel in non-chitinolytic bacteria. **J. Biol. Chem.** 291(26): 13622-13633.
- Soysa, H. S. M., Schulte, A. and Suginta, W. (2017). Functional analysis of an unusual porin-like channel that imports chitin for alternative carbon metabolism in *Escherichia coli*. **J. Biol. Chem.** 292(47): 19328-19337.
- Suenaga, A., Komeiji, Y., Uebayasi, M., Meguro, T., Saito, M. and Yamato, I. (1998). Computational observation of an ion permeation through a channel protein. **Biosci. Rep.** 18(1): 39-48.
- Suginta, W., Chumjan, W., Mahendran, K. R., Janning, P., Schulte, A. and Winterhalter, M. (2013a). Molecular uptake of chitooligosaccharides through chitoporin from the marine bacterium *Vibrio harveyi*. **PLoS One** 8(1): e55126.
- Suginta, W., Chumjan, W., Mahendran, K. R., Schulte, A. and Winterhalter, M. (2013b). Chitoporin from *Vibrio harveyi*, a channel with exceptional sugar specificity. **J. Biol. Chem.** 288(16): 11038-11046.
- Suginta, W. and Smith, M. F. (2013). Single-molecule trapping dynamics of sugar-uptake channels in marine bacteria. **Phys. Rev. Lett.** 110(23): 238102.
- Suginta, W., Winterhalter, M. and Smith, M. F. (2016). Correlated trapping of sugar molecules by the trimeric protein channel chitoporin. **BBA-Biomemb.** 1858(12): 3032-3040.

- Szmelcman, S. and Hofnung, M. (1975). Maltose transport in *Escherichia coli* K-12: involvement of the bacteriophage lambda receptor. **J. Bacteriol.** 124(1): 112-118.
- Vogel, J. and Papenfort, K. (2006). Small non-coding RNAs and the bacterial outer membrane. **Curr. Opin. Microbiol.** 9(6): 605-611.
- Wang, Y. F., Dutzler, R., Rizkallah, P. J., Rosenbusch, J. P. and Schirmer, T. (1997). Channel specificity: structural basis for sugar discrimination and differential flux rates in maltoporin. **J. Mol. Biol.** 272(1): 56-63.
- Watanabe, M., Rosenbusch, J., Schirmer, T. and Karplus, M. (1997). Computer simulations of the OmpF porin from the outer membrane of *Escherichia coli*. **Biophys. J.** 72(5): 2094-2102.



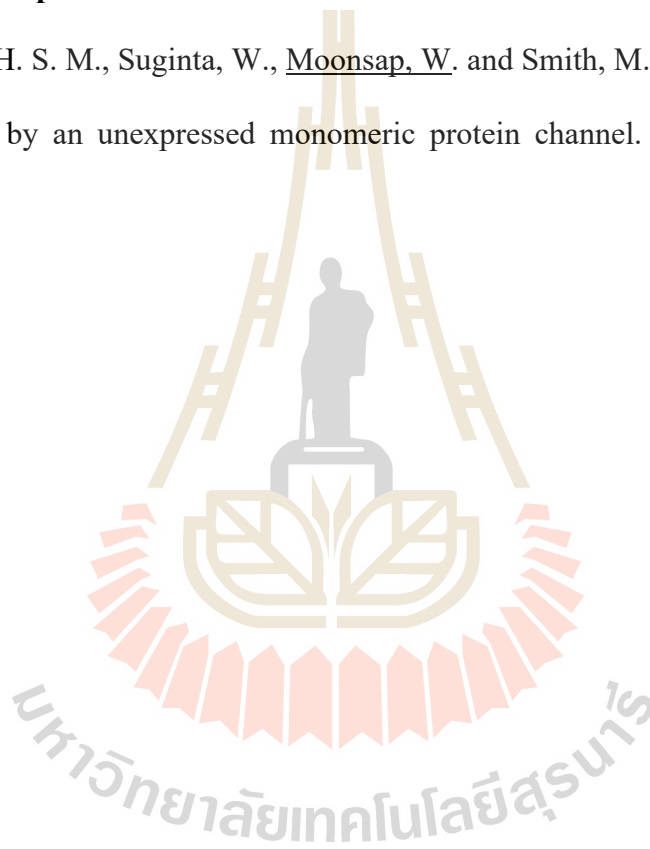


APPENDIX

PUBLICATION

Publication outputs:

Soysa, H. S. M., Suginta, W., Moonsap, W. and Smith, M. F. (2018). Chitosugar translocation by an unexpressed monomeric protein channel. **Phys. Rev. E** 97(5): 05241.



Chitosugar translocation by an unexpressed monomeric protein channel

H. Sasimali M. Soysa and Wipa Suginta

Biochemistry-Electrochemistry Research Unit, School of Chemistry, Institute of Science, Center of Excellence in Advanced Functional Materials, Suranaree University of Technology, Nakhon Ratchasima 30000, Thailand

Watcharaporn Moonsap and M. F. Smith

School of Physics, Institute of Science, Suranaree University of Technology, Nakhon Ratchasima 30000, Thailand

 (Received 26 December 2017; revised manuscript received 24 March 2018; published 31 May 2018)

The outer membrane protein channel *EcChiP*, associated with a silent gene in *E. coli*, is a monomeric chitoporin. In a glucose-deficient environment, *E. coli* can express the *ChiP* gene to exploit chitin degradation products. Single-channel small ion current measurements, which reveal the dynamics of single sugar molecules trapped in channel, are used here to study the exotic transport of chitosugars by *E. coli*. Molecules escape from the channel on multiple timescales. Voltage-dependent trapping rates observed for charged chitosan molecules, as well as model calculations, indicate that the rapid escape processes are those in which the molecule escapes back to the side of the membrane from which it originated. The probability that a sugar molecule is translocated through the membrane is thus estimated from the current data and the dependence of this translocation probability on the length of the chitosugar molecule and the applied voltage analyzed. The described method for obtaining the translocation probability and related molecular translocation current is applicable to other transport channels.

DOI: [10.1103/PhysRevE.97.052417](https://doi.org/10.1103/PhysRevE.97.052417)

I. INTRODUCTION

Gram-negative bacteria ingest sugar through their outer membrane using outer membrane protein (OMP) channels that can be solute specific [1–6]. *Escherichia coli* bacteria utilize glucose-enriched nutrients, so they express the protein channel maltoporin (LamB) to transport maltodextrins, which are glucose-containing oligomers [7–10]. LamB is a trimeric channel, composed of three identical monomers, each of which is barrel shaped with a minimum diameter of a few angstroms [11–16]. A structurally similar trimeric channel called chitoporin (*ChiP*) is used by species of marine *Vibrio* including *Vibrio harveyi* to transport chitooligosaccharides, allowing the bacteria to utilize chitin biomaterials [17–25].

Studies of *E. coli* and *Salmonella* have revealed that non-coding small RNA control OMP expression, selecting OMP genes in response to growth and stress conditions [26–28]. An unexpressed chitoporin gene was identified in *E. coli*. In the absence of the appropriate inducer, this gene is kept silent by the action of small RNA [29]. However, if *E. coli* is deprived of maltodextrins and exposed to chitooligosaccharides, the chitoporin *EcChiP* is expressed, allowing the bacteria to access the available substrate [30].

Recently, we identified and characterized *EcChiP* using the black lipid membrane (BLM) reconstitution technique and proved that *EcChiP* can readily form a stable pore (see Fig. 1) in artificial phospholipid membranes [31,32]. Microcalorimetry measurements indicate that chitohexaose, a chitosugar, has a strong affinity to *EcChiP*. In contrast, no binding affinity for maltohexaose was observed. Here we analyze single-channel current measurements, and the associated sugar trapping and escape dynamics, for the *EcChiP* channel.

In the single-channel current measurements [33–36], a potential V is applied across a bilipid membrane perforated

with one protein channel in an electrolyte solution with a concentration $[c]$ of sugar on one side of the membrane. The small-ion current $I(t)$ through the open channel is monitored. Since the current decreases to near zero when a sugar molecule is trapped in the channel, $I(t)$ reveals the single-molecule trapping and escape dynamics.

The $I(t)$ data (Fig. 2) for *EcChiP* fluctuate between two broad levels, one having a mean value I_0 , corresponding to the conductance of the open channel, and the other having a mean I_1 that is essentially zero. In contrast, the current through *VhChiP* and *EcLamB* fluctuates [25,37,38] among four levels $I_n \approx I_0(3 - n)$, where I_n is the mean current through a trimer with n monomers blocked by sugar [34,36]. This indicates that *EcChiP* is a monomer and thus a convenient system to analyze trapping and escape dynamics free from intermonomer correlations [15,25,38].

The monomer is partly characterized by a trapping rate $k_{\text{on}}[c]$ and residence time τ_C , the average time it takes for a trapped sugar molecule to escape the channel. The rate that molecules are transported through the channel Q_T is given by

$$Q_T = k_{\text{on}}[c]P_T(1 + K)^{-1}, \quad (1)$$

where $K = k_{\text{on}}[c]\tau_C$ and it is assumed that no more than one molecule can occupy the channel at a time. The probability P_T that a trapped sugar molecule will be translocated through the channel (as opposed to escaping back to the side of the membrane from which it entered) cannot be obtained directly from the $I(t)$ data. Without some estimate of this parameter, the channel transport efficiency cannot be evaluated.

Below we claim that an estimate of P_T can be obtained from $I(t)$ data. The first step is to extract the probability distribution for the time that molecules remain trapped in the *EcChiP* channel, of which τ_C is the mean. This distribution has a

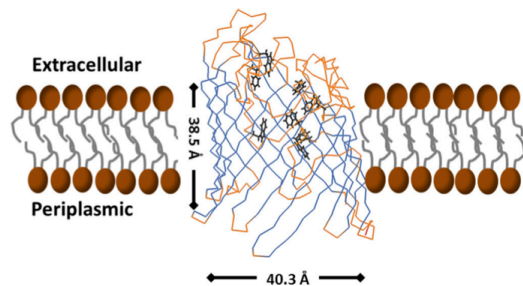


FIG. 1. Illustration of the *EcChiP* channel. The ribbon 3D model was generated by SWISS-MODEL [42] using the unpublished structure of *EcChiP* complexed with chitohexaose as the structure template. The modeled structure was edited and displayed in PyMOL (for education use only version). The β strands are shown in marine blue (for noncolor plots, the strands in the channel bulk), turns and loops in orange (mainly near the extracellular side in noncolor plots), and the amino acid residues that potentially interact with sugar substrate in the channel are shown as sticks (dark gray hexagonal shapes).

characteristic time dependence: It exhibits rapid (submillisecond) escape and much slower (10–100 ms) escape. We associate the rapid rate with backward escape processes. Translocation, which requires molecules to negotiate the angstroms wide, nanometers long monomer, proceeds more slowly. The ability to distinguish rapid escape processes, which are dominated by backward escape, from slow escape processes, which likely include a significant contribution from translocation, makes an inference of P_T possible.

We use this analysis to more fully characterize *EcChiP*. The escape rate of neutral sugar molecules from *EcChiP* is voltage dependent. More precisely, the rapid backward escape rate increases with $|V|$, which lowers transport efficiency. This phenomenon, and other features of trapping and escape processes in *EcChiP*, are studied below.

II. MATERIALS AND METHODS

The single-channel current measurements¹ [39–41] employed a cuvette divided into two chambers that are separated by a 25- μm -thick Teflon barrier with a circular aperture 60–100 μm in diameter. An electrolyte solution, 2.5 ml of 1 M KCl in 20 mM HEPES pH 7.5, is introduced to both chambers and Ag/AgCl electrodes are positioned on respective sides of the barrier. When 2–5 μL of 5 mg mL⁻¹ 1,2-diphytanoyl-*sn*-glycero-3-phosphatidylcholine (Avanti Polar Lipids, Alabaster, AL) in *n*-pentane is added to both chambers, a lipid bilayer forms over the aperture after the lipid concentration in the electrolyte is gently raised and lowered several times by pipetting. To perforate the lipid bilayer with a single channel, 50–100 ng/mL of *EcChiP* is added to one *cis* side of the membrane with a potential ± 100 mV across the artificial

¹All current measurements were performed with an Axopatch 200B amplifier (Molecular Devices, Sunnyvale, CA, USA) in the voltage clamp mode, with the internal filter set at 10 kHz.

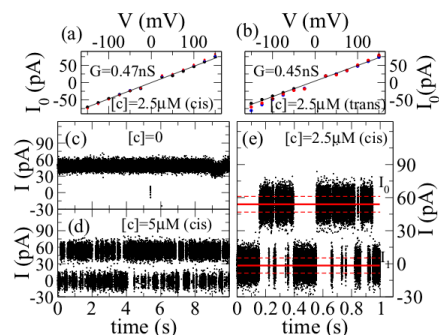


FIG. 2. Current I through a single monomeric channel of *EcChiP* with a concentration $[c]$ of chitohexaose in solution, plotted versus applied voltage V and time t . (a) With a concentration $[c] = 2.5 \mu\text{M}$ on the *cis* side of the channel, the average current I_0 when the channel is unblocked by sugar versus V satisfies Ohm's law with the conductance G indicated. (b) Same as (a) but with sugar on the *trans* side of the channel. (c) Current $I(t)$ with $[c] = 0$ versus time (the range of time is a small fraction of the total measurement duration). Note that $I(t) \approx I_0$ because the channel is always unblocked. (d) Current $I(t)$ with $[c] = 5 \mu\text{M}$ on the *cis* side of the channel. The current changes from $I(t) \approx I_0$ to $I(t) \approx I_1$ when a single sugar molecule blocks the channel. (e) Current $I(t)$ with $[c] = 2.5 \mu\text{M}$ on the *cis* side of the channel. The horizontal solid lines indicate the current averages I_0 (when the monomer is unblocked) and I_1 (blocked). The dashed lines shown are one standard deviation from these averages.

membrane, until a step increase of the ionic current $I(t)$ is observed. The protein solution is then diluted by sequential additions of electrolyte to prevent further channel insertions.

The potential of the electrode in the *cis* chamber, to which *EcChiP* is added, is defined to be zero. A potential V that can be positive or negative is applied to the electrode on the *trans* side. Sugar is added to one side of the membrane, so in some cases the sugar diffusion current flows in the same direction as the electric current and in others it flows against it.

From the raw $I(t)$ data (Fig. 2), it is possible to distinguish states with $I(t) \approx I_0$, when the *EcChiP* monomer is open, from states with $I(t) \approx I_1$, when the monomer is blocked. In the absence of sugar, the current $I(t)$ fluctuates about an average value I_0 . With $V = 100$ mV, we see a mean $I_0 \approx 45$ pA (corresponding to a conductance $G = 0.45$ nS) and standard deviation σ_0 of about 8 pA. When sugar is added, larger fluctuations in $I(t)$ are observed: The current drops to a value near zero [after the current decrease, $I(t)$ fluctuates about an average value I_1 of a few picoamperes with a standard deviation similar to σ_0].

Using the pCLAMP10 software, we record stable events in which $I(t)$ remains near I_j for a time greater than $t_{\min} = 0.1$ ms. If one zooms in on $I(t)$ data to see the transition between I_j levels, the duration of a transition is smaller than t_{\min} by a factor of order unity (when a molecule blocks the channel current, it creates an effective capacitor that requires finite time to charge or discharge). Since $I(t)$ requires time of order t_{\min} to respond to a trapping or escape event, shorter events are unobservable in the experiment.

Regarding the chitosugars used for the current measurements, chitooligosaccharides, including chitopentaose, chito-hexaose, and chitosan hexaose, were purchased from Dextra Laboratories (Science and Technology Centre, Earley Gate, Reading, United Kingdom) and Megazyme (IDA Business Park, Bray, Co., Wicklow, Ireland).

To obtain the structural prediction illustrated in Fig. 1, the amino acid sequence of the EcChiP (UniProtKB entry P75733) was submitted to SWISS-MODEL [42] for tertiary structure prediction using the three-dimensional (3D) structure of *Pseudomonas aeruginosa* OprD (pdb 2odj) as structural template [43]. The annotated structures were edited and displayed in PyMOL [44].

III. RESULTS AND DISCUSSION

A. Single-channel current data and its analysis

The current $I(t)$ passes through a single EcChiP channel embedded in the bilipid membrane. An illustration of the channel appears in Fig. 1. The length of the channel is several nanometers and the diameter of its mouth is similar. The internal structure of the channel, formed from a polypeptide chain with both the N and C terminals on the periplasmic side, is complex. Within the channel interior, the effective diameter is as small as a few angstroms. There are numerous amino acid residues, also shown in Fig. 1, arranged on the outer wall of the channel barrel with others part of extracellular loops. Fluorescence results indicate an interaction between sugar molecules and the tryptophan members, in particular, of the amino acid residues [32].

The structure has significant *cis-trans* asymmetry. In previous studies with *E. coli* LamB [40,43,45,46], it was observed more than 70% of the reconstituted channels are oriented with the extracellular side facing the chamber to which the channel precursor was added. If this tendency holds for the EcChiP channels studied here, then the *cis* end of the channel in typical current measurements should correspond to the extracellular side *in vivo*. This is further suggested by the EcChiP channel structure itself, with long hydrophilic extracellular loops that are likely not amenable to channel insertion. However, we will not assume that the *cis* side of the membrane corresponds to the extracellular solution below, and will compare $I(t)$ data with sugar introduced to each chamber.

In Fig. 2, a one-second segment of a current trace is shown. Transitions between the I_0 and I_1 states are clear. The time-averaged current passing through an open channel I_0 is plotted versus the applied voltage in the presence of chito-hexaose on the *cis* or *trans* sides of the membrane. The current satisfies Ohm's law with $I_0 = GV$ and $G \approx 0.45$ nS with a fitting error of 2% over the range indicated (the error in the time-averaged current and the applied potential are too small to appear on this scale; one expects t - and V -dependent changes in the complex monomer to introduce greater uncertainty). If we write the conductance as $G = (\pi a^2/d)\rho^{-1}$ with a and $d = 4$ nm the effective radius and length of the channel, respectively, and ρ the resistivity of the KCl solution, then we find an effective channel diameter of $2a \approx 0.5$ nm. (This diameter, considerably smaller than that of the channel mouth seen in Fig. 1, corresponds to the narrow channel interior.) In

comparison, an open channel of trimeric *VhChiP* has a larger conductance of 1.6–1.8 nS.

The statistical description of the I_j events can be displayed using a cumulative histogram that counts the number of events with a duration greater than a given t . We define $f_j(t)$ as the fraction of I_j events having a duration greater than t (the height of the cumulative histogram divided by the total number of I_j events). For an infinite number of events, $f_j(t)$ would be a continuous function giving the probability for an I_j event that began at $t = 0$ to survive beyond t . The smooth curves of $f_j(t)$ data approximate this probability. The average trapping rate $k_{\text{on}}[c]$ and residence time τ_C are simply related to $f_0(t)$ and $f_1(t)$,

$$1/k_{\text{on}}[c] = \int_0^\infty dt f_0(t), \quad \tau_C = \int_0^\infty dt f_1(t). \quad (2)$$

Since $f_j(t)$ decreases by orders of magnitude over the time range of interest, it is convenient to introduce logarithms. These logarithms have a simple physical interpretation. The slope $d/dt[-\ln f_0(t)]$ is the instantaneous trapping rate, i.e., the probability rate for a monomer that has been continuously open for time t to become blocked. If this trapping rate is a constant then $\ln f_0(t)$ is linear in time: $\ln f_0(t) = -k_{\text{on}}[c]t$ and thus $f_0(t)$ is a simple exponential $f_0(t) = \exp(-k_{\text{on}}[c]t)$. Similarly, $d/dt[-\ln f_1(t)]$ is the escape rate, the probability rate for a monomer that has been continuously blocked for time t to become unblocked. If the escape rate is constant and equal to k_{off} then $\ln f_1(t) = -k_{\text{off}}t$ with $k_{\text{off}} = 1/\tau_C$ and $f_1(t) = \exp(-k_{\text{off}}t)$.

In all data considered, the initial number of events $N_j(t_{\text{min}})$ varied between several hundred (at low $[c]$) to more than 5000 and decreased according to $N_0(t) = N_0(t_{\text{min}})f_0(t)$ and $N_1(t) = N_1(t_{\text{min}})f_1(t)$. At small t , the sampling error, proportional to $\sqrt{N_j(t)}$, is of order 1% of the measured $N_j(t)$. At large times, the sample size has decreased to a point that the sampling error is a significant fraction of $N_j(t)$. This is reflected by the noisy appearance of $f_1(t)$ at large t . One sees significant variation between $f_1(t)$ curves measured for different EcChiP channels. With regard to prediction of transport properties, this channel-to-channel variance is the greatest source of uncertainty. The probabilities $f_0(t)$ and $f_1(t)$ are defined over a range $t_{\text{min}} < t < t_{\text{max}}$, where $t_{\text{min}} = 0.1$ ms is the threshold for observable events, with $f_0(t_{\text{min}}) = f_1(t_{\text{min}}) = 1$ and t_{max} defined such that at least ten I_j events survive until t_{max} .

B. Trapping and detrapping of sugar by chitoporin

Figure 3 presents experimental results for $f_0(t)$ and $f_1(t)$ obtained with varying chito-hexaose concentration $[c]$ introduced to the *cis* and *trans* chambers. For these data, the applied voltage was fixed at $V = -100$ mV, so the electric current flows from the *cis* to the *trans* chamber. As seen in Fig. 3, the histograms of $f_0(t)$ and $f_1(t)$ are difficult to interpret visually, but their logarithms yield smooth curves that are more convenient to analyze.

The plots of $\ln f_0(t)$ show a linear t dependence, with a slope that increases with sugar concentration $[c]$. The trapping probability $f_0(t)$ is strongly dependent on concentration $[c]$, so $-\ln f_0(t) \approx k_{\text{on}}[c]t$, where the slope $k_{\text{on}}[c]$ increases monotonically with sugar concentration $[c]$.

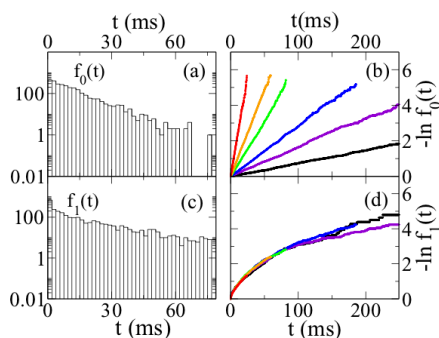


FIG. 3. Channel trapping and escape probabilities versus time t with a concentration $[c]$ of sugar on the *cis* side of the channel. (a) Histogram, for $[c] = 20 \mu\text{M}$, of the probability $f_0(t)$ for the channel to remain unblocked beyond time t given that it became unblocked at $t = 0$. (b) Logarithm of $f_0(t)$. The curves (black, violet, blue, green, orange, and red, from the bottom to the top) show $[c] = 1.25, 5, 10, 20, 40,$ and $80 \mu\text{M}$, respectively. They are linear with a slopes indicating the rate at which sugar molecules are trapped. (c) Histogram, with $[c] = 20 \mu\text{M}$, of the probability $f_1(t)$ for the channel to remain blocked beyond time t after becoming blocked at $t = 0$. (d) Logarithms of $f_1(t)$ for different values of $[c]$ (same values and colors as in (b)); for noncolor plots, the result is approximately $[c]$ independent). The nonlinear curves indicate that sugar molecules can escape the channel at multiple rates.

On the other hand, $\ln f_1(t)$ is approximately $[c]$ independent and nonlinear in time. As seen in Fig. 4, its behavior is similar whether sugar approaches from the *cis* or *trans* chambers. The escape rate, given by the slope of $\ln f_1(t)$, is largest at the minimum time of $t = t_{\min}$, decreases with t , and appears to approach a constant at large t . Linear fits to the curves yield slopes that are two orders of magnitude larger at t_{\min} than at large t . That is, molecules that have recently become trapped in the channel escape at a much higher rate than those that have already been bound for an extended period.

In Fig. 4, the evolution of $\ln f_1(t)$ is described in terms of two distinct regions. At low t , in the so-called region 1, the $\ln f_1(t)$ curve is nonlinear and changes rapidly with time. At large t , region 2, the curve is linear with a much smaller slope and can be approximated by

$$-\ln f_1(t) \approx B_0 + \lambda_1 t \quad (\text{large } t), \quad (3)$$

where λ_1 is the slope at large t and B_0 is the extrapolated $t = 0$ intercept. Data below indicate that behavior in the two regions responds differently to control parameters like applied voltage and the size of the sugar molecule.

A plausible picture, illustrated by the cartoon in Fig. 4(c), is that the behavior of $f_1(t)$ in region 1 is dominated by events in which a molecule that has just been trapped escapes back to the side of the channel from which it entered. The small- t dependence of $f_1(t)$ is attributable to backward escape of molecules. Slower events, in which the molecule traverses the length of the channel and is translocated to the other side of the membrane, contribute to $f_1(t)$ in region 2. That is, during the large- t region in which $\ln f_1(t)$ is linear, translocation events

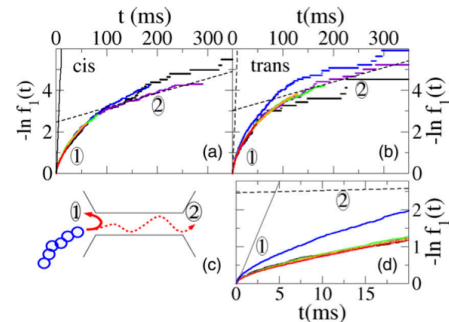


FIG. 4. Inferring the probability of sugar translocation from the nonlinear time dependence of $\ln f_1(t)$. (a) Logarithm of $f_1(t)$ for sugar concentration $[c] = 1.25, 5, 10, 20, 40,$ and $80 \mu\text{M}$ on the *cis* side of the chamber (black, violet, blue, green, orange, and red curves; for noncolor plots, the $[c]$ dependence is weak). The two thin lines show linear fits made at small t and large t . (b) Same as (a) but with sugar on the *trans* side. The $\ln f_1(t)$ curves exhibit a rapid t dependence at small t , the region labeled 1, and a slow linear dependence at large t , labeled 2. (c) A plausible picture, illustrated by the cartoon, is that 1 is associated with chitohexaose molecules escaping back to the side of the channel from which they entered, while translocation through the channel occurs during 2. (d) Same data as in (b) plotted on a timescale within region 1. The linear fit from region 2 is shown as the dashed line.

are likely. If this picture turns out to be valid, then the time dependence of $f_1(t)$ can be used to estimate the translocation probability P_T .

Suppose we make the bold assumption that all translocation occurs during the large- t regime (region 2) and all backward escape occurs earlier (during region 1). Then the fraction P_T of I_1 events that end with translocation is equal to the fraction of events that end during the large- t regime. That is, $P_T \approx \exp(-B_0 - \lambda_1 t^*)$, where t^* is the time when the large- t region begins. Since $B_0 > \lambda_1 t^*$ in Fig. 4, we can approximate this by $P_T \approx \exp(-B_0)$. So

$$\tilde{P}_T \equiv \exp(-B_0) \quad (4)$$

would provide an experimental measurement of the translocation probability P_T . For the data of Fig. 4 it gives $\tilde{P}_T = 0.1$ and 0.05 for sugar approaching from the *cis* and *trans* sides. The uncertainty in these estimates may be as high 50% (though much less in favorable examples). The standard error of linear fits is small (usually less than 1%), but a greater uncertainty may be associated with choosing the high- t range over which to fit. If one sees significant variation of \tilde{P} with concentration $[c]$ (and assumes that such a $[c]$ dependence is not a real effect) then the difference between \tilde{P}_T values obtained from different $[c]$ curves may be considered a measure of uncertainty as well.

In the Appendix, we consider a simplified model of monomers and calculate $f_1(t)$ and P_T . We model the monomer as a sequence of many trapping sites, through which a sugar molecule performs a random walk. The resulting $f_1(t)$ is qualitatively similar to the data of Fig. 3. According to the model results, the initial slope of $\ln f_1(t)$ corresponds to events where a molecule escapes backward immediately after

being trapped. At small t (prior to the large- t linear regime), molecules can wander a few steps into the channel before escaping backward. Translocation events occur at longer t and contribute a significant fraction to the large- t linear regime of $f_1(t)$. The quantity \tilde{P}_T agrees roughly with P_T (overestimating it by a factor of order unity that depends on the details of the random-walk parameters).

We are claiming that \tilde{P}_T is a reasonable proxy for the translocation probability P_T . If a distinct t -linear region of $\ln f_1(t)$ is observed at large t then \tilde{P}_T can be measured.² In the following sections, we provide some experimental support for this claim.

C. Voltage-dependent trapping of charged chitosan

Chitosan hexaose is structurally similar to chitohexaose. At neutral pH , the molecule lacks the N -acetyl group at C2 of the glucosyl ring and is electrically neutral. However, in acidic solutions, it acquires a positive charge via the primary amine at the C2 position. We have measured the single-channel current through *EcChiP* in an acidic solution, pH of 5.5, with a concentration $[c]$ of chitosan hexaose (instead of the usual chitohexaose).

The trapping of chitosan hexaose is strongly voltage dependent because the charged molecule experiences the electric field associated with V . We can exploit this dependence to show that the small- t behavior of $f_1(t)$ is dominated by backward escape.

When chitosan hexaose is introduced to the *cis* chamber with $V < 0$ or the *trans* chamber with $V > 0$, the molecular diffusion current flows in the same direction as the electric current. Molecules are pushed towards the channel by the electric field, so $k_{on}[c]$ should increase with $|V|$. Once a molecule is trapped, the field pushes it deeper into the channel, so the probability of translocation P_T should increase with increasing $|V|$. With the sign of V reversed, the trapping rate should be small and backward escape dominant over translocation.

In Fig. 5, we show plots of the logarithms of $f_0(t)$ and $f_1(t)$ measured for $[c] = 5 \mu M$ of chitosan hexaose introduced to the *cis* side and *trans* sides of the channel for different values of V . The main panels describe molecules flowing with the electric current.

The function $\ln f_0(t)$ is linear in t with a slope $k_{on}[c]$. When chitosan hexaose flows with the electric current, $k_{on}[c]$ increases with $|V|$. When it flows against the current [shown in the insets of Figs. 5(a) and 5(b)], the logarithm of $f_0(t)$ is noisy and does not exhibit a systematic $|V|$ dependence.

In Figs. 5(c) and 5(d), the logarithm of $f_1(t)$ exhibits its usual nonlinear t dependence. There is an evident V dependence, with $f_1(t)$ changing less rapidly at small t when

²In some $f_1(t)$ data, the high- t linear regime is limited to a relatively small number of events or perhaps not evident at all. Intercepts extrapolated from high t will then tend to give \tilde{P} that are too large. These cases correspond to small P_T , where low- t (back-escape) processes dominate the data. So \tilde{P}_T provides an estimate of P_T when translocation is likely and a useful upper limit when translocation is rare.

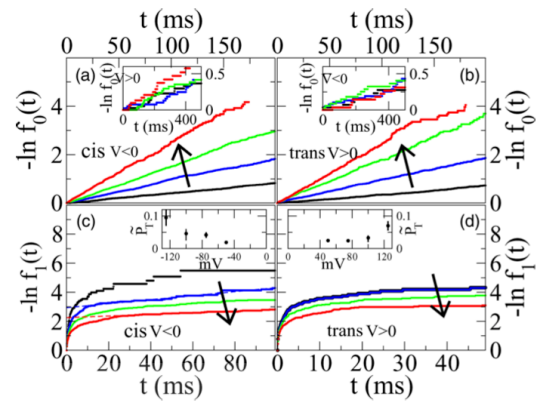


FIG. 5. Trapping and escape with a concentration $[c] = 5 \mu M$ of chitosan hexaose molecules in acidic solution, in which the molecule acquires a positive charge, with the electrode on the *trans* side at a voltage V relative to the *cis* side of the membrane, driven towards the channel by the voltage $|V| = 50, 75, 100,$ and 125 mV (respectively, along the arrow). The trapping rate, given by the slope of $\ln f_0(t)$, increases with driving voltage. The inset shows that the polarity of the potential is reversed, so molecules are pushed away from the channel. (b) Same as in (a) but with the chitosan on the *trans* side of the channel. (c) Plots of $\ln f_1(t)$ for the same conditions as in (a). The escape rate, given by the slope of $\ln f_1(t)$, decreases with driving voltage at small t but is approximately V independent at large t . The inset shows that the parameter \tilde{P}_T , which we propose as the approximate probability for molecules to be translocated through the channel, increases with driving voltage. (d) Same as in (c) but with the chitosan on the *trans* side of the channel.

$|V|$ is increased. That is, when the applied voltage V pushes the chitosan hexaose molecules into the channel, the probability of rapid escape decreases with the driving force $|V|$. This trend is understandable if $f_1(t)$ is dominated by backward escape for $t < 1$ ms. As $|V|$ is increased, the rate of backward escape is reduced, which explains why the escape rate at low t decreases.

Fits of $-\ln f_1(t) \approx B_0 + \lambda_1 t$ at large t yield λ_1 values that are weakly $|V|$ dependent and an intercept B_0 that decreases with increasing $|V|$. The plot of \tilde{P}_T versus V in Fig. 5 shows that this quantity increases rapidly with voltage when sugar molecules flow with the electric current, as expected. (The error bars were obtained by selecting various possible high- t ranges over which to perform linear fits.) In equilibrium, a trapped molecule with charge q is more likely to escape to the low- V side by a factor $\exp(qV/kT)$. This factor is large (between 7 and 400) over the range of V shown, so the relatively small \tilde{P}_T may indicate a large kinetic barrier that acts against translocation. The data here are not sufficient to analyze this feature quantitatively.

The qualitative results of Fig. 5 indicate that the physics of the rapid escape processes that determine $f_1(t)$ at small t is different from that of processes that determine $f_1(t)$ at large t . The large- t , V -independent detrapping processes must be associated with either translocation or backward escape occurring at a rate slower by two orders of magnitude than

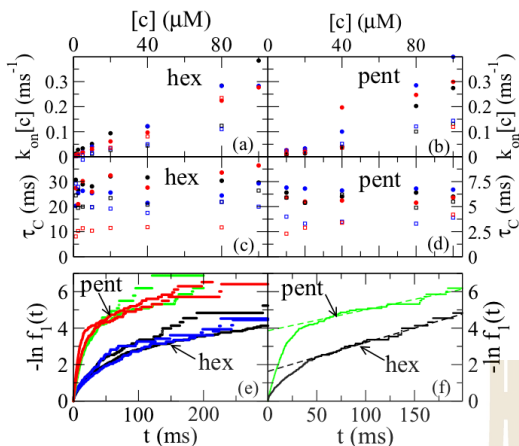


FIG. 6. Trapping and escape rates of different chitosugar molecules with concentration $[c]$ and an applied voltage $|V| = 100$ mV. (a) Trapping rate $k_{\text{on}}[c]$ of chitohexaose on the *cis* side (closed circles) and *trans* side (open squares) of the channel. Different curves are different channel samples measured under the same conditions. (b) Same as (a) but for chitopentaose. (c) Average residence time of chitohexaose τ_C , for the same experiments as in (a). (d) Same as in (c) but with chitopentaose. (e) Logarithm of $f_1(t)$, measured for two channel samples with sugar added to the *cis* (black and green) and *trans* (blue and red) sides at concentration $[c] = 1.25 \mu\text{M}$ for chitohexaose and $[c] = 10 \mu\text{M}$ for chitopentaose (for noncolor plots, differences between colored curves are insignificant). (f) Two curves from (e), with linear fits made at high t shown as dashed lines.

occurs at small t . When chitosan hexaose flows opposite to the electric current, $f_1(t)$ can only be measured (data not shown) at extremely small t . There were no observed I_1 events with a duration of more than a few milliseconds, so the long- t behavior of $f_1(t)$ is absent.

The data of Fig. 5 indicate that the rapid initial variation of $f_1(t)$ is due mainly to backward escape of chitosan hexaose molecules. The measured $f_1(t)$ curves are qualitatively similar for chitosan hexaose and chitohexaose, so it is reasonable to attribute the small- t behavior of $f_1(t)$ with backward escape for chitohexaose as well. We have no direct evidence for translocation of chitohexaose from the current measurements but, given the biological function of the channel, it presumably occurs [30]. This translocation can only happen for larger values of t , after the initial rapid variation of $f_1(t)$ has ended. In light of chitosan data, the claim that $\tilde{P}_T \approx P_T$ seems more likely.

D. Comparing the translocation probability of different chitosugars

We study the dependence of $k_{\text{on}}[c]$, τ_C , and \tilde{P}_T on experimental variables. In particular, we can compare the single-molecule dynamics for different-sized chitosugars: chitohexaose and chitopentaose. In Fig. 6, the trapping rate $k_{\text{on}}[c]$ and residence time τ_C are shown for several different channel

samples, with sugar at a concentration $[c]$ introduced to the *cis* and *trans* sides.

When trapping is measured for different channel samples, significant differences are seen. This variation between samples is the largest source of error in characterizing transport properties (the statistical fitting error in k_{on} and τ_C , which are obtained from data sets with several thousand points, are negligible in comparison and would not even be visible on this scale).

For chitohexaose introduced to the *cis* side of the membrane, the three channels have trapping rates that differ by about 30% at high $[c]$. Larger differences are seen with sugar approaching from the *trans* side of the membrane. The magnitude of $k_{\text{on}}[c]$ for chitohexaose and chitopentaose appear similar in these data. The residence time τ_C is independent of $[c]$, varies significantly from sample to sample, and is roughly five times larger for chitohexaose than for chitopentaose.

The logarithm of $f_1(t)$ is shown for both chitohexaose and chitopentaose on the *cis* and *trans* sides of the membrane. The quantitative details depend on the sample and on whether sugar approaches from the *cis* or *trans* side but the qualitative t dependence is robust. A difference between $f_1(t)$ measured for chitohexaose and chitopentaose is evident: The latter changes more rapidly at small t . The chitopentaose data shown were obtained at higher $[c]$, because the rapid drop of $f_1(t)$ depletes the sample size of events and limits the measurable range at low $[c]$. Since $f_1(t)$ is $[c]$ independent, we choose $[c]$ values that give a larger range and less noisy data.

In Fig. 6(f), representative plots of $\ln f_1(t)$ for chitohexaose and chitopentaose are compared and high- t linear fits shown. The large- t slope, indicating the escape rate of the longest-residing sugar molecules, is similar for the two sugars. However, the rapid initial change of f_1 for chitopentaose results in a larger B_0 value. The associated value of \tilde{P}_T is roughly 0.2 for chitohexaose and 0.02 for chitopentaose.

When chitopentaose is trapped within the *EcChIP* channel, it has a high probability to escape within a millisecond. Trapped chitohexaose molecules are less likely to escape so rapidly and have a relatively high probability to be retained within the channel for a duration of 10 ms or greater. The larger chitohexaose molecules thus enjoy a greater opportunity to be translocated and would, according to Eq. (1) under the assumption $P_T \approx \tilde{P}_T$, be transported through the membrane ten times more rapidly at low $[c]$.

E. Voltage-dependent trapping dynamics for neutral chitohexaose

In Fig. 7, the trapping and detrapping characteristics for chitohexaose are shown as a function of applied voltage. The charged chitosan hexaose molecules were understandably affected by the applied potential. For neutral chitohexaose, the V dependence is more difficult to predict. It turns out that there is a significant V dependence, especially in $f_1(t)$, but it is qualitatively different from that seen for chitosan hexaose. The trapping and escape dynamics for neutral chitohexaose are sensitive to the magnitude $|V|$ of the potential, but independent of its sign.

In Fig. 7, the trapping rate $k_{\text{on}}[c]$ at a fixed $[c] = 5 \mu\text{M}$ is plotted versus applied voltage. With sugar on the *cis* side of the

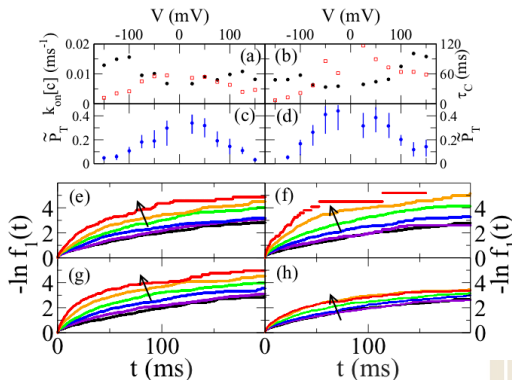


FIG. 7. Trapping and escape of neutral chitohexaose molecules as a function of the voltage V of the electrode on the *trans* side (with the *cis* electrode at ground). (a) Average trapping rate $k_{\text{on}}[c]$ (closed circles) and residence time τ_c (open squares) with sugar concentration $[c] = 5 \mu\text{M}$ on the *cis* side of the channel. (b) Same as in (a) but with sugar on the *trans* side. (c) Parameter \tilde{P}_T , proposed as the probability for sugar molecules to be translocated through the channel, for the same conditions as in (a). (d) Same as in (c) but with sugar on the *trans* side. (e) Logarithm of $f_1(t)$, with $[c] = 5 \mu\text{M}$ on the *cis* side and $V > 0$. Different curves are for $|V| = 25, 50, 75, 100, 125,$ and 150 mV along arrow (black, violet, blue, green, orange, and red curves, respectively). (f) Same as in (e) but with sugar on the *trans* side and $V < 0$. (g) Same as in (e) but with $V < 0$. (h) Same as in (f) but with $V > 0$.

membrane, the sugar flows in the same direction as the electric current when $V < 0$ and in the opposite direction when $V > 0$. Starting from large negative values of V and increasing, the trapping rate first decreases, with an interpolated minimum at $V = 0$, and then slightly recovers at large positive V . The changes in $k_{\text{on}}[c]$ with V are of the order 50% of its maximum value. The data for sugar on the *trans* side exhibit a V dependence that mirrors the result with sugar on the *cis* side. The fitting error in the $k_{\text{on}}[c]$ and τ_c values shown is of order 1% but, as discussed in the preceding section, the much larger variation between channels gives a better indication of their uncertainty.

The effect of varying V on the probability $f_1(t)$ for chitohexaose is shown in Figs. 7(e)–7(h). For sugar on either side of the channel and either sign of V , the function $f_1(t)$ increases more rapidly at small t as the strength of the driving potential is increased. [The magnitude of $\ln f_1(t)$ at $t = 1$ ms increases by a factor of 2 when V increases from 25 to 150 mV.] That is, an applied voltage apparently increases the rate of backward escape by recently trapped chitohexaose molecules. The probability of translocation, as indicated by \tilde{P}_T , decreases with $|V|$. The large- t escape rate λ_1 is approximately independent of $|V|$.

The dependence of $f_1(t)$ on $|V|$ is suggestive of an induced polarization effect. Suppose that the large (and assumed constant) electric field in the channel $|E| \approx |V|/d$, where the channel length $d \approx 4$ nm, results in an average polarization density $\mathbf{P} = \chi \epsilon_0 \mathbf{E}$. If the polarization of a monomer in an

open state is different from that of a monomer obstructed by a sugar molecule then, when the sugar molecule escapes, there is a change in electrostatic energy $\Delta E = -\epsilon_0 \chi (V/d)^2 \Delta\Omega$, where $\Delta\Omega$ is a parameter with the dimension of volume that is used to account for the polarization change. (A change in the susceptibility χ can be absorbed into $\Delta\Omega$ and thus χ taken to be the same for both states.)

The energy difference appears in a Boltzmann factor modifying the reaction rate for a molecule to transition from a bound state inside the channel to an itinerant state in the ambient solution. In a model with multiple bound states for a sugar molecule (like that considered in the Appendix), the measurable escape rate of sugar molecules depends not only on this final reaction rate, but also on the rate of transitions between the internal bound states (which would presumably be weakly affected by the polarization energy and potential V). However, if the Boltzmann factor is rate limiting for the rapid escape observed at the time $t = t_{\text{min}}$, then $\Lambda = \Lambda(V) \equiv -(1/f[t_{\text{min}}]) \ln f_1[t_{\text{min}}]$ should be proportional to this Boltzmann factor

$$\Lambda(V) \approx \Lambda(0) \exp\left(C \frac{[eV]^2}{[k_B T]^2}\right), \quad (5)$$

where

$$C = \Delta\Omega \frac{\chi \epsilon_0 k_B T}{e^2 d^2}. \quad (6)$$

For positive $\Delta\Omega$ values, Eq. (5) predicts that the escape rate $\Lambda(V)$ will increase with $|V|$.

In the data shown above, the factor $(eV)^2/(k_B T)^2$ varies from roughly 1 to 36. For an order-of-magnitude upper estimate of C , we describe the channel as a number volume n of independent molecular dipoles in thermal equilibrium that are aligned by the field and write $\chi \epsilon_0 \approx ne^2 a^2/k_B T$, where a is a length scale for the dipole, giving $C = (n \Delta\Omega)(a/d)^2$. Taking a to be an atomic distance, $n \approx 1/a^3$, and $\Delta\Omega$ to be the volume of the channel interior, we get $C \approx 1/20$. This value would result in Λ changing by a factor of more than 6 when V increases over the measured range. While this is clearly a crude treatment, it does provide a possible approach to understanding the qualitative V dependence of the detrapping characteristics. It may be noted that, in Ref. [41], the authors suggested that a V -dependent τ_c observed in LamB may arise because an applied voltage may cause, in addition to a dipole energy effect, a transition of an open monomer to a different configuration with a reduced sugar-binding affinity (i.e., a gating transition). However, if the small ion conductance of the two configurations is different, then Ohm's law would be violated, which does not appear to be compatible with Fig. 1.

As seen earlier for charged chitosan hexaose, the small- t behavior of $f_1(t)$ changes with V but the large- t escape rate λ_1 is V independent. Upon initially being trapped, the molecule has a backward escape rate that increases with $|V|$. Once a molecule moves into the channel, it is no longer susceptible to backward escape. If it maneuvers to a position from which it can escape to the opposite chamber, then this final escape rate would be enhanced by $|V|$ according to the energetic argument above. However, the long-term escape rate will be independent of V provided the propagation through the channel is rate

limiting (the model calculations in the Appendix are relevant to this discussion).

IV. DISCUSSION

In the results above and those of our earlier studies of *VhChiP*, the probability for the channel to remain unoccupied $f_0(t)$ decays as a single exponential with a $[c]$ -dependent rate. The statistics of trapping can thus be characterized by a single value, the rate $k_{\text{on}}[c]$. This quantity is linear in $[c]$, as seen in Fig. 6, giving a value of k_{on} that is $[c]$ independent. Its value varies considerably from channel sample to sample and depends on the applied voltage, but it is roughly the same whether sugar approaches from the *cis* or *trans* side of the membrane and is of order $2 \times 10^5 \text{ M}^{-1} \text{ s}^{-1}$ for $V = 100 \text{ mV}$. This value of $k_{\text{on}}[c]$ is close, at a given value of $[c]$, to the trapping per monomer observed in *VhChiP*.

The probability for the channel to remain occupied by sugar $f_1(t)$ does not decay as a single exponential. The escape statistics cannot be described by a single parameter, such as the average residence time τ_C or its inverse $k_{\text{off}} = 1/\tau_C$. The effective escape rate changes depending on how long the sugar molecule has remained bound in the channel. Molecules bound for the minimum measurable duration of t_{min} have an escape rate of order 1 ms^{-1} , while those that remain in the channel for at least tens of milliseconds escape at a slower rate of $\lambda_1 \approx 10 \text{ s}^{-1}$.

The average time that a chitohexaose molecule remains bound τ_C , which varies considerably from sample to sample and depends on the applied voltage is, for $|V| = 100 \text{ mV}$, of order 20 ms (it does not depend much on whether sugar was introduced to the *cis* or *trans* side of the channel). Combining these average results, one obtains an equilibrium constant $k_{\text{on}}\tau_C$ of order 10^5 M^{-1} . These values are consistent with values obtained from current averages for other samples and reported in Ref. [32].

The time dependence of the effective escape rate lends itself to physical modeling of the monomer. The simplest model has a single trapping configuration for a sugar molecule. A molecule approaching from either side of the membrane can be trapped in this configuration and may later escape to either side. Assuming constant trapping and escape probability rates, $f_1(t)$ is a simple exponential function, inconsistent with the experimental data. We are thus led to consider models with multiple trapping configurations. We suppose that a molecule that approaches from the *cis* end of the channel and becomes trapped within the monomer can immediately escape back to the *cis* side. If the molecule is to escape to the *trans* side, it must first progress via intermediate transition states, delaying translocation.

A simple example of this latter type of model is the 1D random walk of the Appendix, in which a series of binding sites is located along the channel length. It produces $f_1(t)$ behavior in qualitative agreement with the data. The probability $\ln f_1(t)$ changes rapidly at small t because of the high rate for recently trapped molecules to escape back into the chamber from which they just arrived. If the molecule remains bound for an extended time then it typically moves deep into the channel. From here, escape becomes more difficult and the associated rate decreases, but the molecule can eventually

escape to either side of the channel. The probability $f_1(t)$ is a single exponential with an escape rate λ_1 at large t . If such a model is applicable, then it is possible to estimate the probability of sugar translocation from the $f_1(t)$ data.

Our recent attempt [32] to characterize the *EcChiP* channel suggests the complex structure of Fig. 1. There are numerous amino acid residues arranged along the length of the channel interior. Fluorescence results indicate an interaction between sugar molecules and the Trp residues, in particular, offering some insight into the sugar binding and transport mechanism. It is plausible that the locations of the residues are important trapping sites and may be associated with an observable sugar binding energy.

Microcalorimetry measurements revealed a binding energy of order a significant fraction of 1 eV for a single chitohexaose molecule. The Boltzmann factor associated with escaping such a bound state is of order 10^{-9} . If we assumed a preexponential frequency typical of molecular vibrations, then this would suggest an escape rate of order 0.1 ms^{-1} or smaller. However, any attempt to make a quantitative comparison between the thermodynamic binding energy and a measured escape rate like the large- t rate λ_1 is complicated by several factors. For example, we do not know the maximum escape rate because only molecules bound for more than t_{min} can be observed via the current measurement (thus, a basic escape rate like Λ_0^- used in the model of the Appendix is not observed via the current measurement). Also, in a model with multiple binding configurations with different energies, we would have to obtain an effective binding energy as an appropriate weighted average. Nevertheless, establishing a connection between the phenomenological model of sugar transport discussed in this paper and a more realistic description of the monomer structure is of interest (see, for example, Ref. [47]).

The complex three-dimensional structure of the monomer bears little resemblance to the one-dimensional chain described in the Appendix. Moreover, the model structure of Fig. 1 exhibits a pronounced *cis-trans* anisotropy, which was not evidenced by the trapping and escape statistics: $f_0(t)$ and $f_1(t)$ were qualitatively similar for sugar approaching from either end of the channel. However, making a correspondence between the realistic structure and model calculations, one must consider the following. Different binding configurations could describe not only the physical position of the sugar molecule, but also conformational changes of the molecule within the monomer. The position of the binding site along the chain can be interpreted as a more general reaction coordinate that spans the range of accessible bound configurations. As a minimal assumption, we could suppose that all such bound states can be roughly grouped into three categories: states accessible to a molecule entering (i) from the *cis* chamber, (ii) from neither chamber, and (iii) from the *trans* chamber. This is sufficient to obtain a $f_1(t)$ function with the same qualitative time dependence as the experimental result with translocation mainly occurring on long- t scales. Thus, just as in the simplistic chain model detailed in the Appendix, translocation probability can be approximated from $f_1(t)$. The one-dimensional picture may be regarded as an illustrative example of the class of models needed to understand the $I(t)$ data and its relation to sugar transport.

The $I(t)$ data do not reveal to which side of the channel a trapped molecule escapes. Our argument that the translocation probability P_T can nonetheless be inferred from $I(t)$ data is based on the following points. First, $f_1(t)$ has a qualitative t dependence that is compatible with models that predict backward escape at small t and translocation at large t . Second, $f_1(t)$ for charged chitosan hexaose has the same t dependence as chitohexaose but for chitosan hexaose the initial escape rate is decreased when the potential V drives molecules further into the chamber. So the small- t behavior of $f_1(t)$ for chitosan hexaose, and by assumption chitohexaose, is dominated by backward escape. Finally, since $EcChiP$ can be expressed by $E. coli$ when only chitosugars are available and its average binding characteristics k_{on} and τ_C are similar to those of other chitosugar transporters, it is likely that chitohexaose translocation proceeds with reasonable efficiency. Together this implies that translocation occurs, but only at large t , and that the translocation probability P_T is similar to the measurable parameter \tilde{P}_T .

The value of the transport current Q_T in Eq. (1) could be measured directly. If the sugar concentration on both sides of the membrane was measured as a function of t then the current could be obtained. (One would have to account for the affect of backflow occurring as the concentration on the two sides of the membrane approached equilibrium.) The sugar current Q_T through a single channel, which cannot exceed $k_{on}[c]$, is limited to a few hundred molecules per second at a concentration of $[c] = 100 \mu M$. Thus a viable measurement of Q_T would require a membrane perforated with a large number of channels that conduct sugar in parallel. Since the qualitative behavior of $f_1(t)$ is robust, the average of $f_1(t)$ over many channels would give the nonlinear curve and a measurable \tilde{P}_T . The results of this measurement could be used to obtain P_T and the claim that $\tilde{P}_T \approx P_T$ tested.

V. CONCLUSION

The current $I(t)$ through a single channel of $EcChiP$, a monomeric protein channel for chitosugars that is associated with a silent gene in $E. coli$, has been measured and analyzed. The measured probability $f_1(t)$ for a sugar molecule to remain trapped within the monomer beyond time t exhibits a distinctive t dependence, with an initial rapid decay followed by much slower decay. The initial decay is, based on its V dependence for charged chitosan hexaose, dominated by events in which the sugar escapes back to the side of the membrane from which it entered. The slow long- t escape rate λ_1 is independent of V and likely receives a contribution from successful translocation events, in which the molecule escapes to the opposite side of the membrane. We claim that a valuable estimate for the probability P_T that sugar is translocated through the membrane may be obtained from the measurable property \tilde{P}_T , the extrapolated intercept of the high- t behavior of $f_1(t)$.

These results emphasize the need to go beyond τ_C , which is often used as the only characteristic of escape dynamics, in the characterization of the transport channel. By studying the detailed t dependence of $f_1(t)$, for $EcChiP$, occurring when chitohexaose was replaced with chitopentaose or as a function of V , we were able to develop a phenomenological picture useful for connecting the $I(t)$ data with sugar transport.

ACKNOWLEDGMENTS

Funding was provided by Suranaree University of Technology and the Office of the Higher Education Commission under the NRU project of Thailand. H.S.M.S. was supported by Suranaree University of Technology through an SUT-OROG grant. This author's ten-month research visit in Germany was supported by the Deutscher Akademischer Austausch Dienst. W.S. acknowledges the Thailand Research Fund and Suranaree University of Technology through a Basic Research Grant (No. BRG578001) and an SUT grant (No. SUT1-102-60-36-13). W.M. was supported by a DPST scholarship provided by the Royal Government of Thailand. We thank the group of Professor Mathias Winterhalter at Jacobs University, Bremen, Germany for generously providing access to high-time-resolution BLM equipment and supplies.

H.S.M.S. and W.S. designed and performed single-channel BLM experiments. W.M. and M.F.S. performed data analysis and theoretical calculations. M.F.S. wrote the paper.

APPENDIX: RANDOM-WALK MODEL OF INTRAMONOMER DYNAMICS

There is a substantial amount of literature devoted to modeling OMP channels that utilize molecular dynamical simulations based on a realistic description of the channel structure and other techniques [5,6,48]. For our purposes, a phenomenological description of the monomer that illustrates the relationship between $f_1(t)$, P_T and \tilde{P}_T , in the simplest context, is sufficient. We model the monomer as a series of N trapping sites with sugar molecules undergoing 1D Brownian motion among these sites [49,50]. Trapping sites are labeled $\alpha = 0, 1, 2, \dots, N-1$ from the *cis* end to the *trans* end (see Fig. 8). A sugar molecule that enters the channel from the *cis* chamber becomes bound in the zeroth site at time $t = 0$ and can hop from site to site. When any site is occupied, the ionic current is assumed to be $I(t) \approx I_1$.

At time $t > 0$, the probability of finding the molecule at site α is $g_\alpha(t)$, so $f_1(t) = \sum_\alpha g_\alpha(t)$. The rate for a molecule to hop from the α site to the $\alpha \pm 1$ site Λ_α^\pm is constant in time. Here Λ_0^- is the backward escape rate into the *cis* chamber that determines the initial slope, i.e., $\Lambda_0^- = -f_1'(0)$. A dimensionless time variable τ is defined by

$$\tau \equiv \Lambda_0^- t. \quad (A1)$$

Hopping rates are similarly expressed in units of Λ_0^- so $\Lambda_0^- \equiv 1$ and all Λ_α^\pm are dimensionless.

At time $\tau = 0$, the molecule is bound in the $\alpha = 0$ site, so $g_\alpha(0) = \delta_0^\alpha$. We solve $d\mathbf{g}/d\tau = \mathbf{\Lambda}\mathbf{g}$, where $\mathbf{g}(\tau)$ is a vector with components $g_\alpha(\tau)$ and $\mathbf{\Lambda}$ is a matrix with all elements equal to zero except $\Lambda_{\alpha,\alpha} = -\Lambda_\alpha^+ - \Lambda_\alpha^-$ and $\Lambda_{\alpha,\alpha\pm 1} = \Lambda_{\alpha\pm 1}^\mp$. This gives $\mathbf{g}(\tau) = \exp(\mathbf{\Lambda}\tau)\mathbf{g}(0)$, where the exponential of the matrix is shorthand for the Taylor series $\exp(\mathbf{\Lambda}\tau) \equiv \mathbf{1} + \mathbf{\Lambda}\tau + \mathbf{\Lambda} \cdot \mathbf{\Lambda}\tau^2/2 + \dots$, where $\mathbf{1}$ is the $N \times N$ unit matrix.

The behavior of $f_1(\tau)$ at small times, obtained from the first few terms of the Taylor series, is

$$-\ln f_1(\tau) \approx \tau - \Lambda_0^+ \frac{\tau^2}{2} + \Lambda_0^+(\Lambda_0^+ + \Lambda_1^- - 1) \frac{\tau^3}{6} + \dots \quad (\text{small } \tau). \quad (A2)$$

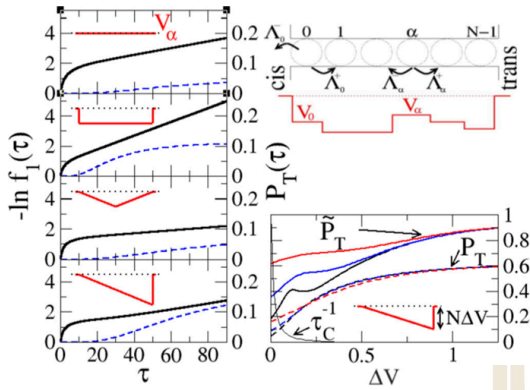


FIG. 8. Escape of a molecule from the channel, modeled as a 1D random walk. The top right shows the model monomer with N trapping sites $\alpha = 0, 1, 2, \dots$ from *cis* to *trans* sides. A molecule hops at rate Λ_α^\pm from α to $\alpha \pm 1$ so $\Lambda_0^- = -f_1'(0)$ is the escape rate to the *cis* chamber. These Λ_α^\pm depend on effective potential V_α . Shown on the left are simulation results from the model for various effective potentials V_α (indicated in red and labeled in the top panel) and $N = 20$. The solid black curves show the logarithm of $f_1(\tau)$, the probability for the molecule to remain in the channel beyond time τ , where τ is the time variable. Dashed blue curves show the probability $P_T(\tau)$ for the molecule to be translocated from the *cis* to the *trans* side before time τ . The bottom right shows the wedge potential with steepness ΔV and probability $P_T = P_T(\infty)$ (dashed line) compared to \tilde{P}_T (solid line) for $N = 20, 10, 5$ from bottom to top. The residence time τ_C in arbitrary units is shown for $N = 20$.

The first term in the series describes molecules that escape back to the *cis* chamber immediately after being trapped at $\alpha = 0$. The next few terms describe molecules that undertake short walks into the monomer before escaping back to the *cis* chamber. Translocation processes do not occur until the N th-order term, which is negligible at small time τ .

More explicitly, the solution can be written $g_\alpha(\tau) = \sum_n u_{n,\alpha} u_{n,0} \exp(-\lambda_n \tau)$ with $f_1(\tau) = \sum_{n=1}^N p_n \exp(-\lambda_n \tau)$ and $p_n = (\Lambda_0^- u_{n,0} + \Lambda_{N-1}^+ u_{n,N-1}) u_{n,0} \lambda_n^{-1}$, where each λ_n is an eigenvalue of $\mathbf{\Lambda}$ and $u_{n,\alpha}$ is the α th component of the corresponding eigenvector. These eigenvalues satisfy $\sum \lambda_n p_n = \Lambda_0^-$.

The simplest nontrivial version of this model has $N = 2$ trapping sites and two eigenvalues λ_n that are functions of the three independent hopping parameters. If applied to the $f_1(t)$ data above, one has to select hopping parameters with a large variation so that the slope of $\ln f_1(t)$ changes by orders of magnitude. Having done this, the calculated curve $\ln f_1(t)$ tends to exhibit a sharp elbow where the slope changes from a large value to a small value. It is difficult to reproduce the smooth evolution of the $\ln f_1(t)$ data with this model. We instead consider models with a much larger number of sites, which have the correct qualitative behavior. [If the hopping parameters are assumed to be equal, as in model (i) below, we can solve the above equations analytically for any N and thus gain some physical insight.]

At large times τ , the sum of exponentials is dominated by the term with the smallest positive eigenvalue, which we denote by λ_1 . This gives

$$-\ln f_1(\tau) \approx B_0 + \lambda_1 \tau + \dots \quad (\text{large } \tau), \quad (\text{A3})$$

with $\tilde{P}_T = \exp(-B_0) = p_1$. The probability of translocation $P_T(\tau)$ occurring before time τ is

$$P_T(\tau) = \int_0^\tau d\tau' g_{N-1}(\tau') \Lambda_{N-1}^+ \quad (\text{A4})$$

with the total probability of translocation $P_T \equiv P_T(\infty)$. Both P_T and \tilde{P}_T can be calculated and the claim that the measurable quantity \tilde{P}_T is an approximation to the translocation probability P_T can be tested within the context of this model.

Sample calculations of $f_1(\tau)$ and $P_T(\tau)$, for an arbitrary channel size $N = 20$, are shown in the left panels of Fig. 8. The Λ_α^\pm values are written in terms of a dimensionless potential energy V_α , which binds the sugar molecule at each trapping site, according to $\Lambda_\alpha^\pm = \exp(V_\alpha - V_{\alpha\pm 1})$ with zero potential outside the monomer. The V_α indicated in Fig. 8 are, from top to bottom, (i) $V_\alpha = 0$, giving all $\Lambda_\alpha^\pm = 1$, (ii) $V_\alpha = -1$, giving fast intramonomer hopping with slower escape at each end of the channel, (iii) a symmetric wedge potential with $V_\alpha = -0.1(\alpha + 1)$ for $\alpha < N/2$, and (iv) an asymmetric wedge potential $V_\alpha = -0.1(\alpha + 1)$ for all α .

The calculations of $f_1(\tau)$ have similar qualitative behavior to the data of Figs. 4 and 5. That is, the curve $\ln f_1(\tau)$ changes rapidly at small τ and then the slope approaches a constant with a much smaller value at large τ . The small- τ behavior is sensitive to the binding potential at the *cis* mouth. The final slope λ_1 is largely determined by the length of the channel, since propagation through a long channel is the rate-limiting mechanism. For the cases shown, $P_T(\tau)$ is negligible at small τ and does not start to increase appreciably until $f_1(\tau)$ is approaching its large- τ limit.

In the bottom right plot, P_T is compared to \tilde{P}_T for the asymmetric wedge potential. They follow a similar trend with variation of the wedge steepness ΔV . At large ΔV , the descending linear potential gives a transmission probability P_T that approaches unity. The average time that the monomer remains blocked τ_C increases rapidly with ΔV .

The connection between \tilde{P}_T and P_T is evident from the results above. Both $f_1(\tau)$ and P_T are given by sums over eigenvectors n . If we approximate each sum by the $n = 1$ term associated with the smallest eigenvalue then we find

$$\tilde{P}_T \approx (1/\lambda_1) (u_{1,0}^2 \Lambda_0^- + u_{1,0} u_{1,N-1} \Lambda_{N-1}^+) \quad (\text{A5})$$

and

$$P_T \approx (1/\lambda_1) u_{1,0} u_{1,N-1} \Lambda_{N-1}^+. \quad (\text{A6})$$

The first term on the right-hand side of Eq. (A5) describes backward escape to the *cis* side during the large- τ regime. The second term, also appearing in Eq. (A6), describes large- τ translocation. An equality is established between \tilde{P}_T and P_T by making two assumptions: (a) The second term in Eq. (A5) dominates over the first and (b) the sum over n that determines P_T is well approximated by its $n = 1$ term. The validity of these two assumption depends on V_α .

When $V_\alpha = 0$ and all hopping rates are equal to one, the equations above can be evaluated analytically. The eigenvalues

are

$$\lambda_n = 2 - 2 \cos \left[\frac{n\pi}{N+1} \right], \quad (\text{A7})$$

with $n = 1, 2, \dots, N+1$ varying over a range of order $1/N^2$ and producing a $f_1(t)$ function with the same qualitative behavior as the data when N is large. The weights p_n satisfy

$$p_n = \cos^2 \left(\frac{n\pi}{2(N+1)} \right) [1 - (-1)^n]. \quad (\text{A8})$$

Further, the analytic results yield $P_T = 1/(N+1)$ and, assuming $N \gg 1$, $\tilde{P}_T = 4/(N+1)$. The two terms in Eq. (A5) are equal and the $n = 1$ term is twice as large as the full series giving P_T . Combining the errors in both assumptions,

\tilde{P}_T overestimates P_T by a factor of 4. For the remaining examples of the left-hand side of Fig. 8, \tilde{P}_T overestimates P_T by factors 4, 2.6, and 2.2, respectively. The estimate becomes more accurate as the steepness of the asymmetric wedge potential ΔV increases.

Generally, \tilde{P}_T gives the probability that a molecule is retained in the channel for a time much greater than required for initial backward escape. It does not tell us whether the molecule will be translocated. For effective potentials V_α that present large barriers to translocation, one finds $\tilde{P}_T \gg P_T$ and $P_T \ll 1$. For a channel designed to translocate sugar, one can suppose that translocation is not prevented by a large energy barrier. If this is the case, then reasonable values for V_α result in $\tilde{P}_T \approx P_T$ to within a factor of order unity.

- [1] H. Nikaido, *J. Bioenerg. Biomembr.* **25**, 581 (1993).
 [2] C. Andersen, M. Jordy, and R. Benz, *J. Gen. Physiol.* **105**, 385 (1995).
 [3] C. Andersen, R. Cseh, K. Schülein, and R. Benz, *J. Membr. Biol.* **164**, 263 (1998).
 [4] S. M. Bezrukov, *J. Memb. Biol.* **174**, 1 (2000).
 [5] H. Nikaido, *Microbiol. Mol. Biol. Rev.* **67**, 593 (2003).
 [6] B. Roux, T. Allen, S. Berneche, and W. Im, *Q. Rev. Biophys.* **37**, 15 (2004).
 [7] S. Szmelcman and M. Hofnung, *J. Bacteriol.* **124**, 112 (1975).
 [8] E. G. Saravolac, N. F. Taylor, R. Benz, and R. R. Hancock, *J. Bacteriol.* **173**, 4970 (1991).
 [9] K. Schulein, K. Schmid, and R. Benz, *R. Mol. Microbiol.* **5**, 2233 (1991).
 [10] T. Schirmer, *J. Struct. Biol.* **121**, 101 (1998).
 [11] R. Dutzler, Y.-F. Wang, P. J. Rizkallah, J. P. Rosenbusch, and T. Schirmer, *Structure* **4**, 127 (1996).
 [12] Y.-F. Wang, R. Dutzler, P. J. Rizkallah, J. P. Rosenbusch, and T. Schirmer, *J. Mol. Biol.* **272**, 56 (1997).
 [13] M. Watanabe, J. Rosenbusch, T. Schirmer, and M. Karplus, *Biophys. J.* **72**, 2094 (1997).
 [14] T. Schirmer, T. A. Keller, Y. F. Wang, and J. P. Rosenbusch, *Science* **267**, 512 (1995).
 [15] C. Hilty and M. Winterhalter, *Phys. Rev. Lett.* **86**, 5624 (2001).
 [16] W. Im and B. Roux, *J. Mol. Biol.* **322**, 851 (2002).
 [17] N. O. Keyhani, X. B. Li, and S. Roseman, *J. Biol. Chem.* **275**, 33068 (2000).
 [18] N. O. Keyhani and S. Roseman, *Biochim. Biophys. Acta* **1473**, 108 (1999).
 [19] X. Li and S. Roseman, *Proc. Natl. Acad. Sci. U.S.A.* **101**, 627 (2004).
 [20] B. L. Bassler, C. Yu, Y. C. Lee, and S. Roseman, *J. Biol. Chem.* **266**, 24276 (1991).
 [21] D. E. Hunt, D. Gevers, N. M. Vahora, and M. F. Polz, *Appl. Env. Microbiol.* **74**, 44 (2008).
 [22] C. Pruzzo, L. Vezzulli, and R. R. Colwell, *Env. Microbiol.* **10**, 1400 (2008).
 [23] K. K. Meibom, X. B. Li, A. T. Nielsen, C. Y. Wu, S. Roseman, and G. K. Schoolnik, *Proc. Natl. Acad. Sci. U.S.A.* **101**, 2524 (2004).
 [24] W. Suginta, W. Chumjan, K. R. Mahendran, A. Schulte, and M. Winterhalter, *J. Biol. Chem.* **288**, 11038 (2013).
 [25] W. Suginta, M. Winterhalter, and M. F. Smith, *Biochim. Biophys. Acta* **1858**, 3032 (2016).
 [26] T. Mizuno, M. Y. Chou, and M. Inouye, *Proc. Natl. Acad. Sci. U.S.A.* **81**, 1966 (1984).
 [27] M. Guillier, S. Gottesman, and G. Storz, *Genes Dev.* **20**, 2338 (2006).
 [28] J. Vogel and K. Papenfort, *Curr. Opin. Microbiol.* **9**, 605 (2006).
 [29] A. A. Rasmussen, J. Johansen, J. S. Nielsen, M. Overgaard, B. Kallipolitis, and P. A. Valentin-Hansen, *Mol. Microbiol.* **72**, 566 (2009).
 [30] N. Figueroa-Bossi, M. Valentini, L. Malleret, F. Fiorini, and L. Bossi, *Genes Dev.* **23**, 2004 (2009).
 [31] H. S. M. Soysa and W. Suginta, *J. Biol. Chem.* **291**, 13622 (2016).
 [32] H. S. M. Soysa, A. Schulte, and W. Suginta, *J. Biol. Chem.* **292**, 19328 (2017).
 [33] R. Benz, A. Schmid, and G. H. Vos-Scheperkeuter, *J. Membr. Biol.* **100**, 21 (1987).
 [34] M. Winterhalter, *Curr. Opin. Colloid Interface Sci.* **5**, 250 (2000).
 [35] E. Berkane, F. Orlik, A. Charbit, C. Danelon, D. Fournier, R. Benz, and M. Winterhalter, *J. Nanobiotech.* **3**, 3 (2005).
 [36] L. Kullman, P. A. Gurnev, M. Winterhalter, and S. M. Bezrukov, *Phys. Rev. Lett.* **96**, 038101 (2006).
 [37] W. Suginta, W. Chumjan, K. R. Mahendran, P. Janning, A. Schulte, and M. Winterhalter, *PLoS One* **8**, e55126 (2013).
 [38] W. Suginta and M. F. Smith, *Phys. Rev. Lett.* **110**, 238102 (2013).
 [39] M. Montal and P. Mueller, *Proc. Natl. Acad. Sci. U.S.A.* **69**, 3561 (1972).
 [40] C. Danelon, T. Brando, and M. Winterhalter, *J. Biol. Chem.* **278**, 35542 (2003).
 [41] G. Schwarz, C. Danelon, and M. Winterhalter, *Biophys. J.* **84**, 2990 (2003).
 [42] <http://swissmodel.expasy.org/>
 [43] S. Biswas, M. M. Mohammad, D. R. Patel, L. Movileanu, and B. van den Berg, *Nat. Struct. Mol. Biol.* **14**, 1108 (2007).
 [44] www.pymol.org
 [45] C. Andersen, B. Schiffler, A. Charbit, and R. Benz, *J. Biol. Chem.* **277**, 41318 (2002).
 [46] L. Kullman, M. Winterhalter, and S. M. Bezrukov, *Biophys. J.* **82**, 803 (2002).
 [47] C. Calero, J. Faraudo, and M. Aguilera-Arzo, *Phys. Rev. E* **83**, 021908 (2011).
 [48] P. Hanggi and F. Marchesoni, *Rev. Mod. Phys.* **81**, 387 (2009).
 [49] R. Phillips, J. Kondev, J. Theriot, and H. G. Garcia, *Physical Biology of the Cell* (Garland, New York, 2013).
 [50] N. G. Van Kampen, *Stochastic Processes in Physics and Chemistry* (Elsevier, Amsterdam, 1992).

CURRICULUM VITAE

Name Miss Watcharaporn Moonsap

Date of Birth 1 December 1991

Place of Birth Roi-Et, Thailand

Education

- 24 April 2014, Bachelor Degree of Science in Physics (First Class Honours), Khon Kaen University.

Publication

- Soysa, H. S. M., Suginta, W., Moonsap, W. and Smith, M. F. (2018). Chitosugar translocation by an unexpressed monomeric protein channel. **Phys. Rev. E** 97(5): 052417.

Awards -

Grants and Fellowships

2007 – Present, The Development and Promotion of Science and Technology Talents Project (DPST Scholarship)